

PHOTOACOUSTIC INVESTIGATION OF PHASE TRANSITIONS IN SELECTED SOLIDS

JOHNEY ISAAC

**THESIS SUBMITTED
IN PARTIAL FULFILMENT OF THE REQUIREMENTS
FOR THE DEGREE OF
DOCTOR OF PHILOSOPHY**


**DEPARTMENT OF PHYSICS
COCHIN UNIVERSITY OF SCIENCE AND TECHNOLOGY
KOCHI - 682 022
INDIA**

1991

CERTIFICATE

Certified that the work presented in this thesis is based on the bona fide work done by Mr.Johney Isaac under my guidance in the Department of Physics, Cochin University of Science and Technology, and has not been included in any other thesis submitted previously for the award of any degree.

Cochin 682 022
April 23, 1991



23/4/91
Dr.Jacob Philip
Supervising Teacher



DECLARATION

Certified that the work presented in this thesis is based on the original work done by me under the guidance of Dr.Jacob Philip, Professor, Department of Physics, Cochin University of Science and Technology, and has not been included in any other thesis submitted previously for the award of any degree.

Cochin 682 022
April 23, 1991


is absorbed light

Johney Isaac

PREFACE

The photoacoustic (PA) effect has widely been used in recent years for the investigation of the optical and thermal properties of materials. It has been an intense field of research ever since Rosencwaig and Gersho developed a general theory of the PA effect about a decade ago. There are many distinct advantages for this new technique compared to conventional techniques. One of them is that it enables one to obtain a spectrum similar to the optical absorption spectrum of any type of solid or semisolid material which cover a wide range of organic, inorganic, biological and medical specimens. Another principal advantage is that non-radiative transitions can be directly detected by this technique which is especially powerful for studying optical properties of semiconductors. Moreover, photoacoustic technique finds extensive applications in the study of thermal properties of materials. These include measurement of thermal diffusivity, thermal wave imaging and investigation of phase transitions in solids.

The PA effect is the generation of acoustic signals when a sample placed inside an enclosed cell is irradiated by an intensity modulated beam of light. The absorbed light

is converted into heat waves through non-radiative relaxation processes and the thermal waves generated within the sample are diffused to the surrounding gas causing corresponding pressure fluctuations which can be detected by a sensitive microphone suitably placed. The amplitude of the acoustic signal and its phase relative to the incident modulated light depend, among others, on the thermal diffusivity of the sample and should therefore be sensitive to any thermodynamic process occurring within the sample. Such a process could for instance be a phase transition in a solid. The PA effect is especially attractive for the study of the changes in the thermal and optical properties of solids near phase transition temperatures. The first attempt to study phase transitions employing the PA effect was by Florian et al., who studied first order phase transitions in selected materials.

Although there has been a few other papers on this topic, attempts for a quantitative evaluation of the features of phase transitions are rare. We have carried out systematic investigations on a few selected type of phase transitions existing in solids using PA technique. The systems studied are the following. (i) High temperature superconductors with $\text{YBa}_2\text{Cu}_3\text{O}_7$ and Pb doped Bi-Sr-Ca-Cu-O as representative samples in order to study the transition from the normal to

the superconducting state. (ii) Ferroelectrics with KNO_3 and Triglycine Sulphate (TGS) as examples to investigate features of the para-ferroelectric phase transitions. (iii) Photo-ferroelectric transition with SbSI as example which shows large variation in optical energy gap around the para-ferroelectric transition point. The thesis contains a detailed account of the work done on the above topic, the results obtained and analysis of the results. In the following paragraphs a brief chapterwise summary is outlined.

The first chapter of the thesis is intended to provide an introduction to the photoacoustic effect, phase transitions in solids and photoacoustic study of phase transitions. This is necessary to follow the material presented in the later chapters. Written in two parts, the first part describes the basic principles of the PA effect based on the theory of Rosencwaig and Gersho (RG theory) highlighting its merits and advantages with emphasis on topics related to the work presented in the thesis. Other theories on PA effect, which are either extensions or modifications of the RG theory are also briefly outlined. In the second part, we discuss the application of photoacoustic technique for the investigation of phase transitions in solids. This section also includes a review of the work already done in the field and an analysis of the current status of this area of research.

The second chapter is devoted to instrumentation which has been used to carry out the work presented in the later chapters. The design and fabrication of a variable temperature photoacoustic cell, design and fabrication of a temperature controller and setting up the PA spectrometer from the core of this chapter. A block diagram and description of our PA spectrometer are given in this chapter. The heart of the experimental set up, the PA cell, has been designed and fabricated in our laboratory and can be used to take measurements over a wide range of temperature from ≈ 85 K to ≈ 420 K. A sensitive electret microphone has been used to detect the acoustic signals. An accurate temperature controller which is essential for phase transition studies has also been designed and fabricated in our laboratory. It is a PID controller utilizing a platinum resistor as the temperature sensor. It can be used to control the temperature anywhere in the range -200°C to $+200^{\circ}\text{C}$ with a set point resolution of 0.1°C and stability within $\pm 0.01^{\circ}\text{C}$. The details of the design and fabrication of the PA cell and temperature controller are given in this chapter.

In chapter 3 we present our studies on the high temperature ceramic superconductor $\text{YBa}_2\text{Cu}_3\text{O}_7$. Chapter 3 begins with the necessary general remarks on the research activities on high T_c superconductivity and outlines the

various properties of the new materials, particularly $\text{YBa}_2\text{Cu}_3\text{O}_7$. Following this a brief description of the method used by us to prepare the samples using the well established solid state reaction method is given. The electrical resistivity and magnetic susceptibility of the samples have been measured and are included in this chapter. A brief review of other measurements on $\text{YBa}_2\text{Cu}_3\text{O}_7$ especially specific heat and thermal conductivity, which are most relevant to the study of high T_c superconducting transitions using PA technique is given. Photoacoustic study of the superconducting transition in $\text{YBa}_2\text{Cu}_3\text{O}_7$ is the core of chapter 3. The amplitude of the PA signal and its phase relative to the incident chopped light beam have been measured as a function of temperature, down to 85 K during both cooling and heating cycles. It is found that the amplitude of the PA signal does not show any appreciable change in the vicinity of the superconducting transition whereas the phase shows an anomalous change near the transition point. Qualitative explanations for the results are given. The second phase of measurements involves the determination of the absolute value of the thermal diffusivity of $\text{YBa}_2\text{Cu}_3\text{O}_7$ as a function of temperature using PA technique. This has been done by measuring the chopping frequency dependence of the amplitude of the PA signal of a thin sample mounted on an aluminium disc which acts as a backing material, at various fixed temperatures above and

below T_c . The thermal diffusivity is found to undergo an abrupt increase below T_c , in a manner opposed to that of a normal superconductor. The results obtained from these studies are presented and discussed in detail in this chapter.

In chapter 4, we present the results of the photoacoustic measurements performed on Pb-doped Bi-Sr-Ca-Cu-O high T_c superconducting samples. The thermal diffusivity has been determined as a function of Pb concentration above and below T_c . It is found that below T_c the thermal diffusivity saturates below certain Pb doping level. The results are explained on the basis of phonon-defect scattering

Both Pottasium Nitrate (KNO_3) and Triglycene Sulphate (TGS) show para-ferroelectric phase transitions as the sample temperature is varied and a photoacoustic study of these transitions form the content of chapter 5. We begin with a brief introduction to the nature of transitions in KNO_3 and TGS and outline the preparation of the samples for PA measurements. Systematic measurements of the variation of PA amplitude on KNO_3 as a function of temperature are given along with results of Differential Scanning Calorimetric studies made with Perkin-Elmer model DSC-7. It is found that

the PA amplitude undergoes distinct variations near phase transition temperatures. PA measurements on TGS are also included in this chapter. The results of all the above investigations are analysed in detail.

In chapter 6, we describe the determination of the optical energy gap of the photoferroelectric material SbSI using PA technique. A brief outline of the nature of the transition in SbSI is given. The optical absorption spectra of these samples have been obtained at various temperatures by plotting the amplitude of the PA signal against the incident photon wavelength. The temperature coefficient of the energy gap in SbSI is found to undergo a marked increase below the para - ferroelectric transition point which can be attributed mainly to the lattice elongation due to the spontaneous polarization below the transition temperature. A detailed discussion of the results with necessary theoretical interpretation is presented in this chapter.

Chapter 7 provides an overall summary and conclusion of the whole work presented in the thesis. The potentiality of the photoacoustic technique as a tool for the investigation of different types of phase transitions is emphasised. Further scope of work in this field of research is also analysed.

Most of the work presented in this thesis has been published/accepted for publication in the form of the following papers.

1. Anomalous change in photoacoustic phase near superconducting transition in $\text{YBa}_2\text{Cu}_3\text{O}_7$, Pramana--J.Phys. 31, L153 (1988).
2. Abrupt increase in thermal diffusion below T_c in $\text{YBa}_2\text{Cu}_3\text{O}_7$, Pramana--J.Phys. 32, L167 (1989).
3. A low cost high precision PID temperature controller, Ind.J.Pure & Appl.Phys. 29, 195, (1991).
4. Stability of the ferroelectric phase in polycrystalline KNO_3 investigated by photoacoustic and calorimetric techniques, J.Appl.Phys. 69, , (1 May 1991).
5. Temperature dependence of the absorption edge in the ferroelectric phase of SbSI using photoacoustic technique, Phys.Stat.Solidi (a), (in press).
6. Thermal diffusivity of Bi-Sr-Ca-Cu-O superconductor: Effect of Pb doping, Phys.Rev. B, (in press).

CONTENTS

	<u>Page</u>
Chapter 1 INTRODUCTION	
PART A: PHOTOACOUSTICS AND PHOTOACOUSTIC SPECTROSCOPY	
1.1 Introduction	1
1.2 Theory of photoacoustic effect in solids	6
1.3 Theory of Rosencwaig and Gersho (R-G theory)	9
1.4 Application of the photoacoustic effect	23
PART B: PHOTOACOUSTIC INVESTIGATION OF PHASE TRANSITIONS IN SOLIDS	
1.5 Phase transitions in solids	28
1.6 Photoacoustic investigation of phase transitions	33
References	43
Chapter 2 INSTRUMENTATION	
2.1 Photoacoustic spectrometers in general	52
2.2 The experimental set up	61
2.3 Design, fabrication and characterization of the variable temperature PA cell	64
2.4 Design and fabrication of a PID temperature controller	73
References	84
Chapter 3 PHOTOACOUSTIC INVESTIGATIONS ON THE HIGH T_c SUPERCONDUCTOR $YBa_2Cu_3O_7$	
3.1 Introduction to high T_c superconductivity	87
3.2 Thermal properties of high T_c superconductors	91

3.3	Preparation and characterization of YBa ₂ Cu ₃ O ₇ samples	97
3.4	Photoacoustic measurements on YBa ₂ Cu ₃ O ₇	101
3.5	Results and discussion	105
	References	117
Chapter 4	PHOTOACOUSTIC STUDY OF THE THERMAL PROPERTIES OF THE HIGH T_c SUPERCONDUCTOR Bi-Sr-Ca-Cu-O	
4.1	Introduction	123
4.2	Sample preparation	128
4.3	Thermal diffusivity measurements	129
4.4	Results and discussion	130
	References	143
Chapter 5	PHOTOACOUSTIC INVESTIGATIONS OF THE PHASE TRANSITIONS IN KNO₃ AND TGS	
5.1	Introduction	147
5.2	Experimental method	149
5.3	Results and discussion	150
	References	162
Chapter 6	PHOTOACOUSTIC INVESTIGATION OF THE PARA - FERROELECTRIC PHASE TRANSITION IN PHOTOFERROELECTRIC SbSI	
6.1	Introduction to photoferroelectric phenomena	164
6.2	Photoacoustic determination of the temperature variation of the optical energy gap of SbSI	169
6.3	Results and discussion	171
	References	179
Chapter 7	SUMMARY AND CONCLUSION	181

Chapter 1

INTRODUCTION

PART A: PHOTOACOUSTICS AND PHOTOACOUSTIC SPECTROSCOPY

1.1 Introduction

Light interacts with matter at the atomic or molecular levels and this makes it one of the most powerful tools for the study of various microscopic phenomena. Optical spectroscopy has largely contributed to the enormous growth of atomic and molecular physics and to the development of quantum theory during the early years of this century. Spectroscopy is now a science encompassing many disciplines and several techniques. The non-destructive nature, versatility and range have made optical spectroscopy a widely used and very important tool for the investigation and characterization of materials.

One major drawback of conventional optical spectroscopy is that it is very difficult to perform with samples which are very weak or very strong absorbers of light or highly light scattering ones; the basic reason being that the technique depends on the detection of photons. In case of a weakly absorbing sample, for example, a transparent gas

containing minute quantities of absorbing centres such as pollutants, the absorption measurement involves the detection of minute variations in the intensity of a strong, essentially unattenuated transmitted light beam. Various techniques developed to overcome this difficulty such as derivative spectroscopy have proven to be generally inadequate. For an opaque sample, whose dimensions far exceed the optical penetration depth, there is essentially no transmitted photons and absorption measurements become difficult, if not impossible. Several techniques have been developed to overcome the difficulties encountered with opaque and highly light scattering substances and the most common of these are diffuse reflectance [1], attenuated total reflection (ATR) and internal reflection spectroscopies [2], and Raman scattering [3]. Eventhough such techniques have been very useful each suffers from serious limitations. In particular, each method is applicable only to a limited category of materials and each is useful only over a small wavelength range and the data obtained are often difficult to interpret.

The photoacoustic technique has evolved over the past one and a half decades as a very powerful method to study those materials that are unsuitable by conventional transmission or reflection methodologies [4-7]. This technique, based on the photoacoustic effect originally

detected by Alexander Graham Bell in 1880 [8,9], possesses some unique features mainly due to the fact that eventhough the incident energy is in the form of photons, the interaction of these photons with the sample is studied not through subsequent detection and analysis of some of the photons, but through a direct measurement of the energy absorbed by the material as a result of its interaction with the incident photon beam.

The photoacoustic (PA) effect is the generation of an acoustic signal when the sample under investigation, placed inside a closed cell, is irradiated by an intensity modulated beam of light. In case of gas and liquid samples, the sample fills the entire volume of the cell and the acoustic signals are detected by a microphone and a piezo-electric transducer respectively. In the case of solid samples, the sample fills only a portion of the cell and the remaining volume of the cell is filled with a non-absorbing gas such as air, and a sensitive microphone is suitably placed inside the cell to pick up the acoustic signals. The internal energy levels of the sample are excited by the absorption of incident radiation and upon subsequent deexcitation, all or part of the absorbed photon energy is converted into heat through non-radiative deexcitation processes. In the case of gas and liquid samples, this

internal heating causes pressure fluctuations having the same frequency as that of the modulation of the incident beam, which can be detected by the acoustic transducer. In the case of solid samples, the periodic heating of the sample results in a periodic heat flow from the interior of the sample to the surrounding gas which in turn produces pressure fluctuations in the gas which can be detected as an acoustic signal by the microphone. It is also possible to measure the heat generated in a bulk solid sample through the subsequent pressure or stress variation in the sample itself by means of a piezoelectric detector in intimate contact with the sample. Eventhough the sensitivity in this case is better it is not always possible to employ a piezoelectric detector due to the limitations imposed by the nature of the sample. Also the use of piezoelectric transducers is very difficult for PA measurements that involve variation of the sample temperature over a wide range.

Photoacoustics is essentially a combination of optical absorption spectroscopy and calorimetry. From the calorimetric viewpoint, the heat input into the sample is supplied indirectly by the incident beam of light and the rise in temperature is detected by another indirect method using an acoustic transducer instead of a thermal detector.

For a typical solid sample, using gas microphone detection system, temperature rise of $\sim 10^{-6} \text{ }^\circ\text{C}$ can be detected. This acoustic detection has several advantages over conventional thermal detection using temperature sensors such as thermistors or thermopiles in terms of sensitivity, detector rise time and the speed at which measurements can be made.

The advantages of photoacoustics as a form of spectroscopy are evident from the very nature of the technique. Since absorption of optical or electromagnetic radiation is essential for the generation of the PA signal, light that is transmitted or elastically scattered by the sample does not interfere with the inherently absorptive PA measurements. This enables one to work with essentially transparent media or highly light scattering materials such as powders, amorphous solids, gels and colloids. On the other hand, since the technique does not depend upon the detection of photons, it is possible to obtain optical absorption spectra of materials that are completely opaque to transmitted light. The advantages offered by photoacoustics over other conventional spectroscopic techniques due to the two basic aspects viz., the insensitivity to the non-absorbed light and the non-dependence on the detection of photons, cannot be over-emphasized.

Spectroscopy is, however, only one of the several applications of PA effect. In the spectroscopic regime itself, photoacoustics can be used to measure the absorption and excitation spectra, the life time of excited states, and the quantum yield of radiative processes. In addition to this, the calorimetric or thermal aspect associated with the PA effect offers a wide range of applications to study the thermal and elastic properties of materials. In such studies the calorimetric or acoustic aspect of photoacoustics plays the dominant role, while the optical part is simply a convenient mechanism for heat generation. Such applications include measurement of thermal parameters, thermal wave imaging and study of phase transitions in solids. A more detailed account of the applications of photoacoustic effect, as used in this work is given later in this chapter.

1.2 Theory of photoacoustic effect in solids

Eventhough the PA effect was discovered more than a century ago, the potentiality of the technique remained almost unexploited until recently. There had been some work during the thirties and fourties--with the advent of microphone--to study infrared absorption in gases to evaluate concentration of gaseous species in gas mixtures, and to study deexcitation and energy transfer processes in gases [10-15].

The principles underlying the PA effect in gases had been well known during that time. But a proper theoretical understanding of PA effect in solids was lacking despite several attempts during the early years of the discovery. Bell himself was aware of the intrinsic optical absorptive dependence of the photoacoustic effect and he correctly deduced that the PA effect is due to the internal heating of the sample by the absorbed radiation energy [9]. But there were several opinions on how the acoustic signal is generated due to this heating. Bell hypothesized that the acoustic signals are generated as a result of periodic expulsion of gases from air spaces or pores within the solid sample due to the alternate expansion and contraction of the sample caused by the periodic heating by the incident radiation. In the case of a thin membrane or disc type sample, he supported the theory of Lord Raleigh [16], who concluded that the primary source of the PA signal was the thermally induced mechanical vibrations of the disc. Another explanation put forward by Mecardier [17] was that the sound is due to the vibrating movement, determined by the alternate heating and cooling produced by the intermittent radiation, principally in the gaseous layer adhering to the solid surface. A more or less similar kind of explanation was also given by Preece [18].

Experiments performed during the last few years indicate that the primary source of PA signal from a solid sample, as measured by the gas-microphone method, arises from the periodic heat flow from the sample to the surrounding gas with the subsequent change in the gas pressure within the cell. Although Mercardier and Preece were closest to the truth, the two mechanisms invoked by Rayleigh and Bell had also contributed to the explanations at various proportions.

The present understanding of the PA effect in solids is based on modern theories developed during the seventies. The first attempt to develop an exact theory of PA effect in solids was carried out by Parker [19] in order to give a quantitative explanation for the PA signal emanating from cell windows while performing PA measurements on gases. This was followed by the pioneering works of Rosencwaig and co-workers which resulted in enormous uprise of interest in this field. The general theory of photoacoustic effect in solids developed by Rosencwaig and Gersho (R-G theory) [20,21] has been found to be very successful in interpreting most of the experimental observations. The theory shows that in a gas microphone PA cell, the signal depends both on the generation of an acoustic pressure disturbance at the sample-gas interface and on the transport of this pressure disturbance through the gas to the microphone.

The pressure fluctuations at the sample-gas interface are caused by the periodic heat flow from the sample which is governed by thermal diffusion equations. Rosencwaig and Gersho solved the thermal diffusion equations for the sample, the backing material on which the sample is mounted and the gas in the cell, and obtained exact expressions for the periodic temperature at the sample-gas interface. Although the thermal part of the theory has been treated exactly, the acoustic part is treated in an approximate heuristic manner, which is however valid for most experimental conditions. Since R-G theory is extensively used in interpreting the results of the present work, we feel it would be appropriate to present the salient features of the theory in this introductory chapter.

1.3 Theory of Rosencwaig and Gersho (R-G theory)

R-G theory is a one-dimensional analysis of the production of a photoacoustic signal in a simple cylindrical cell as shown in fig.1.1. The cell has a diameter D and length L . It is assumed that the length L is small compared to the wavelength of the acoustic signal and the microphone (not shown in the figure) detects the average pressure in the cell. The solid sample is considered to be in the form of a

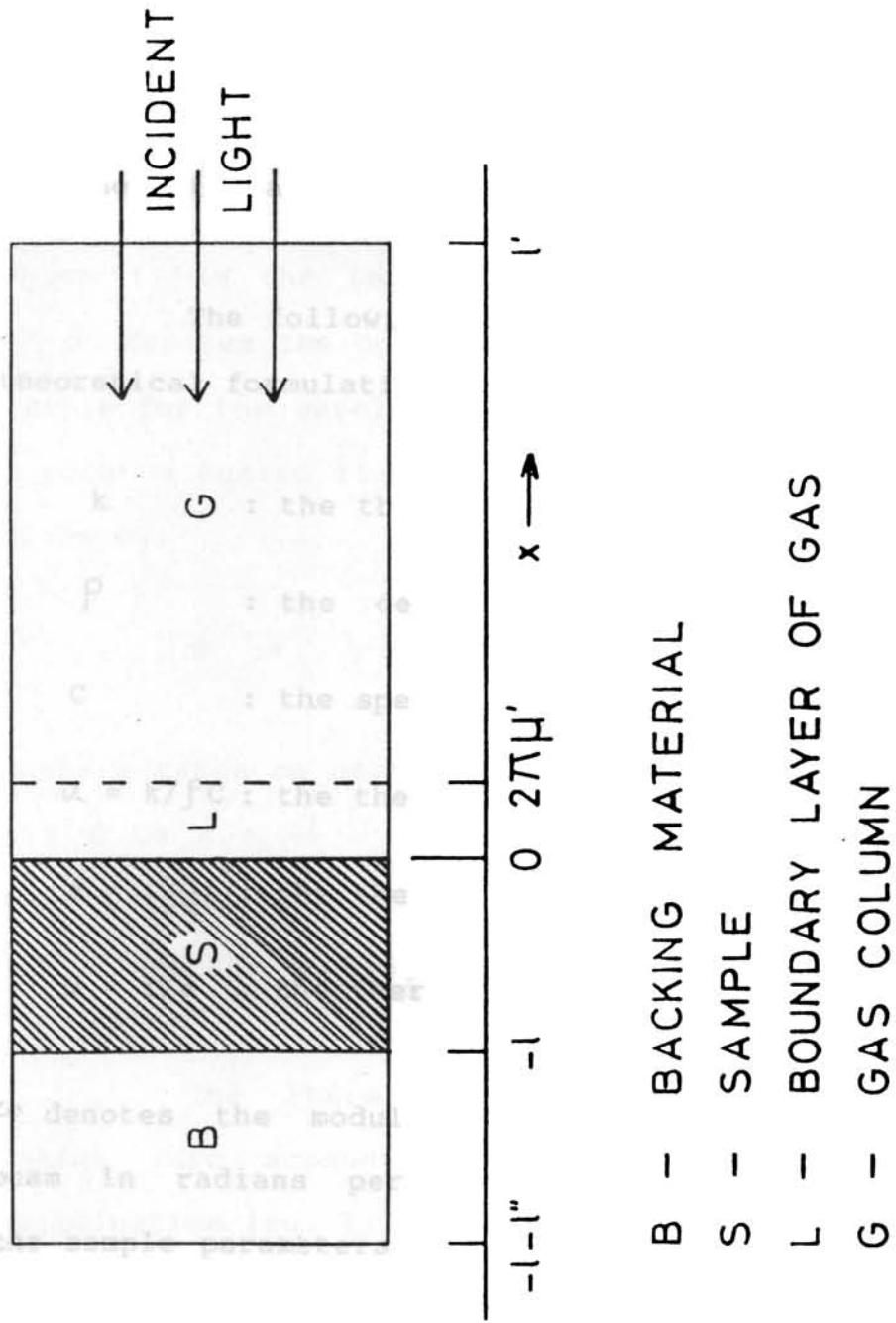


Fig.1.1: Cross sectional view of a simple cylindrical PA cell.

disc having diameter D and length l . The sample is mounted so that its back surface is against a poor thermal conductor of thickness l'' . the length of the gas column in the cell is given by l' . It is also assumed that the gas and the backing material are not absorbers of light.

The following parameters which are important in the theoretical formulation are defined as:

- k : the thermal conductivity ($\text{cal.cm}^{-1}\text{sec}^{-1}\text{.}^{\circ}\text{C}^{-1}$)
- ρ : the density (gm cm^{-3})
- C : the specific heat ($\text{cal.gm}^{-1}\text{.}^{\circ}\text{C}^{-1}$)
- $\alpha = k/\rho C$: the thermal diffusivity ($\text{cm}^2 \text{sec}^{-1}$)
- $a = (\frac{\omega}{2\alpha})^{\frac{1}{2}}$: the thermal diffusion coefficient (cm^{-1})
- $\mu = 1/a$: the thermal diffusion length (cm).

ω denotes the modulation frequency of the incident light beam in radians per second. In the following treatment the sample parameters are represented by unprimed symbols and the gas and backing material parameters by singly primed and doubly primed letters respectively.

The intensity I of a sinusoidally modulated monochromatic beam of light with wavelength λ incident on the sample is given by,

$$I = [\frac{1}{2}] I_0 (1 + \cos \omega t) \quad (1.1)$$

where I_0 is the incident monochromatic light flux (W/cm^2). If β denotes the optical absorption coefficient of the solid sample for the wavelength λ , the heat density H produced at a point x due to light absorbed at this point in the solid is given by,

$$H = \frac{1}{2} \beta I_0 e^{\beta x} (1 + \cos \omega t) \quad (1.2)$$

where x takes on negative values since the solid extends from $x = 0$ to $x = -l$, with the light incident at $x = 0$. Note also from fig.1.1 that the gas column extends from $x = 0$ to $x = l'$ and the backing from $x = -l$ to $x = -(l + l'')$.

The thermal diffusion equation for the sample taking into account the distributed heat source due to illumination (eq. 1.2) can be written as

$$\frac{\partial^2 \theta}{\partial x^2} = \frac{1}{\alpha} \frac{\partial \theta}{\partial t} - A e^{\beta x} (1 + e^{i\omega t})$$

for $-l \leq x \leq 0$ (1.3)

with $A = \frac{\beta I_0 \eta}{2K}$ (1.4)

where θ is the temperature and η is the efficiency with which the absorbed light is converted into heat through non-radiative relaxation process. The value of η is taken as unity in the following treatment; a reasonable assumption for most solids at room temperature. The thermal diffusion equations for the backing material and the gas are respectively given by,

$$\frac{\partial^2 \theta}{\partial x^2} = \frac{1}{\alpha''} \frac{\partial \theta}{\partial t}, \quad -l'' - l \leq x \leq -l \quad (1.5)$$

$$\frac{\partial^2 \theta}{\partial x^2} = \frac{1}{\alpha'} \frac{\partial \theta}{\partial t}, \quad 0 \leq x \leq -l' \quad (1.6)$$

The real part of the complex valued solution $\theta(x,t)$ of equations (1.3) to (1.6) is the solution of physical interest and represents the temperature in the cell relative to ambient, as a function of position and time. To completely specify the solution $\theta(x,t)$ the appropriate boundary conditions are obtained from the requirement of temperature and heat flux continuity at the boundaries $x = 0$ and $x = -l$, and from the constraint that the temperature at the cell walls $x = l'$ and $x = -l - l''$ is at ambient.

The general solution for $\theta(x,t)$ in the cell neglecting transients can be written as,

$$\theta(x,t) = \begin{cases} \frac{1}{l''}(x+l+l'')W_0 + W e^{\sigma''(x+l)} e^{i\omega t}, & -l-l'' \leq x \leq -l \\ b_1 + b_2 x + b_3 e^{\beta x} + (Ue^{\sigma x} + Ve^{-\sigma x} - Ee^{\beta x}) e^{i\omega t}, & -l \leq x \leq 0 \\ (1 - \frac{x}{l'}) F + \theta_0 e^{-\sigma' x} e^{i\omega t}, & 0 \leq x \leq l' \end{cases} \quad (1.7)$$

where W, U, V, E and θ_0 are complex valued constants, b_1, b_2, b_3, W_0 and F are real valued constants, and $\sigma = (1+i)a$. θ_0 and W represent the complex amplitudes of the periodic temperatures at the sample-gas boundary ($x = 0$) and the sample-backing boundary ($x = -l$) respectively. The quantities W_0 and F denote the d.c. components of the temperature at the sample surface $x = 0$ and $x = -l$ respectively. The quantities E and b_3 , determined by the forcing function in eq.(1.3) are given by,

$$b_3 = \frac{-A}{\beta^2} \quad (1.8)$$

$$E = \frac{A}{(\beta^2 - \sigma^2)} = \frac{\beta I_0}{2K(\beta^2 - \sigma^2)} \quad (1.9)$$

The growing exponential components of the solutions to the gas and backing material are omitted in the general solution (eq.1.7) because for all frequencies ω of interest, the

thermal diffusion length is small compared to the length of the material and hence the sinusoidal components of these solutions are sufficiently damped so that they are effectively zero at the cell walls. Therefore, the growing exponential components of the solutions would have coefficients that are essentially zero in order to satisfy the temperature constraint at the cell walls.

By applying the boundary conditions all the constants of eq.(1.7) and hence the d.c. and a.c. components of the solution can be obtained. Then, the explicit solution for θ_o , the complex amplitude of the periodic temperature at the solid-gas boundary ($x = 0$) is given by,

$$\theta_o = \frac{\beta I_o}{2K(\beta^2 - \sigma^2)} \left[\frac{(r-1)(b+1)e^{\sigma l} - (r+1)(b-1)e^{-\sigma l} + 2(b-r)e^{-\beta l}}{(g+1)(b+1)e^{\sigma l} - (g-1)(b-1)e^{-\sigma l}} \right] \quad (1.10)$$

$$\text{where } b = \frac{K'' a''}{Ka} \quad (1.11)$$

$$g = \frac{K' a'}{Ka} \quad (1.12)$$

$$\text{and } \gamma = (1-i) \frac{\beta}{2a} \quad (1.13)$$

The periodic temperature variation at the sample surface as governed by eq.(1.10) causes thermal waves to diffuse into

the gas. This periodic diffusion process produces a periodic temperature variation in the gas as given by the a.c. component of the solution (1.7).

$$\theta_{ac}(x,t) = \theta_o e^{-\sigma' x} e^{i\omega t} \quad (1.14)$$

The time dependent component of the temperature in the gas (eq.1.14) attenuates rapidly to zero with increasing distance from the surface of the solid. The periodic temperature variation in the gas is effectively fully damped out at a distance of $2\pi/a' = 2\pi\mu'$ where μ' is the thermal diffusion length of the gas. It can be assumed to a good approximation that only this boundary layer of gas as shown in fig.1.1 whose thickness is $2\pi\mu'$ is capable of responding thermally to the periodic temperature at the surface of the sample.

The spatially averaged temperature of this boundary layer of gas as a function of time can be determined as,

$$\bar{\theta}(t) = \frac{1}{2\pi\mu'} \int_0^{2\pi\mu'} \theta_{ac}(x,t) dx \quad (1.15)$$

Substituting θ_{ac} from (1.14) and using the approximation $e^{-2\pi} \ll 1$,

$$\bar{\theta}(t) \approx \frac{1}{2\sqrt{2}\pi} \theta_o e^{i(\omega t - \pi/4)} \quad (1.16)$$

Because of the periodic heating, this boundary layer of gas expands and contracts periodically and thus can be thought of as acting as an acoustic piston on the rest of the gas column, producing an acoustic signal that travels through the entire gas column. The displacement of this gas piston due to the periodic heating can be estimated by the ideal gas law as,

$$dx(t) = 2\pi\mu' \frac{\bar{\theta}(t)}{T_0} = \frac{\theta_0\mu'}{\sqrt{2}T_0} e^{i(\omega t - \pi/4)} \quad (1.17)$$

Assuming that the rest of the gas responds to this acoustic piston adiabatically, the acoustic pressure in the cell due to the displacement of the piston can be obtained from the adiabatic gas law,

$$PV^\gamma = \text{constant}$$

Where P is the pressure, V is the gas volume in the cell and γ is the ratio of specific heats of the gas. Then the incremental pressure is given by,

$$\partial P(t) = \frac{\gamma P_0}{V_0} \partial V = \frac{\gamma P_0}{l'} \partial x(t)$$

where P_0 and V_0 are the ambient pressure and volume respectively, and $-\partial V$ is the incremental volume.

Substituting from (1.17)

$$\begin{aligned} \delta P(t) &= Q e^{i(\omega t - \pi/4)} \\ \text{where } Q &= \frac{\gamma P_o \theta_o}{\sqrt{2} l' a' T_o} \end{aligned} \quad \left. \vphantom{\begin{aligned} \delta P(t) &= Q e^{i(\omega t - \pi/4)} \\ \text{where } Q &= \frac{\gamma P_o \theta_o}{\sqrt{2} l' a' T_o} \end{aligned}} \right\} \quad (1.18)$$

Thus the actual physical pressure variation $\Delta P(t)$ is given by the real part of the $\delta P(t)$ as,

$$\Delta P(t) = Q_1 \cos(\omega t - \pi/4) - Q_2 \sin(\omega t - \pi/4) \quad (1.19)$$

$$\text{or } \Delta P(t) = q \cos(\omega t - \psi - \pi/4) \quad (1.20)$$

where Q_1 and Q_2 are the real and imaginary parts of Q and q and ψ are the amplitude and phase of Q , that is,

$$Q = Q_1 + i Q_2 = q e^{-i\psi} \quad (1.21)$$

Thus Q specifies the complex envelope of the sinusoidal pressure variation, and the explicit formula for Q is obtained by combining (1.10) and (1.18).

$$Q = \frac{\beta I_o \gamma P_o}{2\sqrt{2} T_o K l' a' (\beta^2 - \sigma^2)} \left[\frac{(r-1)(b+1)e^{\sigma l} - (r+1)(b-1)e^{-\sigma l} + 2(b-r)e^{-\beta l}}{(g+1)(b+1)e^{\sigma l} - (g-1)(b-1)e^{-\sigma l}} \right] \quad (1.22)$$

Equation (1.22) gives the amplitude and phase of the acoustic pressure wave generated in the cell by photoacoustic effect.

Special Cases

The complexity and the consequent difficulty in the interpretation of eq.(1.22) can be reduced by examining the following special cases. The special cases are determined by the relative magnitudes of the optical absorption length $l_{\beta} = \frac{1}{\beta}$, the thermal diffusion length μ and the thickness l of the sample respectively. For all cases it is assumed that $g < b$ and $b \sim 1$. Also it is convenient to define

$$Y = \frac{\gamma P_o I_o}{2 \sqrt{2} T_o l'} \quad (1.23)$$

which always appears as a constant factor in the expression for Q .

Case 1: Optically Transparent Solids ($l_{\beta} > l$)

In this case the light is absorbed throughout the length of the sample and some light is transmitted through the sample.

Case 1(a): Thermally Thin Solids ($\mu \gg l$; $\mu > l_{\beta}$)

Here using the approximations $e^{-\beta l} \approx 1 - \beta l$,

$e^{\pm\sigma l} \approx 1$ and $|r| > 1$ in eq.(1.22), the expression for Q is obtained as

$$\begin{aligned} Q &= \frac{Y}{2a'a''K''} (\beta - 2ab - i\beta) \\ &= \frac{(1-i)\beta l}{2a'} \left(\frac{\mu''}{K''}\right) Y \end{aligned} \quad (1.24)$$

Equation (1.24) shows that in this case the acoustic signal is proportional to βl and since $\frac{\mu''}{a'}$ is proportional to $\frac{1}{\omega}$, the acoustic signal has an ω^{-1} dependence. Also, for this thermally thin case of $\mu \gg l$, the thermal properties of the backing material come into play in the expression for Q .

Case 1(b): Thermally Thin Solids ($\mu > l$; $\mu < l_\beta$)

Here setting $e^{-\beta l} \approx 1 - \beta l$, $e^{\pm\sigma l} \approx (1 \pm \sigma l)$ and $|r| < 1$ in eq.(1.22) the expression for Q becomes,

$$Q = \frac{\beta l Y}{4K a' a^3 b} [\beta^2 + 2a^2] + i[\beta^2 - 2a^2] \approx \frac{(1-i)\beta l}{2a'} \left(\frac{\mu''}{K''}\right) Y \quad (1.25)$$

Here again the acoustic signal is proportional to βl and varies as ω^{-1} and depends on the thermal properties of the backing material. Equation (1.25) is identical to (1.24).

Case 1(c): Thermally Thick Solids ($\mu < l$; $\mu \ll l_{\beta}$)

Here setting $e^{-\beta l} \approx 1 - \beta l$, $e^{-\sigma l} \approx 0$ and $|r| \ll 1$ in eq.(1.22).

$$Q = \frac{-i \beta \mu}{2a'} \left(\frac{\mu}{K} \right) \gamma \quad (1.26)$$

In this case the acoustic signal is proportional to $\beta \mu$ instead of βl . This means that only the light absorbed within the first thermal diffusion length contributes to the signal eventhough the absorption takes place throughout the thickness of the solid. Also, since $\mu < l$ the thermal properties of the backing material in eq.(1.24) and (1.25) are replaced by those of the solid sample. The signal in this case varies as $\omega^{-3/2}$.

Case 2: Optically Opaque Solids

In this case most of the light is absorbed within a distance that is small compared to l and essentially no light is transmitted.

Case 2(a): Thermally Thin Solids ($\mu \gg l$; $\mu \gg l_{\beta}$)

Using the approximations $e^{-\beta l} \approx 0$, $e^{\pm \sigma l} \approx 1$ and $|r| \gg 1$

$$Q \approx \frac{(1-i)}{2a'} \left(\frac{\mu''}{K''} \right) \gamma \quad (1.27)$$

In this case the acoustic signal is independent of β . It depends on the thermal properties of the backing material and varies as ω^{-1} .

Case 2(b): Thermally Thick Solids ($\mu < l$; $\mu > l_\beta$)

Setting $e^{-\beta l} \approx 0$, $e^{-\sigma l} \approx 0$ and $|r| > 1$ in (1.22),

$$Q = \frac{Y}{2a'aK\beta} (\beta - 2a - i\beta) \approx \frac{(1-i)}{2a'} \left(\frac{\mu}{K}\right) Y \quad (1.28)$$

Equation (1.28) is similar to (1.27) except that the thermal parameters of the backing material are now replaced by those of the sample. Here also, the acoustic signal is independent of β and varies as ω^{-1} .

Case 2(c): Thermally Thick Solids ($\mu \ll l$; $\mu < l_\beta$)

Setting $e^{-\beta l} \approx 0$, $e^{-\sigma l} \approx 0$ and $|r| < 1$ in (1.22),

$$Q = \frac{-i\beta Y}{4a'a^3K} (2a - \beta - i\beta) \approx \frac{i\beta\mu}{2a'} \left(\frac{\mu}{K}\right) Y \quad (1.29)$$

This is a very interesting case because eventhough the sample is optically opaque, it is not photoacoustically opaque as long as $\mu < l_\beta$, that is the acoustic signal is proportional to β . The signal also depends upon the thermal properties of the sample and varies as $\omega^{-3/2}$.

The essence of the R-G theory as summarized in eqs.(1.24) to (1.29) have successfully been verified by several workers [22-25]. Further improvements to the theory have been made later by treating the transport of the acoustic signal in the gas more exactly with Navier-Stokes Equation [26-29].

McDonald and Wetsel [28] extended the theory to include the effect of thermally induced mechanical vibrations of the sample by solving coupled equations for thermal and acoustic waves in both the sample and gas. Although these refinements did not change the basic results of the R-G theory for most experimental conditions, they were able to account for observed deviations from the R-G theory at very low modulation frequencies.

1.4 Applications of the photoacoustic effect

As we have seen earlier, the PA technique incorporates two aspects viz., spectroscopy and calorimetry. Applications of the PA effect therefore correspondingly fall into two classes. The first one is basically a study of the interaction of photons with matter and the second one is the study of thermal and acoustic properties of materials. During the past few years there have been enormous growth for

applications of the PA technique in various branches of science and technology. The range of applications are so wide that any attempt to summarize them would neither be easy nor short. The following paragraphs outline only some of the principal applications of the PA effect.

Spectroscopy is perhaps the most basic and earliest application of the PA effect. One of the principal advantages of PA spectroscopy is that it enables one to obtain spectra similar to the optical absorption spectra of any type of solid or semisolid material, whether it be crystalline, powder, amorphous, smear or gel. Furthermore, it has been found experimentally that good optical absorption data can be obtained with the PA technique on materials that are essentially transparent [30] or completely opaque [5,31] to incident light. PA spectroscopy has already found important applications in research and analysis of inorganic, organic and biological solids and semisolids [4,31-33].

The sensitivity of measurement of optical absorption in weakly absorbing samples has increased to an extent of $\sim 10^{-10} \text{ cm}^{-1}$ [34] with the advent of laser PA systems. Laser PA technique finds extensive applications in overtone spectroscopy, trace analysis and pollution monitoring [35-39].

The PA technique can be used to study insulator, semiconductor and even metallic systems that cannot be readily studied by conventional absorption techniques. In case of insulators, PA spectra give direct information about the optical absorption bands in the material [4]. Both direct and indirect transitions can be detected using PA technique in semiconductors [5,31].

Applications in the spectroscopic regime also include the study of de-excitation processes in materials. The selective sensitivity of the PA technique to non-radiative de-excitation channel can be used to study fluorescence and photosensitivity of materials. If there are only two competing branches, for example, luminescence and heat producing de-excitation, then by PA monitoring of the non-radiative branch, the quantum efficiency of luminescence under various conditions can be deduced [40-43]. PA effect has been effectively utilized for de-excitation studies in rare earth oxides and in doped crystals [44-45]. A combination of conventional fluorescence spectroscopy and PA spectroscopy can provide information about the relative strength of the radiative and non-radiative de-excitation processes in solids.

The PA technique is very useful in the study of photovoltaic de-excitation processes in semiconductors. In such processes part of the incident radiation is converted into electrical energy resulting in a corresponding reduction in the thermal energy produced and hence the PA signal depends upon the energy conversion efficiency of the process. Measurement of photoelectrical generation efficiency of silicon solar cells using PA technique has been reported by Cahen [46]. There are reports on the use of PA method to determine photoconductive quantum efficiency of a thin organic dye film [47], and photocarrier generation quantum efficiency of a Schottky diode [48]. The PA method has been used to investigate laser annealing of semiconductor surfaces, to monitor dopant concentration and diffusion, to study the degree of recrystallisation and to detect possible damage resulting from laser irradiation [49,50]. It has also been used to study recombination processes in semiconductors along with photoconductivity studies [51,52].

One of the direct results of R-G theory is that only the heat generated within a depth of one thermal diffusion length of the sample contributes to the PA signal. Since the thermal diffusion length is a function of chopping frequency, one can have a depth profile analysis of the sample by varying the chopping frequency. Information from deeper regions within

the sample is obtained by lowering the chopping frequency while near surface features can be monitored using sufficiently high frequencies. This unique capability of the PA technique brings some important applications especially in the case of thin films, layered and opaque samples etc. Depth profiling is also important in the study of doped semiconductors, laser windows etc., whose surface absorption properties are different from that of the bulk.

Recently attention has turned to the possibility of using PA effect for imaging applications [53-56]. By scanning the amplitude modulated focussed light beam across the surface of the sample and recording the amplitude and phase of the photoacoustic response, it is possible to construct an image that is characteristic of the optical and thermal properties within a part of the sample. PA images at various depths can be obtained using different chopping frequencies. The PA image is due to the spatial variation in the optical and thermal properties of the material. This form of imaging is becoming increasingly important for subsurface imaging and detecting flaws in samples such as semiconductor chips. The technique of photoacoustic microscopy makes use of the imaging applications of PA effect.

The PA technique finds extensive applications in the investigation of thermal properties of materials. The thermal and acoustic waves generated by optical irradiation can be used to investigate different properties such as thermal diffusivity, sound velocity, flow velocity, thickness of thin films, sub-surface defects and so on. Adams and Kirkbright [57] were the first to use PA technique to obtain thermal diffusivity values of copper and glass by using rear surface illumination. Later several workers [58-63] investigated the use of PA technique for the measurement of thermal parameters in detail and various methods have developed in this area.

The dependence of the PA signal on the thermal properties of the sample has created a great deal of interest in the technique for the investigation of phase transition in solids. Since this application has special relevance in respect of the work presented in this thesis, a detailed account of this topic is given in the next section of this chapter.

PART B: PHOTOACOUSTIC INVESTIGATION OF PHASE TRANSITIONS IN SOLIDS

1.5 Phase transitions in solids

The cross-disciplinary subject of phase transitions is of great interest in the study of condensed matter on

account of its academic as well as technological relevances. This very interesting phenomena is found to occur in a variety of ways in many physical systems. Literature abounds in theoretical and experimental studies of phase transitions in solids and newer kinds of phase transitions in newer systems are constantly reported. Basic features of phase transitions have been discussed by several authors [64,65]. In the following paragraphs a brief outline of the basic ideas regarding phase transitions in solids is presented.

A homogeneous assembly of atoms or molecules, called a phase, is characterized by thermodynamic properties like volume, pressure, temperature and energy. The stability of an isolated phase is determined by whether its energy--more generally, its free energy--is a minimum for the specified thermodynamic conditions. If the phase is present in a local minimum of free energy instead of a unique minimum and is separated by still lower minima (under the same thermodynamic conditions) by energy barriers, the system is said to be in a metastable state. If barriers do not exist, the state of the system becomes unstable and the system moves into a stable or equilibrium state, characterized by the lowest value for free

energy. As the temperature, pressure or any other variable like an electric or magnetic field acting on a system is varied, the free energy of the system changes smoothly and continuously. Whenever such variations are associated with changes in the structural details of the phase (atomic or electronic configuration) a phase transition is said to occur.

During a phase transition, whereas the free energy of the system remains continuous, thermodynamic quantities like entropy, volume, specific heat etc., undergo discontinuous changes. Ehrenfest [66] classified phase transitions depending upon the relation between the thermodynamic quantity undergoing discontinuity and the Gibb's free energy function. According to this scheme, a transition is said to be of the same order as the derivative of the Gibb's function which shows a discontinuous change at the transition. Thus if there is discontinuity in quantities such as volume and entropy which are first order derivatives of the Gibb's function, the transition is said to be of first order, whereas if specific heat, compressibility, thermal expansion etc., are the quantities undergoing discontinuity, which are second order derivatives of Gibb's free energy function, the transition is said to be of second order and so on. However,

several of the known transitions [67,68] do not strictly belong to any of the above classes. There is superposition of second order behaviour in many first order transitions and vice-versa. It is possible that many of the transitions are really of mixed order.

Phase transitions are always associated with configurational changes within the system. Magnetic phase transitions are driven by the alignment of unpaired spins in a specific direction and one usually does not observe any changes in the atomic configuration. On the other hand, several other types of phase transitions like the ferroelectric transitions are generally associated with atomic rearrangements or structural changes. The change of structure at a phase transition in a solid can occur in two distinct ways. Firstly, there are transitions where the atoms of a solid reconstruct a new lattice as in the case of an amorphous solid changing to the crystalline state. Secondly, there are transitions where a regular lattice is distorted slightly without in any way disrupting the linkage of the network. This can occur as a result of small displacements in the lattice position of single atoms or molecular groups, or the ordering of atoms or molecules among various equivalent positions. Most of the ferroelectric phase

transitions belong to the second group. The displacive type transitions are often driven by the freezing out of a vibrational mode called a soft mode. In case of a ferroelectric transition the soft mode is an optical phonon belonging to the centre of the Brillouin zone while in the case of an antiferroelectric transition is a zone boundary phonon. Soft acoustic phonons are found to be associated with ferroelastic transitions.

Since all phase transitions involve configurational changes, one can always identify a physical quantity that is characteristic of the new ordered configuration. Such a concept of an order parameter was introduced by L.Landau [69] in his thermodynamic theory of phase transitions. The order parameter has a non-zero value in the ordered phase below the transition temperature T_c and is zero above T_c . Thus, in a ferroelectric transition the order parameter is the spontaneous polarization while in a ferroelastic transition it is the spontaneous strain. Landau assumed that the Gibb's free energy can be expanded in powers of the order parameter in the vicinity of a phase transition where the value of the order parameter is very small. The results of Landau theory supports Ehrenfest's classification and reveals many basic features of phase transitions.

Phase transitions in solids are often accompanied by interesting changes in their physical properties. Several techniques are employed to investigate phase transitions depending on the nature of the solid and the properties of interest. Such studies are not only of academic value in understanding the structural and mechanistic aspects of phase transitions, but can also be of technological importance. The literature abounds in studies of phase transitions using a wide range of techniques including light scattering, thermal, optical, electrical, magnetic, dielectric, ultrasonic, spectroscopic and other measurements [68,70-74].

1.6 Photoacoustic investigation of phase transitions

Besides several well established methods such as Raman and neutron scattering, NMR, ultrasound studies etc., photoacoustic technique has gained wide interest as a powerful tool for the study of phase transitions in solids recently. The wealth of information contained in the PA signal can be used to investigate the variations in the optical and thermal properties of materials during phase changes. The PA technique offers several advantages such as easiness in sample preparation, the range of samples that can be studied etc.

In phase transition studies, photoacoustics constitutes a complementary technique to the conventional calorimetric methodology. The amplitude of the PA signal is determined primarily by the amplitude of the temperature oscillation at the sample surface which is governed by the thermal diffusivity of the sample given by,

$$\alpha = \frac{K}{\rho C} \quad (1.30)$$

where K , ρ and C are the thermal conductivity, density and specific heat of the sample respectively. The R-G theory predicts different quantitative relations between α and the PA signal depending upon the experimental condition. Thus for the amplitude I_{PA} of the PA signal from a light absorbing, thermally thick sample we have from eq.(1.28),

$$I_{PA} \propto \left(\frac{\mu}{K}\right) \propto K^{-\frac{1}{2}} C^{-\frac{1}{2}} \quad (1.31)$$

In this case we see that the amplitude of the PA signal is inversely proportional to the square roots of thermal conductivity and specific heat. The above equation is for the case where $\mu > l_{\beta}$. For $\mu < l_{\beta}$, eq.(1.29) as well as (1.26) gives,

$$I_{PA} \propto \frac{\mu^2}{K} \propto C^{-1} \quad (1.32)$$

Here the signal amplitude is independent of the thermal conductivity of the sample and varies inversely as the specific heat.

A significant number of solids undergoing interesting phase transitions are transparent crystals. Direct PA monitoring of transitions in such materials is difficult due to the low signal intensity due to weak absorption with ordinary light sources. This difficulty can be overcome by mixing the sample with absorbing centres like fine particles of carbon black. In such cases, the fine particles will be thermally thin and hence the PA signal will be determined by the thermal properties of the sample which acts as the backing material. Thus the experimental condition becomes that of an optically opaque and thermally thin case, and we get from eq.(1.27) that

$$I_{PA} \propto \frac{\mu''}{K''} \propto K^{-\frac{1}{2}} C^{-\frac{1}{2}} \quad (1.33)$$

Here also the PA signal varies inversely as the square roots of the thermal conductivity and specific heat of the sample. In the above discussions only the sample parameters which affect the PA signal are considered.

There have been several reports on the use of photoacoustic technique for the investigation of phase transitions. We summarize below the work already reported in this field. Florian et al. [75] were the first to publish results of measurements of PA effect in the temperature region of first order phase transitions in solids. In their paper, results of measurements of the PA signal at the liquid-solid transition of gallium and of water and the structural phase transition in K_2SnCl_6 were reported. The amplitude and phase angle of the PA signal were recorded as a function of temperature and both were found to undergo anomalous changes during the phase transitions. Qualitative explanations have been given based on the latent heat of the transition and no attempt has been made to explain the results on the basis of R-G theory.

Pichon et al. [76] examined the specific heat anomaly of thermally thick dielectric samples in the neighbourhood of a magnetic phase transition using PA technique. R-G theory has been used to obtain relative values of the specific heat. Results obtained with $CrCl_3$ and MnF_2 are given therein. In case of MnF_2 the observed anomaly is comparable to that obtained using conventional calorimetric measurements. They also have observed that the shift of the PA signal anomaly from T_C is reduced as the laser power is reduced. For 20 mW of incident power the shift is about 1.3 K from the zero power extrapolated value.

By exploring the dependence of the photoacoustic signal on the thermal properties of the sample, Siqueira et al. [77] demonstrated experimentally the usefulness of photoacoustic effect for investigating phase transitions in solids. Their studies have been on aluminium doped VO_2 . The results are in qualitative agreement with R-G theory. They also described the design of the PA cell used for measurements. The complete characterization of the cell is done by a piece of germanium single crystal, the thermal properties of which are well known.

A theoretical model for the PA effect during a first order phase transition has been described by Korpiun and Tilgner [78]. With this model, called the oscillating interface model, they have solved the differential equation of conduction of heat for a medium exhibiting a temperature gradient superposed by a temperature oscillation due to the absorption of light with sinusoidally varying intensity. In the medium there exists two regions of different thermodynamic phases separated by an interface at the transition temperature. The variation of the intensity of light absorbed at the surface leads to an oscillation of the interface that is accompanied by absorption and emission of latent heat in the sample. This periodic storage of heat by

the sample should as well influence the phase angle between the incident chopped light and the oscillation of temperature at the surface that governs the acoustic signal, as the temperature itself detected as the amplitude of the PA signal. The latent heat for phase transitions is taken into account through boundary conditions for the heat flow at the interface. It is assumed that the optical absorption coefficient is much larger than the thermal diffusion coefficient as realized in strongly absorbing materials. The application of their calculation to measured data is discussed with respect to the technique used to detect the acoustic signal.

Bibi and Jenkins [79] have reported observation of a first order phase transition in $\text{CoSiF}_6 \cdot 6\text{H}_2\text{O}$ using photo-acoustic technique. They observed a large change in phase angle through the phase transition point as predicted. However, the large red shift in the absorption characteristics of $\text{CoSiF}_6 \cdot 6\text{H}_2\text{O}$ on traversing the transition from above, with consequent stronger surface absorption below the phase transition, will itself contribute strongly to a change in the phase angle of the signal and makes it difficult to compare the results with theory. In fact, the red shift probably explains why the phase did not recover below the transition as one usually observes.

Korpiun et al. [80] have investigated the temperature dependence of the PA signal at the solid-liquid phase transition of gallium at 302.8 K, the structural phase transition of VO_2 at 340 K and of BaTiO_3 with 0.45% Fe_2O_3 by weight at 393 K. The temperature behaviour of both amplitude and phase are nearly the same while passing through the transition from above as well as from below. Qualitative interpretations are given to the observations based on the newly developed oscillating interface model [78]. In another paper by Korpiun and Tilgner [81] the above model is applied to thermally thin samples and verified in the case of melting of Indium. It is shown that the shift in the phase angle for a thermally thin sample near the transition is negative, whereas for thermally thick samples it is essentially positive.

The PA technique has been applied to the study of a series of phase transitions in Tetramethylammonium tetrachloro cobaltate (TMATC-CO) by Fernandez et al. [82]. A comparison between calorimetric and PA measurements confirms the great potential and accuracy of the PA method in the study of phase transitions in solids. From PA and specific heat data they calculated the thermal conductivity of the material over a wide range, based on R-G theory. The authors also have described a resonant type PA cell which allows PA measurements over a wide temperature range.

A theoretical model which accounts for the variation of PA amplitude and phase at first and second order phase transitions in solids using a piezoelectric detection scheme has been proposed by Etxebarria et al. [83]. This model is based on a previously published one for the study of phase transitions using microphonic detection [78]. Measurements of the PA signal on CsCuCl_3 and $[\text{N}(\text{CH}_3)_4]_2\text{COCl}_4$ have presented. However, for the PA signal amplitude both models provide almost indistinguishable results. The authors point out the necessity of additional theoretical work for a quantitative application of this experimental technique to phase transitions in solids.

Somasundaram et al. [84] have carried out a systematic study of a few typical phase transitions exhibited by different solids. Among the systems studied are (i) NaNO_2 in single crystal as well as polycrystalline powder forms in order to study the influence of particle size on the para-ferroelectric transition (ii) CuO and BaTiO_3 which show second order anti-ferromagnetic and ferroelectric transitions at 290 and 400 K respectively (iii) inorganic nitrates which exhibit first order transitions (iv) Cu_2HgI_4 which is thermo-chromic, and (v) insulator-metal transition in VO_2 and V_3O_5 . They compared the changes in the PA amplitude with the

published data on specific heat or thermal diffusivity. Their study is not only illustrative of the application of the technique but also shows that the relative changes in the PA signal at a phase transition are independent of some of the parameters that effect the PA intensity. The results reported are not entirely in agreement with R-G theory. One needs to take several factors into account in explaining quantitatively the variation of PA amplitude and phase near critical points.

There have been a few reports on the application of PA technique for the investigation of superconducting transitions. Song et al. [85] have measured the temperature dependence of the PA signal intensity near the superconducting transition temperature in the high temperature superconductor $\text{YBa}_2\text{Cu}_3\text{O}_{7-x}$. They observed a small anomaly in the signal amplitude at the temperature which corresponds to the onset temperature of the superconducting transition in resistivity measurements. The anomalous change of the PA signal intensity is attributed mainly to the specific heat jump associated with the superconducting transitions. In another paper by Song and Chung [86] the relative values of specific heat in the temperature region around the high T_c superconducting transition in $\text{GdBa}_2\text{Cu}_3\text{O}_{7-x}$ and $\text{DyBa}_2\text{Cu}_3\text{O}_{7-x}$ samples are

determined from the PA signal amplitude using thermal conductivity data measured by the longitudinal heat flow method. The specific heat values determined by PA technique show good agreement with those obtained by calorimetric methods. The paper also describes photoacoustic measurements on a $\text{KDP}(\text{KH}_2\text{PO}_4)$ sample near the ferroelectric transition in order to confirm the usefulness of the technique for the measurement of specific heat near phase transitions.

The work done by us on photoacoustic investigation of phase transitions in a number of solids is presented in the following chapters.

REFERENCES

1. W.W.Wendlandt & H.G.Hecht, Reflectance Spectroscopy, Wiley, New York (1966).
2. P.A.Wilks, Jr. & T.Hirschfeld, Appl.Spectrosc.Rev. 1, 99 (1968).
3. G.B.Wright (Ed.), Light Scattering in Solids, Springer-Verlag, Berlin and New York (1969).
4. A.Rosencwaig, Opt.Comm. 7, 305 (1973).
5. A.Rosencwaig, Anal.Chem. 47, 592A (1975).
6. A.Rosencwaig, Advances in Electronics and Electron Physics, Vol.46 (L.Marton, Ed.), Academic Press, New York (1978), pp.207-311.
7. A.Rosencwaig, Photoacoustics and Photoacoustic Spectroscopy, Wiley, New York (1980).
8. A.G.Bell, Amer.J.Sci. 20, 305 (1880).
9. A.G.Bell, Phil.Mag. 11, 510 (1881).
10. M.C.Viengerov, Dokl.Akad.Nauk SSR, 19, 687 (1938).

11. A.H.Pfund, *Science* **90**, 326 (1939).
12. K.F.Luft, *Z.Tech.Phys.* **24**, 97 (1943).
13. M.L.Viengerov, *Dokl.Akad.Nauk SSSR* **54**, 182 (1945).
14. G.Gordik, *Dokl.Akad.Nauk SSSR* **54**, 779 (1946).
15. P.V.Slobodskaya, *Izv.Akad.Nauk SSSR, Ser.Fiz.* **12**, 656 (1948).
16. Lord Rayleigh, *Nature* **23**, 506 (1881).
17. M.E.Mercardier & C.R.Hebd, *Serv.Acad.Sci.* **92**, 409 (1881).
18. W.H.Preece, *Proc.R.Soc. (Lond.)* **31**, 506 (1881).
19. J.G.Parker, *Appl.Opt.* **12**, 2974 (1973).
20. A.Rosencwaig & A.Gersho, *Science* **190**, 556 (1975).
21. A.Rosencwaig & A.Gersho, *J.Appl.Phys.* **47**, 64 (1976).
22. M.J.Adams, G.F.Kirkbright & K.R.Menon, *Anal.Chem.* **51**, 508 (1979).
23. J.F.McClelland & R.N.Kniseley, *Appl.Phys.Lett.* **28**, 467 (1976).

24. G.C.Wetsel Jr. & F.A.McDonald, Appl.Phys.Lett. **30**, 252 (1977).
25. E.M.Monahan Jr. & A.W.Nolle, J.Appl.Phys. **48**, 3519 (1977).
26. H.S.Bennett & R.A.Forman, Appl.Opt. **15**, 2405 (1976).
27. L.C.Aamodt, J.C.Murphy & J.G.Parker, J.Appl.Phys. **48**, 927 (1977).
28. F.A.McDonald & Wetsel Jr., J.Appl.Phys. **49**, 2313 (1978).
29. F.A.McDonald, Appl.Opt. **18**, 1363 (1979).
30. A.Hardwik & Schlossberg, Appl.Opt. **16**, 101 (1977).
31. A.Rosencwaig, Phys.Today **28**, 23 (1975).
32. A.Rosencwaig, Science **181**, 657 (1973).
33. A.Rosencwaig & S.S.Hall, Anal.Chem. **47**, 548 (1975).
34. C.K.N.Patel & R.J.Kerl, Appl.Phys.Lett. **30**, 578 (1977).
35. R.G.Bray & M.J.Berry, J.Chem.Phys. **71**, 4909 (1979).
36. G.Stella, J.Getland & W.H.Smith, Chem.Phys.Lett. **39**, 146 (1976).

37. C.K.N.Patel, *Science* **220**, 157 (1978).
38. T.H.Vansteenkiste, F.R.Faxvog & D.M.Roessler, *Appl.Spectrosc.* **35**, 194 (1981).
39. P.C.Claspy, C.Ha & Y.H.Pao, *Appl.Opt.* **16**, 2972 (1977).
40. W.Lahman & H.J.Ludewig, *Chem.Phys.Lett.* **45**, 177 (1977).
41. M.J.Adams, J.G.Highfield & G.F.Kirkbright, *Anal.Chem.* **49**, 1850 (1977).
42. J.C.Murphy & L.C.Aamodt, *J.Appl.Phys.* **48**, 3502 (1977).
43. R.S.Quimby & W.M.Yen, *Opt.Lett.* **3**, 181 (1978).
44. C.D.Merkle & R.C.Powel, *Chem.Phys.Lett.* **46**, 303 (1977).
45. R.G.Peterson & R.C.Powel, *Chem.Phys.Lett.* **53**, 366 (1978).
46. D.Cahen, *Appl.Phys.Lett.* **33**, 810 (1978).
47. A.C.Tam, *Appl.Phys.Lett.* **37**, 978 (1980).
48. W.Thielemann & H.Neumann, *Phys.Stat.Solidi.(a)* **61**, K123 (1980).

49. J.F.McClelland & R.N.Kniseley, *Appl.Phys.Lett.* **35**, 121 (1979).
50. J.F.McClelland & R.N.Kniseley, *Appl.Phys.Lett.* **35**, 585 (1979).
51. V.A.Sablikov & V.B.Sandomirskii, *Sov.Phys.Semicond.* **17**, 50 (1983).
52. A.Mandelis & E.K.M.Sin, *Phys.Rev.B* **34**, 7209 (1986).
Phys.Rev.B **34**, 7222 (1986).
53. G.F.Kirkbright & R.M.Miller, *Analyst* **107**, 798 (1982).
54. A.Rosencwaig & G.Busse, *Appl.Phys.Lett.* **36**, 725 (1980).
55. Y.H.Wong, R.L.Thomas & G.F.Hawkins, *Appl.Phys.Lett.* **32**, 538 (1978).
56. H.K.Wickramasinghe, R.L.Brag, V.Jipson, C.F.Quate & J.R.Salecda, *Appl.Phys.Lett.* **33**, 923 (1978).
57. M.J.Adams & G.F.Kirkbright, *Analyst* **102**, 281 (1977).
58. P.Charpentier, F.Lepoutre & L.Bertrand, *J.Appl.Phys.* **51**, 608 (1982).

59. O.Pessoa, C.L.Cesar, N.A.Patel, H.Vargas, C.C.Ghizoni & L.C.M.Miranda, *J.Appl.Phys.* **59**, 1316 (1986).
60. P.Korpiun, R.Tilgner & D.Schmidt, *J.Phys.(Paris) Colloq.* **44**, C6 (1983).
61. A.Torres-Filho, L.F.Perondi & L.C.M.Miranda, *J.Appl. Polym.Sci.* **35**, 103 (1988).
62. T.Hashimoto, J.Cao & A.Takaku, *Thermochem.Acta*, **120**, 191 (1987).
63. B.Bonno, J.L.Laporte & Y.Rousset, *J.Appl.Phys.* **67**, 2253 (1990).
64. C.N.R.Rao & K.J.Rao, *Phase Transitions in Solids*, McGraw-Hill, New York (1978).
65. H.E.Stanley, *Introduction to Phase Transitions and Critical Phenomena*, Clarendon Press, Oxford (1971).
66. P.Ehrenfest, *Proc.Amsterdam Acad.* **36**, 153 (1943).
67. K.J.Rao & C.N.R.Rao, *J.Materials Sci.* **1**, 238 (1966).

68. C.N.R.Rao & K.J.Rao, Progress in Solid State Chemistry (H.Reiss Ed.), Vol.4, Pergamon Press, Oxford (1967).
69. L.D.Landau & E.M.Lifshitz, Statistical Physics, Pergamon Press, Oxford (1959).
70. C.N.R.Rao & M.Natarajan, Crystal Structure Transformation in Binary Halides, NSRDS-NBS Monograph 41, National Bureau of Standards, Washington, D.C. (1972).
71. C.N.R.Rao & G.V.Subba Rao, Transition Metal Oxides: Crystal Chemistry, Phase Transition and Related Aspects NSRDS-NBS Monograph 49, National Bureau of Standards, Washington, D.C. (1974).
72. C.N.R.Rao & K.P.R.Pisharody, Transition Metal Sulfides, Progress in Solid State Chemistry, Vol.10, Pergamon Press, Oxford (1975).
73. J.B.Goodenough & J.M.Longo, Crystallographic and Magnetic Properties of Perovskite and Perovskite Related Compounds, Landolt-Bornstein, New Series, Group III, Vol.4a, Springer-Verlag, Berlin (1970).

74. K.A.Muller & H.Thomas (Ed.), Structural Phase Transitions I, Springer Verlag, Berlin, Heidelberg, New York (1981).
75. R.Florian, J.Pelzl, M.Rosenberg, H.Vargas & R.Wernhardt, Phys.Status Solidi (a) **48**, K35 (1978).
76. C.Pichon, M.Leliboux, D.Fournier & A.C.Boccara, Appl. Phys.Lett. **35**, 435 (1979).
77. M.A.A.Siqueira, C.C.Ghizoni, J.I.Vargas, E.A.Menezes, H.Vargas & L.C.M.Miranda, J.Appl.Phys. **51**, 1403 (1980).
78. P.Korpiun & R.Tilgner, J.Appl.Phys. **51**, 6115 (1980).
79. I.Bibi & T.E.Jenkins, J.Phys.C. **16**, L57 (1987).
80. P.Korpiun, J.Baumann, B.Luscher, E.Papamokos & R.Tilgner, Phys.Stat.Solidi (a) **58**, K13 (1980).
81. P.Korpiun & R.Tilgner, Phys.Stat.Sol.(a) **67**, 201 (1981).
82. J.Fernandez, J.Etxebarria, M.G.Tello & A.Lopez Echarri, J.Phys.D: Appl.Phys. **16**, 269 (1983).
83. J.Etxebarria, S.Uriarte, J.Fernandez, M.J.Tello & Gomez Cuevan, J.Phys. C **17**, 6601 (1984).

84. T.Somasundaram, P.Ganguly & C.N.R.Rao, J.Phys.C. 19, 2137 (1986).
85. Yang Sup Song, Ho Keun Lee & Nak Sam Chung, J.Appl.Phys. 65, 2568 (1989).
86. Yang Sup Song & Nak Sam Chung, J.Appl.Phys. 67, 935 (1990).

Chapter 2

INSTRUMENTATION

In this chapter we describe the experimental set up used for the present work. After a short general introduction to PA spectrometers, a detailed description of our system, including the design fabrication and characterization of a variable temperature PA cell, is given. This chapter also describes an accurate temperature controller which we designed and fabricated for the present work.

2.1 Photoacoustic spectrometers in general

The basic modules of a PA spectrometer are (i) a radiation source of sufficient intensity and of the wavelength range of interest (ii) intensity or frequency modulator (iii) PA cell in which the sample is placed, which also incorporates the acoustic transducer and (iv) data processing unit. The block diagram of a basic PA spectrometer is shown in fig.2.1. Various modifications of this fundamental instrumentation has been used for a wide variety of PA experiments by different workers.

2.1.1 Radiation source

Incandescent or arc lamps and lasers are two popular types of light sources currently in use for PA

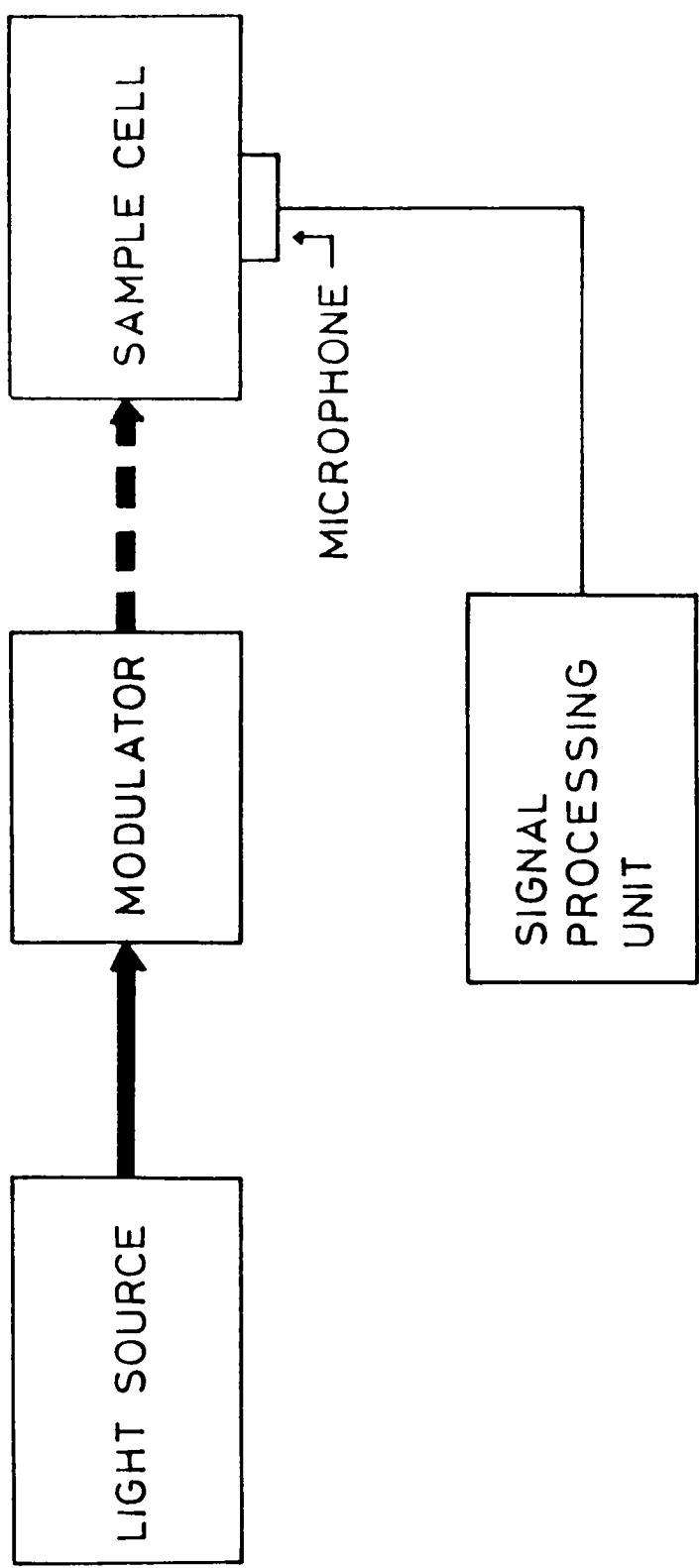


Fig.2.1: Basic set up of a gas - microphone PA spectrometer.

experiments. The lamp-monochromator combination can provide continuous tunability over a wide wavelength range from the infrared to the vacuum ultraviolet. High pressure Xe arc lamps, high pressure Hg lamps, tungsten lamps Nerst glowers etc., are the commonly used incandescent sources. A major drawback of these sources is the relatively low bandwidth throughput product. A monochromator output power of 0.1 mW is typical for 1 nm resolution using a high pressure Xe arc lamp. Consequently, the lamp monochromator combination is used with strongly absorbing samples or where low resolution suffices. Lasers have found wide acceptance as convenient radiation sources in PA spectroscopy owing to their highly collimated beam of high spectral brilliance. The high peak power available from pulsed lasers is especially attractive for measuring very weak absorptions. One main drawback of lasers is their limited tunability.

2.1.2 Modulation

Modulation of the incident light beam is essential for the generation of PA signals. Either the amplitude or frequency of the incident beam can be modulated, amplitude modulation being the more commonly used method. Amplitude modulation can be achieved by one of the several methods such as mechanical, electrical, electro-optic etc. Using a

mechanical chopper is inexpensive, efficient and is the most commonly used method. The depth of modulation in this case is $\sim 100\%$. Care should be taken, while using mechanical chopper, to minimize the vibration noise as this may interfere with the PA signal and cannot be filtered off even by lock-in detection. Output of electric discharge lasers such as CO_2 , CO etc., can be modulated by varying the discharge current. Electro-optic modulation involves changing the plane of polarization of an incoming polarized light beam in a non-linear crystal (such as KDP or ADP) by the application of a modulated electric field across the crystal. Frequency modulation can be employed to eliminate the PA signals generated due to wavelength independent absorption at the cell window. In dye lasers, rapid frequency change can be obtained by using an electro-optic tuner in place of a birefringent filter. Frequency modulation is well suited for narrow linewidth absorbers such as atomic and diatomic species.

2.1.3 The photoacoustic cell

The central part of a PA spectrometer is the PA cell, in which the sample is placed and the PA signal is generated. Proper design of the cell is very important to generate PA signal of detectable amplitude. Some of the major criteria that one should take into account in designing a PA cell are given below.

- i) There should be good acoustic isolation of the cell from the ambient. The cell should be designed with good acoustic seals and with walls of sufficient thickness to form good acoustic barriers. Precautions to isolate the whole PA cell from building vibrations should also be taken.

- ii) To minimize any photoacoustic signal that may arise from the walls and windows of the cell, one should employ windows as transparent as possible in the wavelength range of interest and maintain the interior of the cell highly reflecting. Although the cell walls will absorb some of the incident and scattered light, the resulting PA signal will be quite weak as long as the thermal mass of the walls is very large. One should also design the cell so as to minimize the amount of scattered light that can reach the microphone diaphragm. In addition, all interior surfaces of the cell should be free from any kind of contamination.

- iii) Since the PA signal from a solid sample varies inversely with the volume of the gas inside the cell [1], one should attempt to minimize the volume of the cell. However, care must be taken not to minimize this volume to such a point that the signal suffers appreciable dissipation before reaching the microphone.

The length l' of the gas column between the sample and window should be greater than the thermal diffusion length μ' of the gas at the lowest chopping frequency of interest. It is this layer of gas of thickness μ' at the sample boundary, that acts as an acoustic piston on the rest of the gas column, generating the PA signal [1]. Tam [2] has suggested the optimum gas column length to be $l' \approx 1.8 \mu'$. In determining the passageway dimensions, one should take the thermo-viscous damping into account, since this could be a source of significant signal dissipation at the cell boundaries. Thermo-viscous damping results in a $e^{-\epsilon x}$ damping where ϵ is a damping coefficient given by [3],

$$\epsilon = (1/dv)(\eta_e \omega/2 \rho_0)^{\frac{1}{2}} \quad (2.1)$$

where d is the closest distance between the cell boundaries in the passageway, v is the sound velocity, ω is the frequency, ρ_0 is the density of the gas, and η_e is an effective viscosity which depends both on the ordinary viscosity and the thermal conductivity of the gas. It should be noted that whereas the thermal diffusion length which varies as $\omega^{-\frac{1}{2}}$ is predominant at low frequencies, the thermoviscous damping which varies as $\omega^{\frac{1}{2}}$ is predominant at high frequencies. A cell that is designed to be used over a wide range of frequencies should then have a minimum distance between the

sample and window and minimum passageway dimensions, of the order of 1 - 2 mm [4]. However, how closely one adheres to the above criteria depends on the type of sample to be used, its size and on the type of measurements one wishes to perform (low temperature, high temperature etc.).

Discussions of the operational principles of several different types of PA cells, including resonant and non-resonant cell operations, are given by Rosengreen [5] and Dewey [6]. The most common cell design adopts cylindrical symmetry in which the light beam is centered along the axis. Resonance enhancement of the PA signal is a useful technique to increase sensitivity of PA detection. Several types of acoustic resonance such as longitudinal, azimuthal and radial resonant modes are possible. PA cells with very high quality factor have been constructed [7,8]. Of particular interest is the Helmholtz resonator type configuration [9-11]. In this configuration, the sample and microphone compartments having volumes V_1 and V_2 are connected by a narrow tube of length L and cross-sectional area σ , and the resonance frequency is given by [12],

$$2\pi f = \mathcal{V} \left\{ \frac{[(1/V_1) + (1/V_2)\sigma]}{[L + (\frac{1}{2})(\pi\sigma)^{\frac{1}{2}}]} \right\}^{\frac{1}{2}} \quad (2.2)$$

where \mathcal{V} is the speed of sound. With this configuration,

light scattering from the sample, sample holder and window onto the microphone, causing spurious acoustic signals due to absorption at microphone surface, may be reduced. Also, by using a sufficiently long connecting tube, the sample chamber can be kept at a very high or very low temperature to perform temperature dependent PA studies, with the microphone being kept at room temperature [13,14]. Geometries other than cylindrical symmetry have also been used in PA cell design. Ioli et al. [15] directed the laser radiation transverse to a cylindrical sample cell. This configuration allows the excitation of a lower frequency longitudinal resonance, with simultaneous placement of the microphone along the axis of the PA cell, for a more efficient coupling of the acoustic energy onto a small diaphragm microphone.

The PA cell also incorporates the acoustic transducer, usually a microphone. Both conventional condenser microphones with external biasing and electret microphones with internal self-biasing provided by a charged electret foil, are good ones in use to detect photoacoustic signal.

2.1.4 Signal processing

Since the PA signal is very weak, often several orders of magnitude lower than the ambient noise, special

care must be taken in processing the microphone output signal. The fact that the PA signal has the same frequency as that of modulation enables one to take advantage of the lock-in detection technique [16]. High signal to noise ratios can easily be obtained using a lock-in amplifier. Also, by lock-in detection the amplitude and phase of the PA signal can be measured and by using a dual phase lock-in amplifier the measurements can be made more easily especially when both amplitude and phase vary simultaneously. In cases where a pulsed laser is used as the excitation source, a boxcar averager is used instead of a lock-in amplifier.

In spectroscopy applications one should normalize the PA spectrum with the power spectrum of the radiation source, since the PA signal is proportional to the intensity of the incident beam. The power spectrum of the source can be obtained either by using a conventional power meter or using another reference PA cell with a saturable absorber like carbon black as the sample. While using a reference PA cell, part of the incident modulated beam is allowed to fall into the reference cell using a beam splitter and the signal from the sample cell is divided by that of the reference cell using a ratiometer and the spectrum is directly recorded.

2.2 The experimental set up

In order to carry out temperature dependent studies on different samples, we have developed a photoacoustic set up, block diagram of which is shown in fig.2.2. Different parts of the set up are (i) a 1000 W Xe arc lamp, (ii) a grating monochromator (iii) an electromechanical chopper (iv) a variable temperature PA cell (v) a lock-in amplifier and (vi) a temperature controller.

The light source we have used is a 1000 W high pressure Xe arc lamp (M/s.Spectroscopy Instruments, Model SVX 1000). It has got continuous emission from 280 to 2500 nm with high intensity in the visible region and some intense lines between 800 and 1000 nm. The power of the lamp can be varied between 600 and 1000 W. The intensity of the lamp is found to be highly stable. In situations where a single highly monochromatic source have to be used, the Xe lamp has been replaced by a 5 mW He-Ne laser (Spectra-Physics Model 105-1).

A grating monochromator (Oriel Model 7240) has been used to select the wavelength of the incident radiation. This monochromator can be used over a wide range of wavelengths from 190 nm to 24 μm with appropriate gratings. For

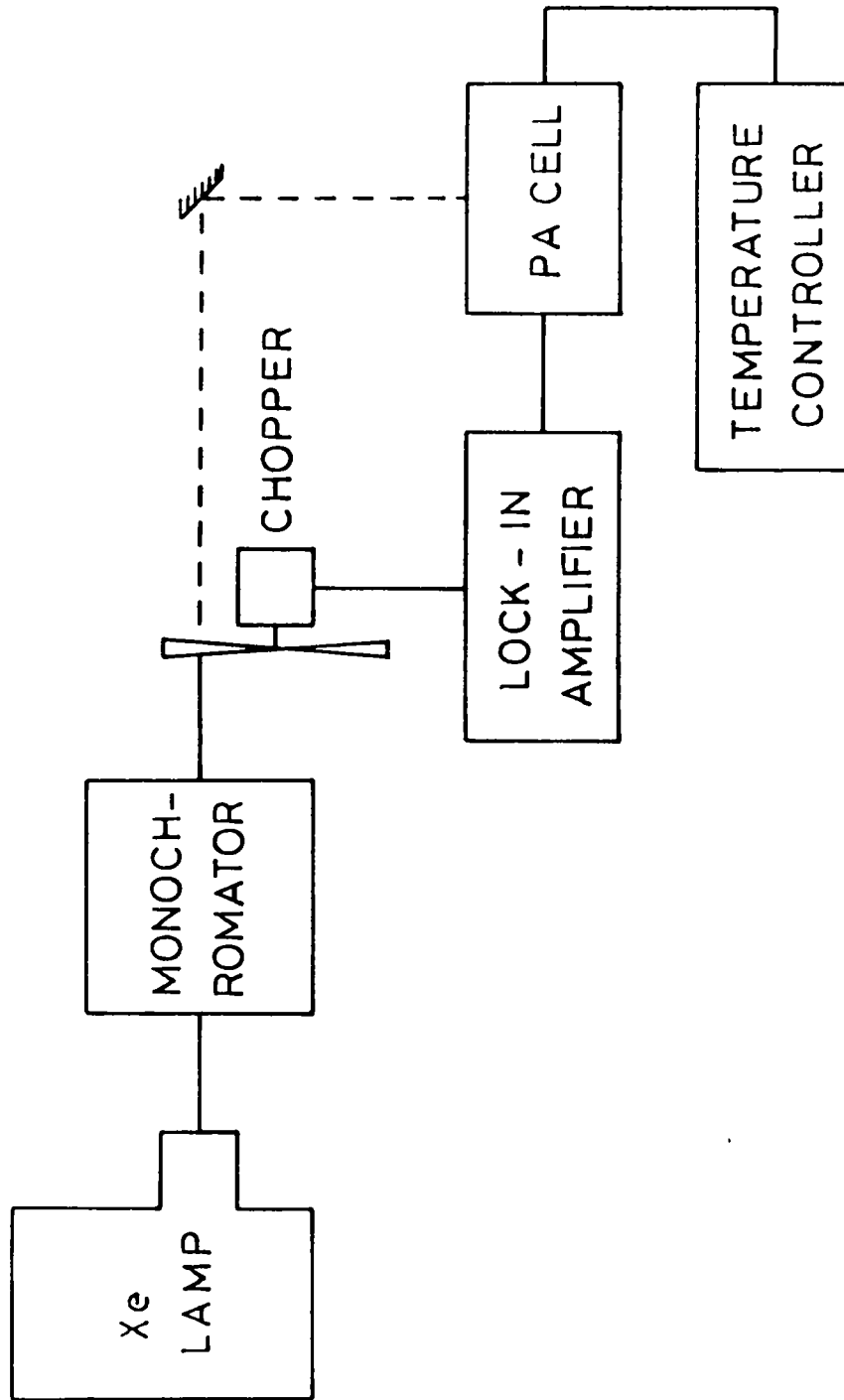


Fig.2.2: Block diagram of the experimental set up.

the present work we have used a grating blazed at 500 nm. A variable slit having adjustable width from 0 to 3.2 mm is used which allows bandwidth of 0.8 to 20 nm in the visible region.

Intensity modulation of the incident light beam is accomplished by an electromechanical chopper (Photon Technology International, Model OC 4000). With the two discs, chopping frequency can be varied continuously from 4 to 4000 Hz. The chopper also provides appropriate reference signal to the lock-in amplifier with excellent phase stability. The chopping frequency is also found to be highly stable.

The PA signal detected by the microphone is processed using a single phase lock-in amplifier (Stanford Research Systems, Model SR 510). The lock-in amplifier has a built in preamplifier providing a full scale sensitivity of 10 nV maximum. It has an operating frequency range from 0.5 Hz to 100 KHz. Phase can be adjusted in large steps of 90° and fine steps of 0.025°.

A detailed description of the other two modules viz., the variable temperature PA cell and the temperature controller are given in the following sections.

2.3 Design, fabrication and characterization of the variable temperature PA cell

A photoacoustic cell which can be used over a wide range of temperature has been designed and fabricated with which measurements can be made from 85 to 450 K. Fig.2.3 shows a schematic diagram of this PA cell. The sample compartment, made out of a brass rod, is in the form of a cold finger, one end of which is in contact with a liquid nitrogen reservoir and is kept inside a vacuum chamber. The liquid nitrogen reservoir, which forms part of the endside wall of the vacuum chamber, has a double walled construction with the vacuum extending throughout the interior of the walls. The sample cell having a volume of $\sim 0.8 \text{ cm}^3$ is sealed with a window against the vacuum outside using an 'O' ring made out of Indium wire. The cell volume can be varied by putting circular buffer metallic discs inside the sample cell. The microphone compartment is integrated with the other endside wall of the outer chamber and is acoustically coupled to the sample cell through a thin walled stainless steel tube of inner diameter 1.6 mm and length 6 cm. The PA cell configuration is thus that of an acoustic Helmholtz resonator [9-11], which for several reasons is an appropriate design for variable temperature PA cells, whether heated [17] or cooled [13]. This configuration permits large

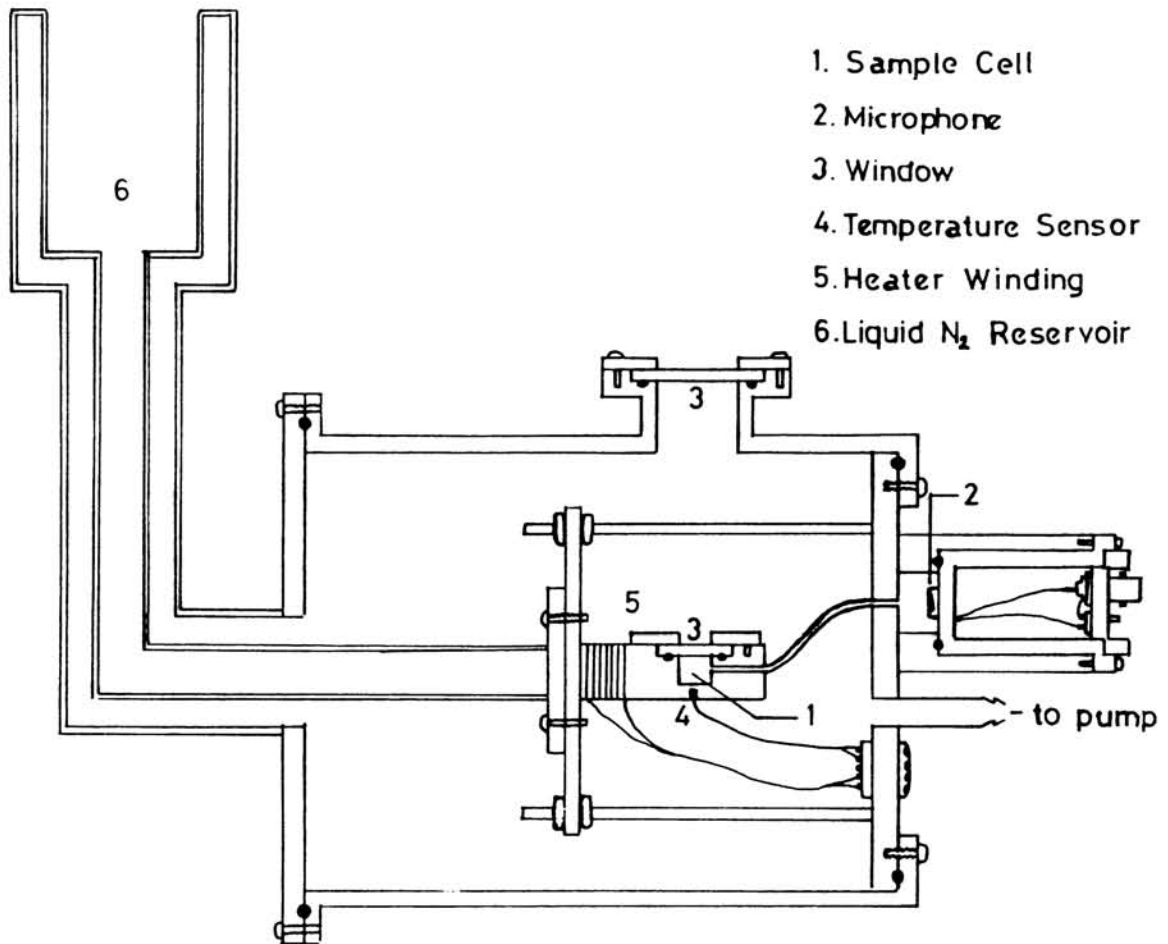


Fig.2.3: Schematic diagram of the variable temperature PA cell.

variations in the sample temperature without altering the microphone temperature appreciably. In order to avoid convection of the gas inside the cell at low temperatures, the microphone chamber is slightly lifted with respect to the sample cell and the corresponding small bend of the connecting tube helps to compensate for thermal contraction. The microphone housing is sealed with a rubber 'O' ring to have good acoustic isolation. The sample temperature is detected by a platinum resistance sensor and can be varied by the heater wound around the cold finger. Both the temperature sensor and heater are connected to a temperature controller.

A small size flat type electret microphone (Knowles, Model BT 1759) is used in the PA cell to pick up the generated acoustic signals. It has got flat frequency response in the range 10 to 5000 Hz, and a high sensitivity of 10 mV/Pascal. The microphone has a built-in FET buffer amplifier in order to provide proper impedance matching. A 3 V cell to supply bias voltage to the FET, a miniature switch and a BNC connector to take the output are all fitted on the microphone housing.

In order to characterize the performance of the fabricated cell, both the modulation frequency and temperature response of the cell have been studied using a carbon black

sample as the standard. Fig.2.4 shows the log-log plots of the amplitude of the PA signal against the modulation frequency, for two different temperatures. As predicted by the R-G theory [1], the amplitude shows a ω^{-1} dependence at low frequencies away from the resonance. However, the slopes of the straight portion of the curves are slightly different from the theoretical value of unity. Similar observations have been reported by Fernelius [10] and Aamodt et al. [18] who attributed this to three dimensional heat flow in the sample cell. The effect of resonance can be clearly seen on both the curves. The resonance peak of the low temperature curve is slightly shifted towards low frequencies due to the decrease in sound velocity in air at low temperatures. The calculated resonance frequency at room temperature is 340 Hz and the observed peak is at 306 Hz. The difference may be due to the ambiguity in determining the effective volumes in the sample cell and the front region of the microphone. Log-log plots of the phase of the PA signal as a function of the modulation frequency is shown in fig.2.5. The phase is more or less stable with respect to frequency in agreement with R-G theory [1]. However, it is different from the theoretically predicted value of $-\pi/4$ and varies slightly with frequency. This can be attributed to the finite non-radiative de-excitation time and various delay times

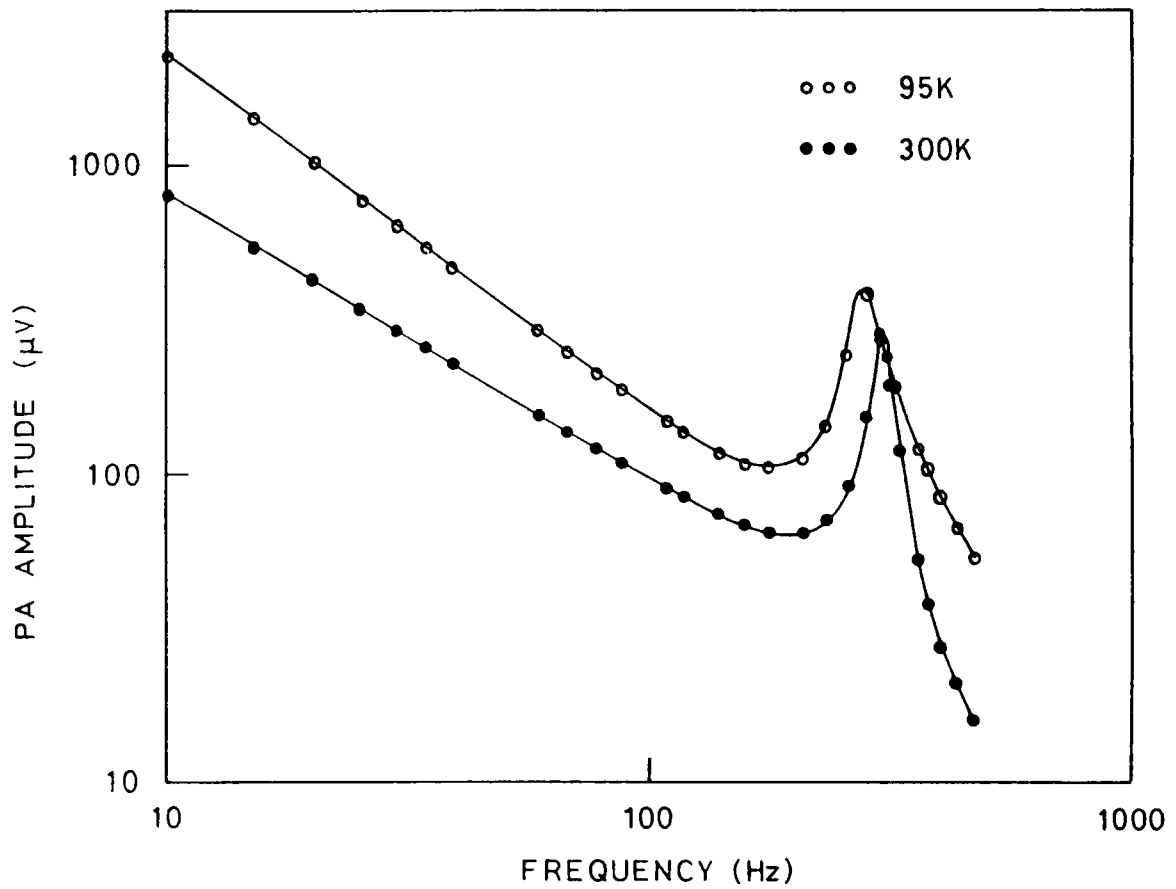


Fig.2.4: Log-log plot of the PA signal amplitude vs chopping frequency of carbon black sample.

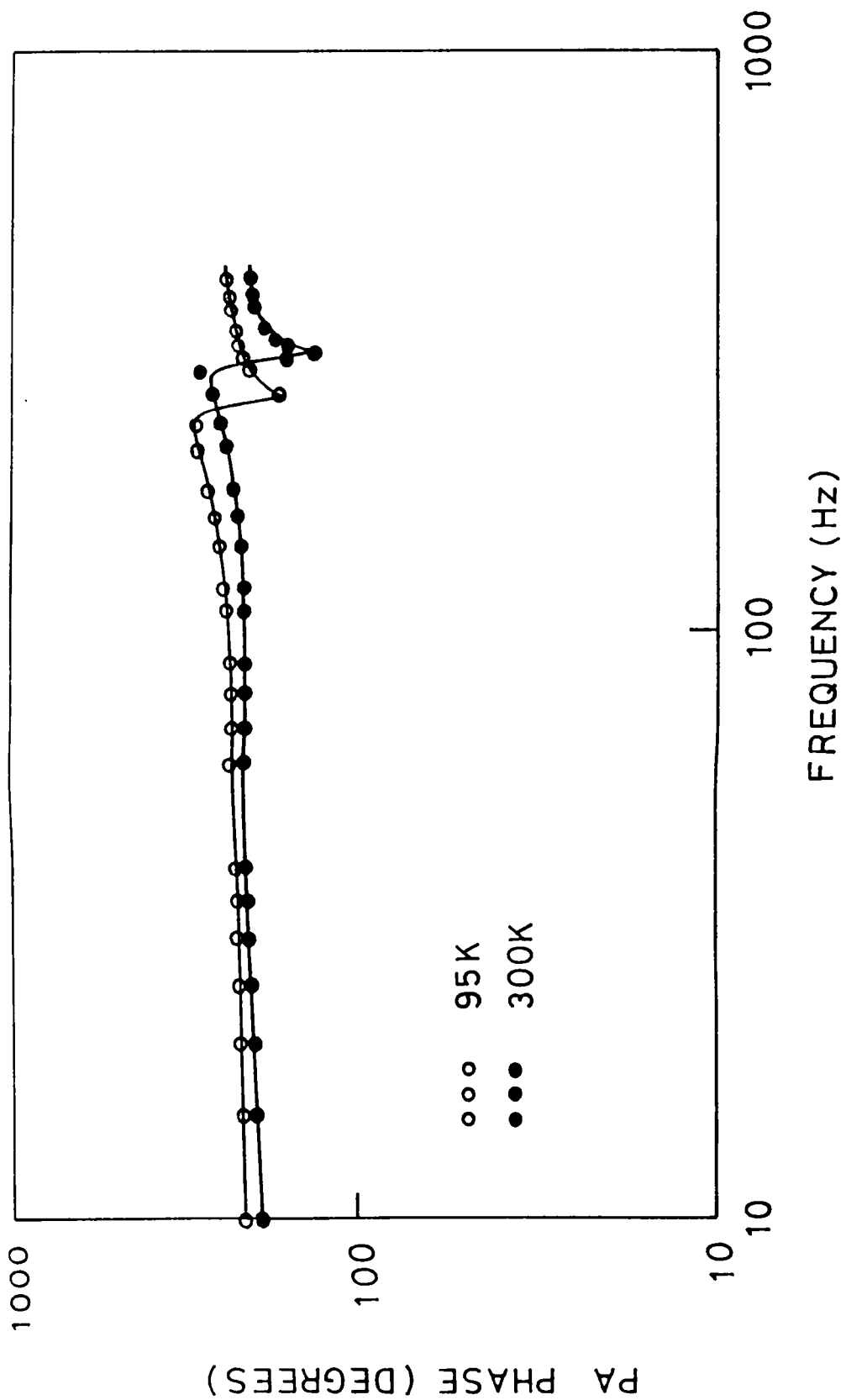


Fig.2.5: Variation of the PA phase with chopping frequency for carbon black sample.

associated with the propagation of sound and the detecting electronics. The large variation in phase at resonance is a true characteristic of the phenomenon.

Variation of the PA signal amplitude as a function of temperature for a thin layer of carbon black coated on an aluminium disc is shown in fig.2.6. At the experimental chopping frequency of 20 Hz, the carbon black layer is thermally thin and hence the amplitude is governed by the thermal properties of the backing material; here aluminium. For such an experimental condition, the R-G theory predicts the amplitude $I_{PA}(T)$ of the PA signal to vary as,

$$I_{PA}(T) \propto F(T) \cdot C(T)^{-\frac{1}{2}} \cdot K(T)^{-\frac{1}{2}} \quad (2.3)$$

where $C(T)$ and $K(T)$ are the specific heat and thermal conductivity of aluminium respectively. The function $F(T)$ takes into account all the temperature dependent properties of the cell, and the gas that affect the PA signal. Therefore, knowing $C(T)$ and $K(T)$, the curve in fig.2.6 can be used to eliminate the function $F(T)$ while performing temperature dependent studies on other samples of unknown thermal parameters. Variation of the PA phase with temperature, is shown in fig.2.7 which again does not follow from R-G theory. The increase in the phase difference can be attributed to the decrease in sound velocity as the temperature decreases.

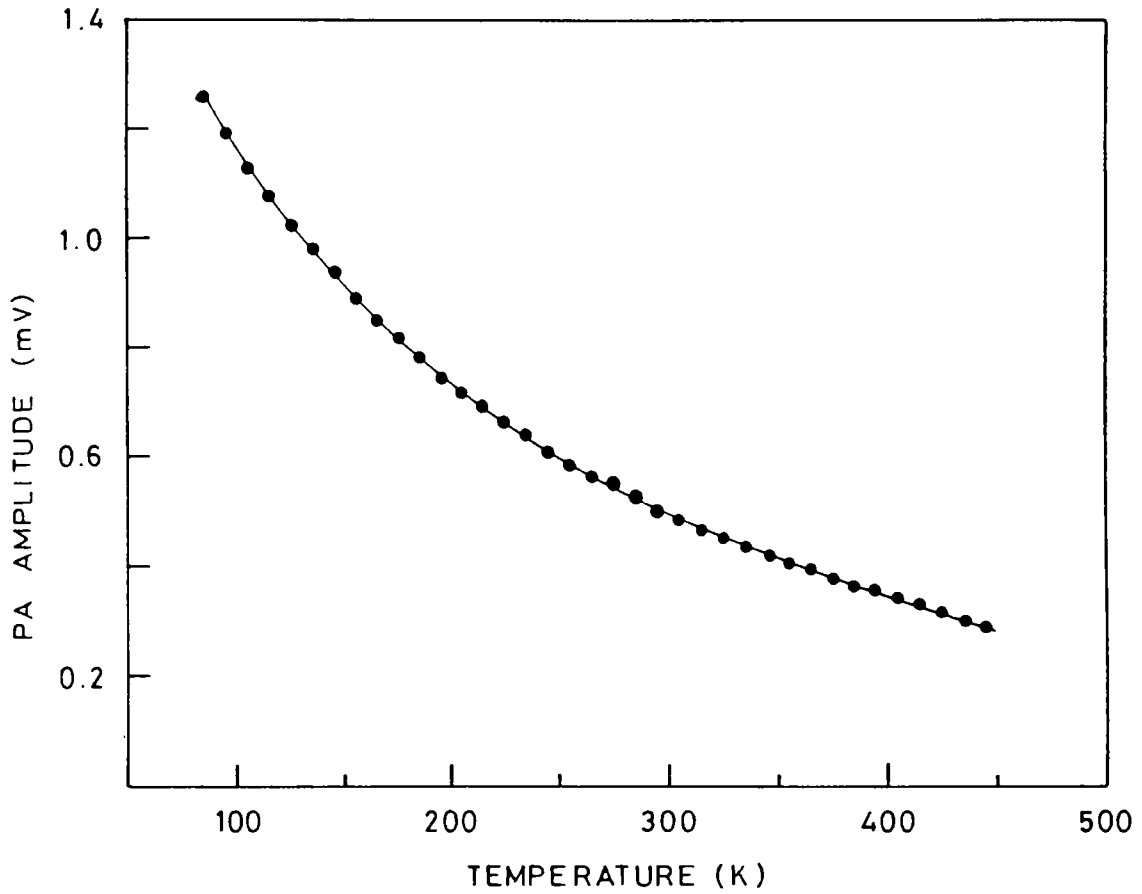


Fig.2.6: Variation of the PA signal amplitude with temperature.

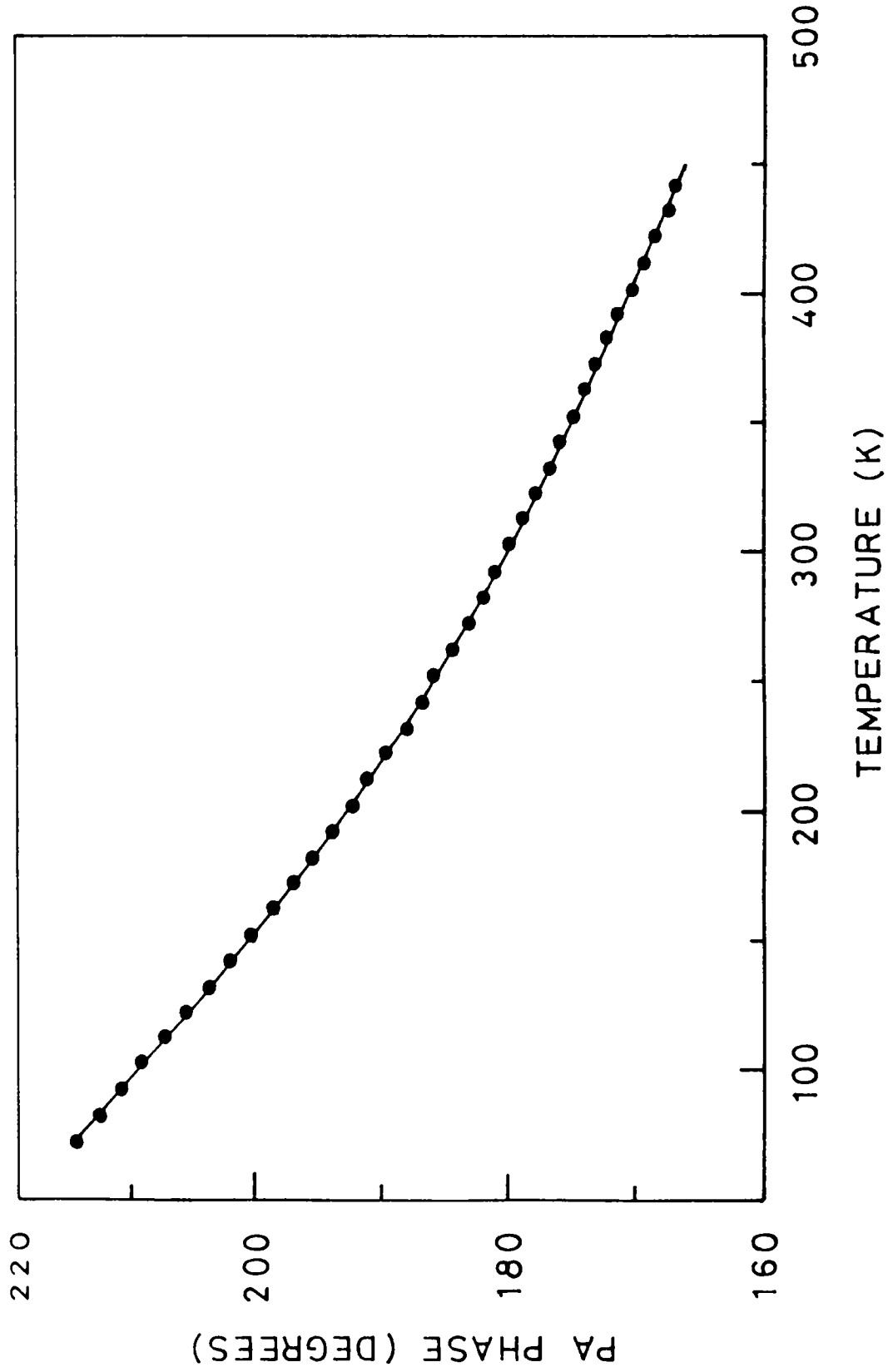


Fig.2.7: Variation of the PA phase with temperature.

2.4 Design and fabrication of a PID temperature controller

Precise control of temperature over a wide range is very important for a variety of experiments in physics and other branches of science and technology. Though it is not very difficult to control the temperature within a few degrees with a simple on-off controller, obtaining a stability of a few millidegrees is not very easy. Temperature controllers having high precision usually employ complex control functions as that of a proportional integral derivative (PID) controller. Several controllers with such complex control and high precision have been described in literature [19-21]. Most of them are designed for operating in a narrow temperature range which makes them unsuitable for many experiments and unacceptable as a general purpose controller.

In designing modern temperature controllers, very sensitive temperature sensors, usually thermistors, are utilized in order to achieve high precision. Thermistors have a large fractional resistance variation per degree variation in temperature, about 20 dB higher than that of a platinum resistor, which makes them attractive in high precision temperature control. But their stability and reproducibility are poor and the large non-linearity restricts their applicability to a small temperature range.

In the following paragraphs we describe the design and working of a precision temperature controller which is capable of maintaining the set temperature constant within $\pm 0.01^{\circ}\text{C}$ anywhere in the range -200°C to $+200^{\circ}\text{C}$. It employs a platinum resistance sensor, a better choice for wide range applications. In spite of the low sensitivity of the sensor, the high precision is achieved by employing stable and sensitive detection and control circuitary using low noise, low drift operational amplifiers now easily available at rather low cost. The sensor is an indigenous one and all the components are available easily.

The present one is a true three mode controller utilizing the proportional, integral and derivative functions. The on-off type controllers have unavoidable overshoots which is a serious drawback for systems having large thermal transfer lag. A proportional mode of control can eliminate the constant oscillations in temperature but its response is very sluggish and introduces a permanent offset in temperature. A finite output power required to maintain the temperature at a steady value is derived only from a finite error and as a result the actual temperature never attains the set value. This offset can be reduced by decreasing the proportional band, but this makes proportional control to

behave almost the same way as an on-off control. Another way to solve this problem is to introduce a control power proportional to the time integral of the error signal. After the proportional control part stops its correcting action, the integral part senses a small error (offset) which is still persisting and continues the correcting action till the error is reduced to zero. The sluggish response of the proportional control can be overcome by adding a third control term which is proportional to the derivative of the error signal, so that the system can follow rapid changes in temperature. Addition of the derivative mode helps to overcome the difficulties associated with the system having long time lag between applying the corrective action and the appearance of the results of that corrective action in the measurement. The working of three mode controllers has been discussed by several authors [23,24] previously.

2.4.1 Circuit description

A simplified description of the present controller is possible with the help of the block diagram shown in fig.2.8. The controller essentially has 9 parts shown as different blocks in fig.2.8. The constant current source, the platinum RTD and the instrumentation amplifier constitute the temperature detection circuitary and direct reading of the measured temperature is possible with the digital panel

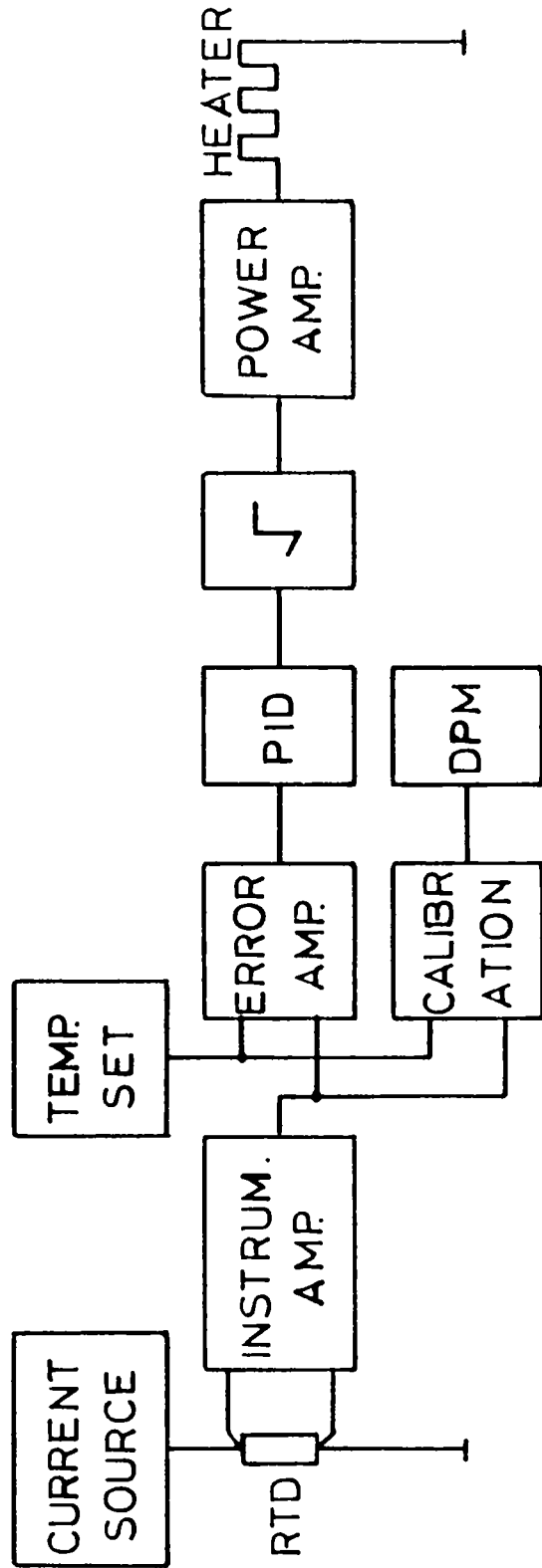


Fig.2.8: Block diagram of the temperature controller.

meter (DPM) after calibration. The error amplifier gives the error signal which is the difference between the set temperature and the actual temperature and it is fed to the PID control network. The PID, consisting of the proportional, integral and derivative functions, derives the control signal from the error signal. The square root converter modifies the control signal before feeding to the power output stage, which is a d.c. amplifier capable of delivering a maximum power of 100 watts to the heater.

The schematic diagram of the controller is given in fig.2.9. The d.c. detection technique employed makes the circuit simple and eliminates troublesome phase adjustments needed in a.c. techniques. Inexpensive integrated circuits are now available with d.c. characteristics that allow performance nearly equal to that attainable with a.c. techniques. Operational amplifier A_1 which forms a stable current source delivers 1 mA excitation current to the platinum resistance sensor (PT 100; Electronics systems and devices) and the voltage developed across it is amplified by the instrumentation amplifier composed of the op amps A_2 and A_3 . This configuration of the instrumentation amplifier has less component count and resistor matching is more easily accomplished because of the lower resistor values. Also the very high input impedance of the amplifier allows to take

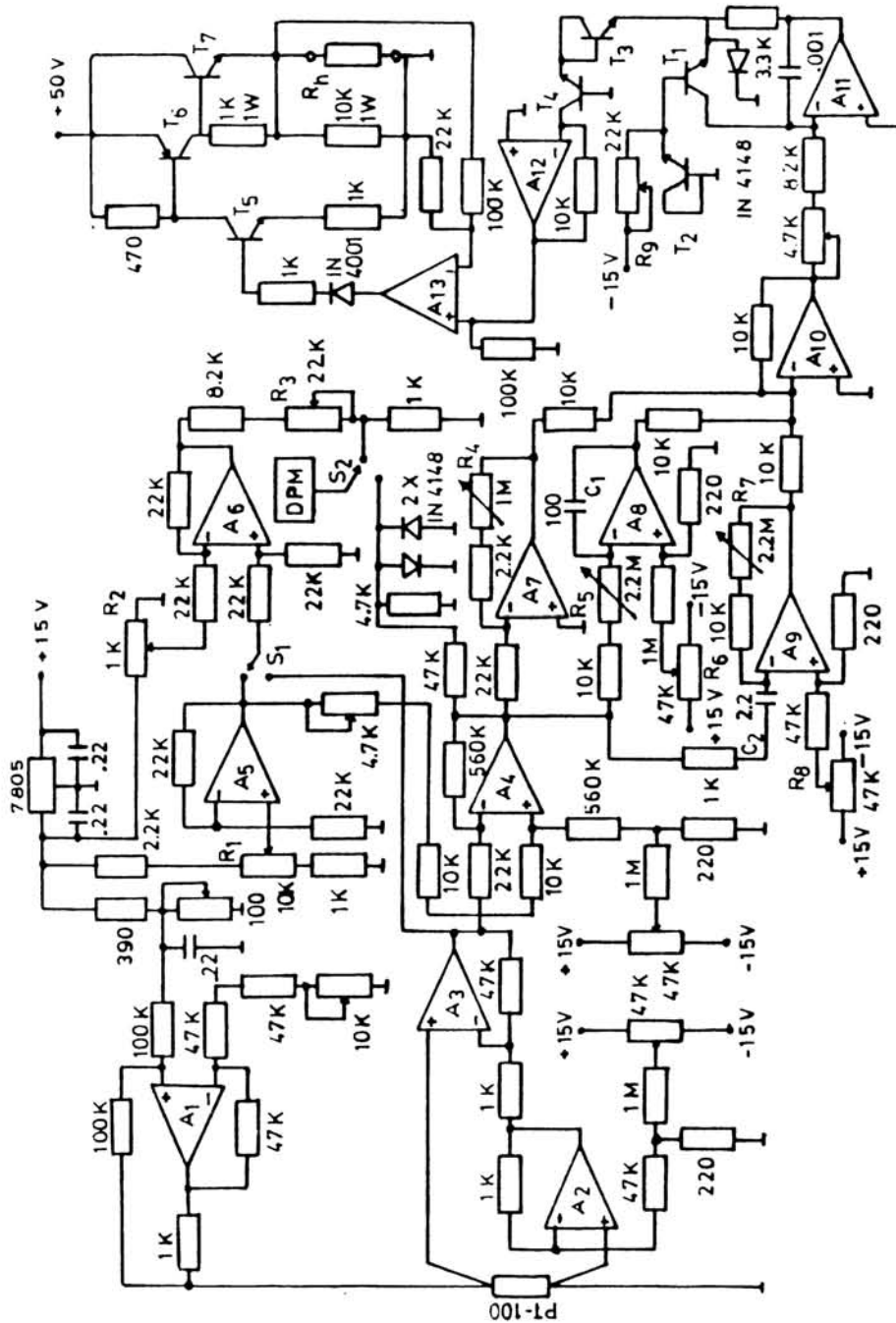


Fig.2.9: Schematic diagram of the temperature controller.
 A₁-A₄, LM725; A₅-A₇ & A₁₀-A₁₃, uA741; A₈-A₉ LF353 JFET input dual op amp
 T₁-T₄, BC108 mounted on a single heat sink. T₅, BD139; T₆, BD140;
 T₇, 2N3055. All resistors are standard metal film resistors 0.25 W, 1%
 except where noted. All capacitances are in microfarads.

advantage of the four-probe detection technique. A_4 is the error amplifier which gives the difference between the amplified sensor voltage and the set point voltage derived from A_5 as output. By adjusting the 10 turn potentiometer R_1 the set point can be selected anywhere in the range -200°C to $+200^\circ\text{C}$ with a resolution of 0.1°C . This configuration has the advantage that one can directly read the set temperature and the actual temperature through the selector switch S_1 with the DPM having $3\frac{1}{2}$ digits. Calibration of the DPM is accomplished with the op amp A_6 and associated network. Potentiometer R_2 is adjusted for reading 0°C and R_3 is adjusted for any other known temperature. Due to the slight non-linearity of the platinum sensor, an exact calibration can be done only externally using conversion tables. The DPM can be used to read either the temperatures or the error signal through the selector switch S_2 .

Op amps A_7 - A_{10} constitute the PID control network. A_7 constitutes the proportional path; its gain is varied from -20 dB to $+40$ dB continuously by R_4 . The A_8 - C_1 circuit is the integrator with integration times from 1s to 220s which can continuously be varied by the potentiometer R_5 . Instead of using an attenuator previous to the integrator to increase the effective time constant [19], we use a large value capacitor because the variation of the output voltage of the

integrator with a large capacitance will be smaller for a given leakage current. Long time constants can be obtained only if capacitor C_1 is of non-electrolytic type and the insulation resistance in the circuit is kept high. Potentiometer R_6 should be adjusted so that the output of the integrator is steady with time when its input is zero. A_9 and associated circuit form the differentiator with time constants continuously variable from 5 ms to 5 s by adjusting R_7 . Potentiometer R_8 should be adjusted for zero output when the input is at zero or a steady voltage.

The proportional, integral and derivative signals are summed by A_{10} and is fed to the square root converter. Taking the square root makes the heater power directly proportional to the control signal. Op amp A_{11} and transistor T_2 form a logarithmic amplifier, transistor T_3 makes the division and A_{12} together with T_4 forms the antilogarithmic amplifier. The output of the square root converter can be expressed by the relation $V_o = (KV_{in})^{\frac{1}{2}}$ where K is a constant. The value of the constant K is set as 10 by adjusting the value of R_9 . This is to make the voltage levels match the voltage of the power amplifier. The power amplifier is composed of the op amp A_{13} and a discrete transistor booster circuit including T_5 - T_7 . The voltage swing capability is increased from 10 V to 50 V by transistors T_5 and T_6 and

transistor T_7 enhances the current capability. The resistance of the heater R_h should be kept greater than 25 ohms in order to limit the output current to 2 A and the power dissipation of T_7 to 25 W. The power amplifier can deliver 100 W to this load if T_7 has an adequate heat sink. Heavy d.c. feedback employed in this circuit ensures high stability and prevent ripple in the +50 V supply from appearing across the heater.

2.4.2 Fabrication of the controller

The complete circuit of the controller excluding the power supply is assembled on two printed circuit boards (PCBs). The main board containing the detection and PID control sections is made by photolithographic method. The square root converter and output power section are assembled on a general purpose PCB. Fig.2.10 shows the diagram of the power supply which is assembled on a separate general purpose PCB. The whole circuit is mounted in an Aluminium chassis. The digital panel meter was supplied by Mecro Instrument Pvt.Ltd. (Type GM-035A). Special care has been taken during the fabrication in determining the positions of different boards and the passage of connecting wires to avoid electrical interferences.

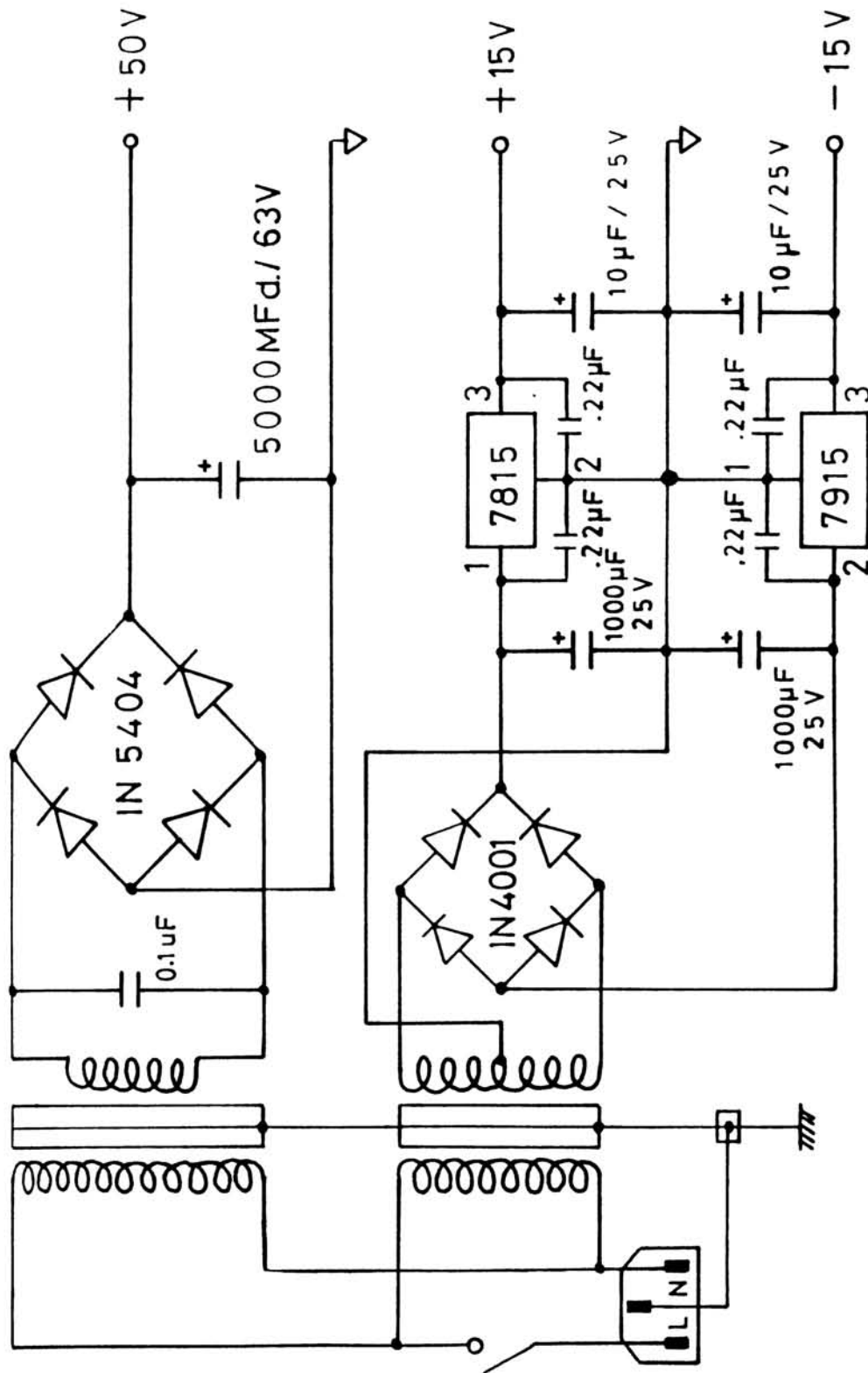


Fig.2.10: Schematic diagram of the power supply.

2.4.3 Performance of the controller

The performance of the controller is ultimately limited by any variations in the circuit that produce a change indistinguishable from a temperature change. These include variations in the value of the standard resistor of the current source, thermal noise in the sensor and input amplifiers and any drift in the offset voltage and common mode rejection ratio of the error amplifier. A rough estimate shows that the temperature error caused by all the above reasons under ordinary conditions is very much less than 0.01°C . The controller is tested with the variable temperature photoacoustic cell at different temperatures and found that it is capable of maintaining the temperature stable within $\pm 0.01^{\circ}\text{C}$ for several hours. The set temperature can be attained within a few seconds if the PID parameters are correctly set. The PID parameters can be determined according to the principles outlined in literature [22,23].

The controller is complete in every respect and can be used as a general purpose controller with any type of thermostats. The controller is designed with cost effectiveness in mind. The sensor and all the components are available indigenously. This is an accurate, precise, low cost temperature controller for the range -200°C to $+200^{\circ}\text{C}$ and is very convenient to be used as a general purpose one for laboratory applications.

REFERENCES

1. A.Rosencwaig & A.Gersho, J.Appl.Phys. **47**, 64 (1976).
2. A.C.Tam, Ultrasensitive Laser Spectroscopy (D.Klinger Ed.), Academic Press, New York (1983).
3. L.E.Kinsler & A.R.Frey, Fundamentals of Acoustics, Chap.9, Wiley, New York (1962).
4. A.Rosencwaig, Rev.Sci.Instrum. **48**, 1133 (1977).
5. L.G.Rosengreen, Appl.Opt. **14**, 1960 (1975).
6. C.F.Dewey, Optoacoustic Spectroscopy and Detection (Y.H.Pao, Ed.), Academic Press, New York (1977).
7. L.D.Thomas III, M.J.Kelley & N.M.Amer, Appl.Phys.Lett. **32**, 736 (1978).
8. E.Nodov, Appl.Opt. **17**, 1110 (1978).
9. N.C.Fernelius & T.W.Hass, Appl.Opt. **17**, 3348 (1978).
10. N.C.Fernelius, Appl.Opt. **18**, 1784 (1979).
11. R.S.Quimby, P.M.Selzer & W.M.Yen, Appl.Opt. **16**, 2630 (1977).

12. Lord Rayleigh, *Theory of Sound*, Vol.2, Dover, New York, (1945), pp.189-192.
13. J.C.Murphy & L.C.Aamodt, *J.Appl.Phys.* **48**, 3502 (1977).
14. P.A.Bechthold, M.Campagna & J.Chatzipetros, *Opt.Commun.* **36**, 369 (1981).
15. N.Ioli, P.Violino & M.Meucci, *J.Phys.E.* **12**, 168 (1979).
16. M.L.Meade, *Lock-in Amplifiers: Principles and Applications*, Peter Peregrinus Ltd., London (1983).
17. P.S.Bechthold, M.Campagna & T.Schober, *Solid State Commun.* **36**, 225 (1980).
18. L.C.Aamodt, J.C.Murphy & J.G.Parker, *J.Appl.Phys.* **48**, 927 (1977).
19. M.A.Handschy, *J.Phys.E: Sci.Instrum.* **13**, 998 (1980).
20. M.Grubic & U.Wurz, *J.Phys.E:Sci.Instrum.* **11**, 692 (1978).
21. D.Sarid & D.S.Cannel, *Rev.Sci.Instrum.* **45**, 1082 (1974).

22. Timothy J. Maloney, *Industrial Solid-State Electronics: Devices & Systems*, Prentice-Hall, New Jersey, 286 (1979).
23. F.M. Forgan, *Cryogenics* **14**, 207 (1974).

Chapter 3

PHOTOACOUSTIC INVESTIGATIONS ON THE HIGH T_c

SUPERCONDUCTOR $YBa_2Cu_3O_{7-x}$

3.1 Introduction to high T_c superconductivity

Vigorous research activity has recently been focussed on the properties of oxygen deficient Perovskite structured ceramics which exhibit superconductivity at remarkably high temperatures. These exotic materials have been the subject of intense research by a large number of scientists from a wide range of fields of basic and applied research. Within a short period of two years, the highest known transition temperature has raised from 23.3 K of the transition metal alloy Nb_3Ge [1,2] to nearly 125 K in Tl-Ca-Ba-Cu-O. The ground work for this extra-ordinary increase in T_c was done by Bednorz and Muller in 1986 [3] who discovered that multiphase mixtures of BaO, LaO and CuO with nominal composition $Ba_xLa_{5-x}Cu_5O_{5(3-y)}$ is superconducting at around 30 K. The superconducting phase was subsequently identified as $La_{2-x}Ba_xCuO_4$ with the highest transition temperature occurring at $x \sim 0.15$ [4]. It was later found that doping with Sr in place of Ba produced higher T_c 's of ~ 36 K [5]. Shortly thereafter another major breakthrough

was achieved when Wu et al. [6] found superconductivity above the boiling point of liquid nitrogen in multi-phase samples with the nominal compositions $Y_{1.2}Ba_{0.3}Cu_2O_{4-x}$ and $Y_{0.6}Ba_{0.4}CuO_{3-x}$. Several groups identified the single phase compound responsible for superconductivity as $YBa_2Cu_3O_{7-x}$ [7-9] with T_c in the 90 K range. Within a short period a number of rare earth based copper oxide ceramics have been synthesized with T_c in the 30 K and 90 K ranges. Superconductivity at temperatures above 100 K has been obtained in Bismuth and Thallium based oxide systems Bi-Ca-Sr-Cu-O ($T_c \approx 110$ K) [10,11] and Tl-Ca-Ba-Cu-O ($T_c \approx 125$ K) [12] in 1988. These systems do not contain any rare earth which were earlier considered essential for the occurrence of high T_c .

A great deal of work has gone into characterizing the superconducting properties of these materials and into the search for new high T_c compounds. In spite of the enormous amount of data taking during the last 3-4 years, many important questions still remain unanswered. In particular, the basic mechanisms that are responsible for superconductivity in these systems at such high temperatures are not yet known. In the conventional superconductors the phonons mediate Cooper pairing of electrons which is evidenced

by isotopes effect and many other properties. The near absence or marginality of isotope effect in these materials, especially in Y-Ba-Cu-O (1:2:3) compound [13-15], is puzzling both to experimentalists and theorists alike. The question that is being asked is whether these are phonon mediated BCS superconductors or not. A number of theoretical models ranging from conventional phonon mediated coupling [16,17] to a variety of exotic mechanisms involving plasmons [18,19], charge transfer excitations [20], polarons and bipolarons [21] and a new electronic ground state [22] have been put forward. Despite all the activities a clear picture of the mechanism of the phenomenon is yet to evolve.

All the high T_c superconducting cuprate systems exhibit certain important common features [23-25] in their properties. All of them possess Perovskite type structures. They all have low dimensional characteristics, the two-dimensional Cu-O sheets being common to them. The 1:2:3 compounds have, in addition, one-dimensional Cu-O chains. They crystallize in orthorhombic or tetragonal structures with the former being more common. The Cu-O bonds are highly covalent and the distances are generally in the $1.90 \pm 0.50 \text{ \AA}$ range. The coordination of Cu is essentially square planar.

	La-(Ca, Sr, Ba)-Cu-O	Y(La)-Ba-Cu-O	Bi-Sr-Ca-Cu-O	Tl-Ca-Ba-Cu-O
T_c	30-40 K	90-100 K	60-110 K	90-125 K
Dimensionality	2 (Cu-O sheets)	2 (Cu-O sheets) +1 (Cu-O chains)	2 (Cu-O sheets)	2 (Cu-O sheets)
Normal state	Marginally metallic	Marginally metallic	Marginally metallic	Marginally metallic
Crystal structure	Orthorhombic	Orthorhombic	Orthorhombic	Tetragonal
Cu-coordination	Square-planar	Square-planar	Square-planar	Square-planar
Short Cu-O distance	1.90	1.90±0.05	1.90	1.93
Oxidation state of Cu as found	1 ⁺ , 2 ⁺	1 ⁺ , 2 ⁺	1 ⁺ , 2 ⁺	1 ⁺ , 2 ⁺

Table 3.1: Salient features of high T_c superconductors.

since these materials superconduct in directions parallel to the copper planes, many theorists believe, this unusual planar arrangement contributes significantly to the remarkable electronic properties of these materials. In table 3.1 a summary of the properties of cuprate superconductors is given.

3.2 Thermal properties of high T_c superconductors

Eventhough there has been frantic experimental activity since the discovery of high T_c superconductors, only relatively few measurements of the thermal properties such as specific heat, thermal conductivity etc., of these materials have been reported. Such measurements are of fundamental importance in understanding many basic features of the phenomenon. For example, specific heat measurements can provide a direct means for verifying BCS and BCS like theories. On the other hand, since heat is conducted both by charge carriers and phonons, a measurement of the thermal conductivity can yield information not only about the spectra of electrons and phonons but also about the interaction between them.

Specific heat measurements are mainly centered around finding solution to two problems. First, to verify

whether at low temperatures there is a contribution to specific heat that varies linearly with temperature. Experimental data on high T_c superconductors indicate that in these materials the electronic specific heat is very small and that existence of a linear term is not certain. Secondly, one can check whether there is a jump in specific heat at T_c and if it exists, to verify whether it is in agreement with the expectations of the BCS theory.

For a conventional superconductor, BCS theory, predicts a jump in specific heat at the transition temperature T_c given by,

$$\Delta C_p = \alpha \Upsilon T_c \quad (3.1)$$

where α is a constant and Υ is the electronic heat capacity coefficient in the normal state. The value of Υ is 1.43 for weak coupling superconductors and can be as large as 2.5 for strong coupling superconductors. In the high T_c superconductors the determination of ΔC_p is hampered due to several reasons. First of all, since the T_c of these materials is high the specific heat jump is only a few per cent of the lattice contribution. Another difficulty is due to the inhomogeneities in the sample which tend to wash out the specific

heat jump. Also, since the fraction of the superconducting phase in the sample is not known with any degree of certainty, it is difficult to deduce ΔC_p for a fully superconducting sample from the measured jump. Finally, since the critical field H_{c2} of these materials is very large, it is almost impossible to drive the material to normal state by the application of a magnetic field to determine from the low temperature specific heat measurements.

Inderhees et al. [26] have reported measurement of the jump in specific heat ΔC_p associated with the superconducting transition in $YBa_2Cu_3O_{7-\delta}$. They found that with decreasing temperature, C_p exhibits a step like increase to a maximum at 90 K corresponding to the completion of the transition. The measured ΔC_p is 6.2 mJ/gm and the ratio $\Delta C_p / \gamma T_c = 1.23$ is close to the value of 1.43 of the weak coupling BCS model. They did not find any critical behaviour (a logarithmic peak in T_c) such as might be expected from a breakdown of the Ginzburg criterion in these materials. Nevitt et al. [27] have measured the specific heat of a single phase sample of $YBa_2Cu_3O_{7-\delta}$ revealing a discontinuity at T_c . Magnetic susceptibility measurements suggest that $\Delta C_p / \gamma T_c$ is close to the weak coupling BCS value of 1.43.

The data of Junod et al. [28] on the specific heat jump in different pellets of $\text{YBa}_2\text{Cu}_3\text{O}_{7-\delta}$ having different densities illustrate the effect of sample quality on the nature of the specific heat jump. Sample which has the highest Meissner fraction of 70% shows the largest jump in $\Delta C_p/T_c = 57 \text{ mJ mole}^{-1}\text{K}^{-2}$. Fossheim et al. [29] who made high resolution specific heat measurements on single crystal of YBCO reports a value of about 30 to 40 $\text{mJ mole}^{-1}\text{K}^{-2}$. There have also been some reports of specific heat measurements on Bi and T based superconductors [30,31]. The behaviour of C_p is similar to that of YBCO system except that the peaks are not as pronounced as in the YBCO system.

All the measurements indicate that a finite jump in specific heat, though very small, is associated with the superconducting transition in all the high T_c materials. There is however no general agreement on the magnitude of ΔC_p which may mainly be due to sample inhomogeneities. It is also not clear whether there is any fluctuation contribution to specific heat around T_c .

It has not yet been answered conclusively whether the electron-phonon interaction produces the high transition temperatures in these materials. In this regard thermal

conductivity measurements are an indispensable tool. The thermal conductivity is a particularly useful transport coefficient in that it can probe scattering processes in both the normal and superconducting states. Thermal conductivity of superconducting materials usually undergoes anomalous changes at the transition point. It either decreases or increases below T_c , depending on the nature of the heat carriers and their interactions. There have been reports of measurements of thermal conductivity of many of the high T_c superconductors such as La-Sr-Cu-O [32], Y-Ba-Cu-O [33-36], Er-Ba-Cu-O [37], Sm-Ba-Cu-O [38], Gd-Ba-Cu-O [39], Bi-Sr-Ca-Cu-O [40,41] and Tl-Ba-Sr-Cu-O [42].

The interpretation of thermal conductivity data on these materials is rendered difficult due to the following reasons:

- i) The normal state electrical resistivity of these materials is of the order of a few milliohm-cm which implies that the phononic contribution may be the dominant mode of heat transport.
- ii) The thermal conductivity of these samples should be anisotropic, but since most of the measurements are made on sintered polycrystalline pellets, one actually measures

the value averaged over all possible orientations of the individual grains. Also the average grain size in different pellets can be different and the grain size and existence of pores can impose serious limitations on the mean free path of phonons at low temperatures.

iii) Oxygen stoichiometry plays an important role on the superconducting properties of these materials. For a given oxygen stoichiometry, the distribution of oxygen atoms do play an important role in defect scattering.

iv) Magnetic excitations which are likely to be present in some of the superconductors can play a part in scattering phonons and even in the transport of heat.

In spite of the complications mentioned above, thermal conductivity measurements on high T_c superconductors have revealed a uniformity in behaviour. In all the high T_c materials the thermal conductivity shows an increase below T_c and exhibits a bump like behaviour at a temperature below T_c . In the case of La-Sr-Cu-O, this effect is very weak and shows only a hint of a small upturn in the thermal conductivity curve close to T_c [32]. This general behaviour is explained on the basis of strong electron-phonon interaction in these materials which causes a reduction in the phonon mean free

path in the normal state. When the material becomes superconducting, the scattering of phonons by electrons are reduced and hence the thermal conductivity increases with decreasing temperature. Ultimately the scattering of phonons by defects, grain boundaries etc., come into play and the conductivity starts decreasing on a further reduction of temperature.

In order to understand the thermal properties of the high T_c superconductors better, we have carried out photoacoustic measurements on YBCO and Bi-Ca-Sr-Cu-O samples. In this chapter the details of the measurements done on YBCO samples and the results obtained are given.

3.3 Preparation and characterization of $\text{YBa}_2\text{Cu}_3\text{O}_7$ samples

The ceramic oxide superconductors are all granular superconductors prepared by sintering the component oxides at high temperatures. Due to their multicomponent nature one usually ends up with a multi-phase bulk containing the required superconducting phase plus other parasitic phases and unreacted oxides. Control of processing conditions during synthesis is very important and has a direct impact on the particle size, stoichiometry, intergrowth of unwanted phases and the stability of the superconducting phase. All these parameters eventually decide the quality of the end

product in terms of basic characteristics like the transition temperature (T_c), critical current density (J_c) and other properties such as Meissner effect and upper critical field.

The following procedure has been adopted for the preparation $YBa_2Cu_3O_7$ samples for the present studies. Appropriate amounts of Y_2O_3 , $BaCO_3$ and CuO (99.9%) are thoroughly mixed and ground with an agate mortar and pestle and the mixture is heated in an alumina crucible at $950^\circ C$ for 24 hours in air. The process is repeated with intermediate grindings and treated in a stream of pure oxygen at $900^\circ C$ for 24 hours. The powder is then cooled to room temperature at a rate of $12^\circ C/hr.$ and is ground again. The powder is then pressed into pellets of 10 mm diameter using a pressure of 20 MPa applied for 10 min. Finally, the pellets are heated to $930^\circ C$ for 24 hrs. in flowing oxygen and slowly cooled to room temperature at the same cooling rate.

In order to characterize the samples electrical resistivity and magnetic susceptibility measurements have been carried out. Fig.3.1 shows the resistivity curve measured using four probe method. The measuring current is kept at 10 mA. The room temperature resistivity is 3.4×10^{-3} ohm cm and decreases almost linearly as the

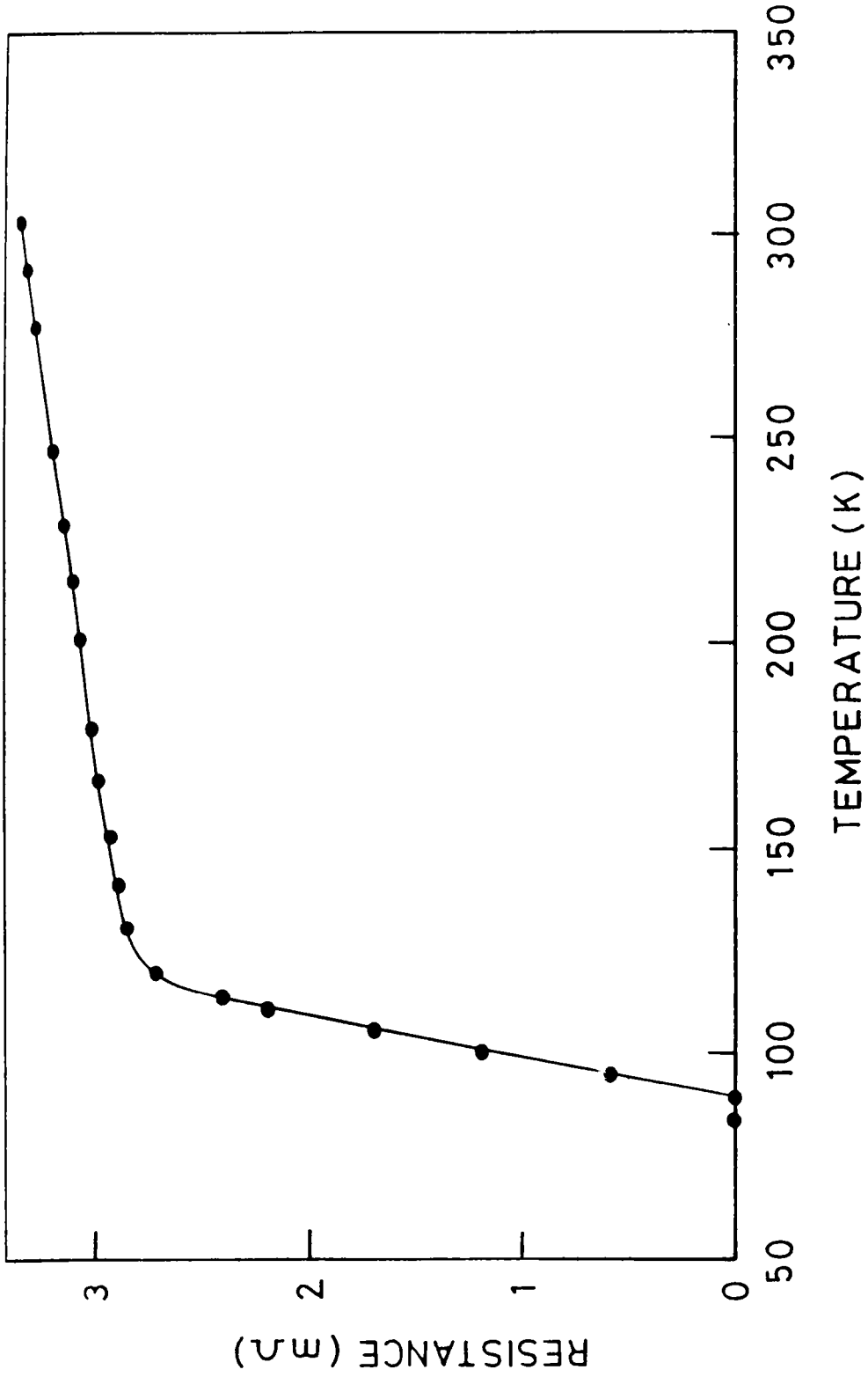


Fig.3.1: Resistance as a function of temperature in $YBa_2Cu_3O_7$.

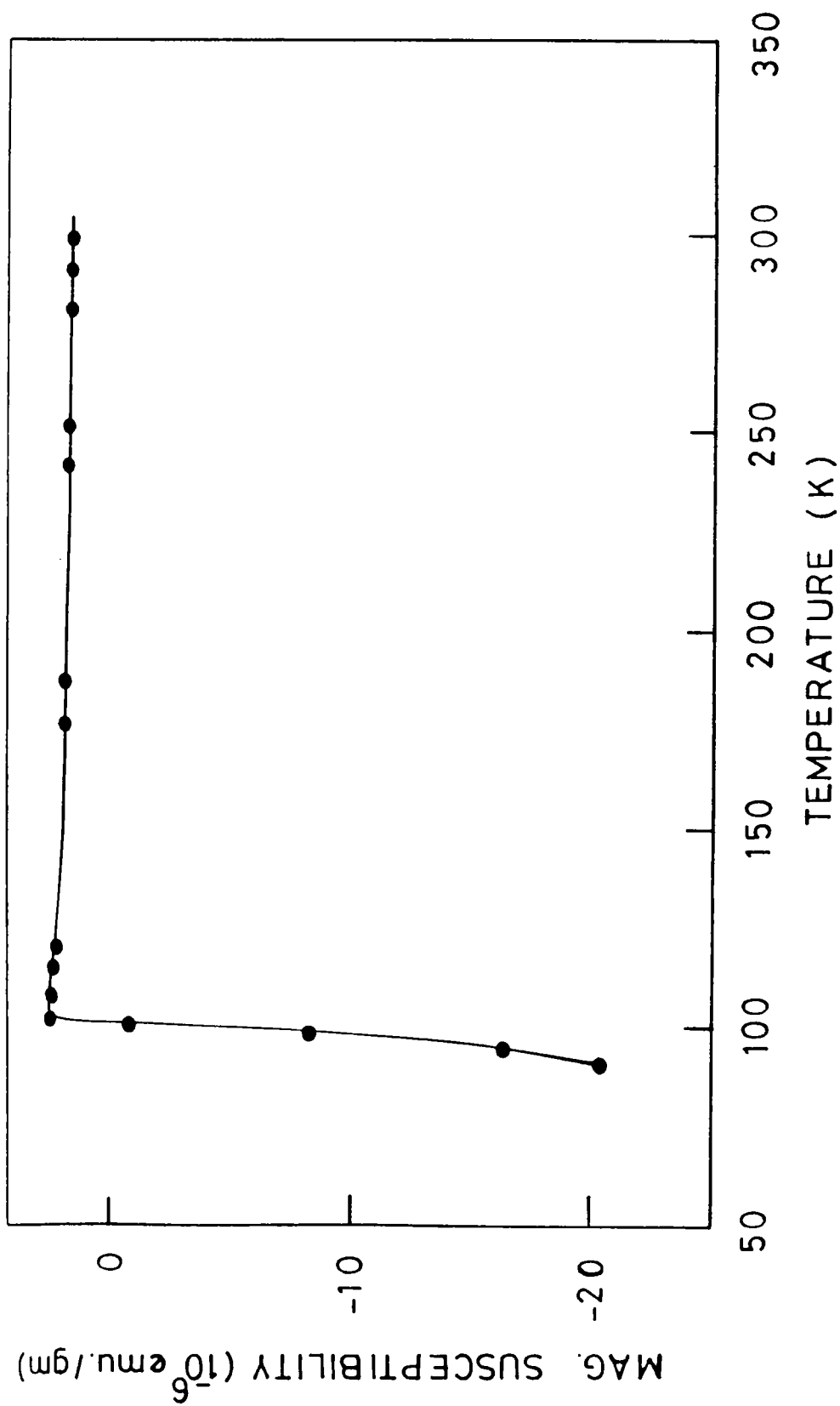


Fig.3.2: Temperature dependence of dc susceptibility in YBa₂Cu₃O₇.

temperature is lowered. The onset of the superconducting transition takes place at ≈ 105 K and the transition is complete at 93 K. In fig.3.2 the d.c. magnetic susceptibility of the sample is plotted against temperature. The curve clearly shows the flux expulsion (Meissner effect) associated with the superconducting transition.

3.4 Photoacoustic measurements on $\text{YBa}_2\text{Cu}_3\text{O}_7$

3.4.1 Amplitude and phase measurements

The amplitude and phase of the PA signal have been measured as a function of temperature on bulk $\text{YBa}_2\text{Cu}_3\text{O}_7$ samples in the range 85-300 K. The experimental set up described in chapter 2 has been used for these measurements. The measurements have been carried out on two superconducting samples (samples I and II) and a non-superconducting sample of the same composition. Sample II has a slightly higher room temperature resistivity, but has almost the same T_c as that of sample I. Pellets having thickness 1 mm and diameter 10 mm have been used for the measurements. The samples are thermally thick at the experimental chopping frequency of 21 Hz. White light with the infrared filtered off is used for optical excitation of the samples. Measurements have been carried out during both heating and cooling cycles. The results are discussed in section 3.5.

3.4.2 Thermal diffusivity measurements

Thermal diffusivity of superconducting $\text{YBa}_2\text{Cu}_3\text{O}_7$ samples have been measured in the temperature range 85–300 K using photoacoustic technique. This has been done by measuring the amplitude of the PA signal as a function of the chopping frequency. One of the parameters which determine the amplitude of the PA signal is the thermal diffusion length μ given by,

$$\mu = [\alpha / \pi f]^{1/2} \quad (3.2)$$

where α is the thermal diffusivity of the sample and f is the chopping frequency. In the thermally thick regime ($\mu < l$ where l is the thickness of the sample) the PA signal is independent of the thermal properties of the backing material on which the sample is mounted, whereas in the thermally thin regime ($\mu > l$) the PA signal gets modified by the thermal properties of the backing material as well. For an appropriate sample thickness, one can obtain a crossover from the thermally thin regime to the thermally thick regime by increasing the chopping frequency. The amplitude versus chopping frequency plot hence shows a change in slope at the characteristic frequency f_c at which the crossover takes place. The characteristic frequency f_c is related to the thermal diffusivity of the sample as follows.

The Rosencwaig and Gersho theory shows that the complex expression for the pressure variations Q inside a photoacoustic cell can be written as,

$$Q = q e^{-i\psi} \quad (3.3)$$

where q is the amplitude of the PA signal and ψ is the phase shift between Q and the excitation. Eq.(3.3) can be written as the product of two terms A and B such that A depends on the modulation frequency f , and B is independent of f as given by,

$$B = \frac{P_o \gamma W_a l^2 \sqrt{\alpha'}}{2 l' T_o K \sqrt{\alpha}} \quad (3.4)$$

$$\text{and } A = \left(1 + g \frac{d^+ + d^-}{d^+ - d^-} \right)^{-1} \left(\frac{d^+ + d^-}{d^+ - d^-} + g \right) \frac{1}{(\sigma l)^2} \quad (3.5)$$

$$\text{where } d^+ = e^{(\sigma l)}$$

$$d^- = e^{-(\sigma l)}$$

$$\sigma = (1+i) \sqrt{\pi f / \alpha} \quad (3.6)$$

and g , the ratio between the effusivities of the backing material (e'') and the sample (e), is given by,

$$g = \frac{e''}{e} = \frac{K''}{K} \frac{\sqrt{\alpha}}{\sqrt{\alpha''}} \quad (3.7)$$

In the above expressions, l , K and α are the thickness, thermal conductivity and thermal diffusivity respectively. Unprimed quantities refer to sample parameters, singly primed quantities refer to gas parameters and doubly primed ones to the backing material. T_0 and P_0 are the static temperature and pressure of the gas respectively. γ is the ratio of specific heats of the gas and W_a is the absorbed light. The effusivity of the gas in the cell is neglected compared to the effusivity of the sample. The term A depends on the modulation frequency through the product σl which can be written as,

$$\sigma l = (1+i) \sqrt{\pi f / \bar{f}_c} \quad (3.8)$$

where the characteristic frequency f_c is defined by,

$$f_c = \alpha / l^2 \quad (3.9)$$

Charpentier et al. [43] have demonstrated the dependence of A on the modulation frequency for different values of g . When $f > f_c$, the variation of A is independent of α and A decreases as f^{-1} . When $f < f_c$ the variation of A depends both on α and the ratio of effusivities, g . Thus it is possible to determine f_c by measuring the amplitude of the

PA signal as a function of f . However, if $g = 1$, (same effusivity for sample and backing) the variation of the amplitude is the same for all frequencies and the determination of f_c becomes impossible. Once f_c is determined, thermal diffusivity can be obtained from eq.(3.9) as,

$$\alpha = f_c l^2 \quad (3.10)$$

Pellets of $\text{YBa}_2\text{Cu}_3\text{O}_7$ samples have been thinned down to approximately 0.2 mm by hand lapping and polishing of both faces to avoid surface effects if any. A thick aluminium disc has been used as the backing material on which the sample is mounted using silver epoxy to ensure good thermal contact between the sample and the backing material. The temperature of the sample is kept constant within $\pm 0.5^\circ\text{C}$ during measurements. Thermal diffusivity is determined at various temperatures by measuring the amplitude of the PA signal as a function of the chopping frequency and determining f_c at each temperature.

3.5 Results and discussion

Fig.3.3 shows the measured photoacoustic phase change relative to the room temperature value as a function of temperature in sample I. Results are shown only in the

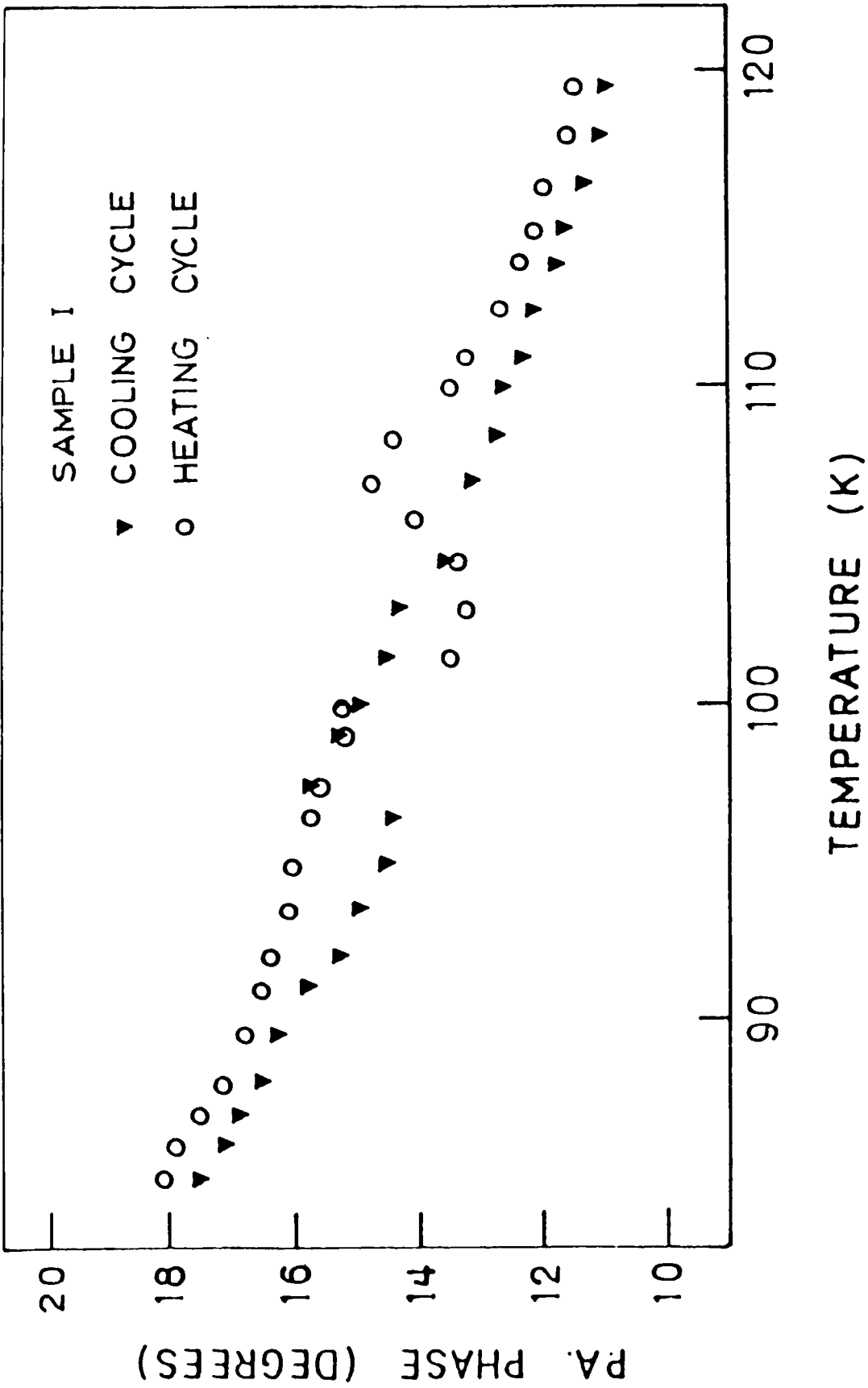


Fig.3.3: Temperature variation of the photoacoustic phase in $\text{YBa}_2\text{Cu}_3\text{O}_7$. (sample I) between 85 K and 120 K.

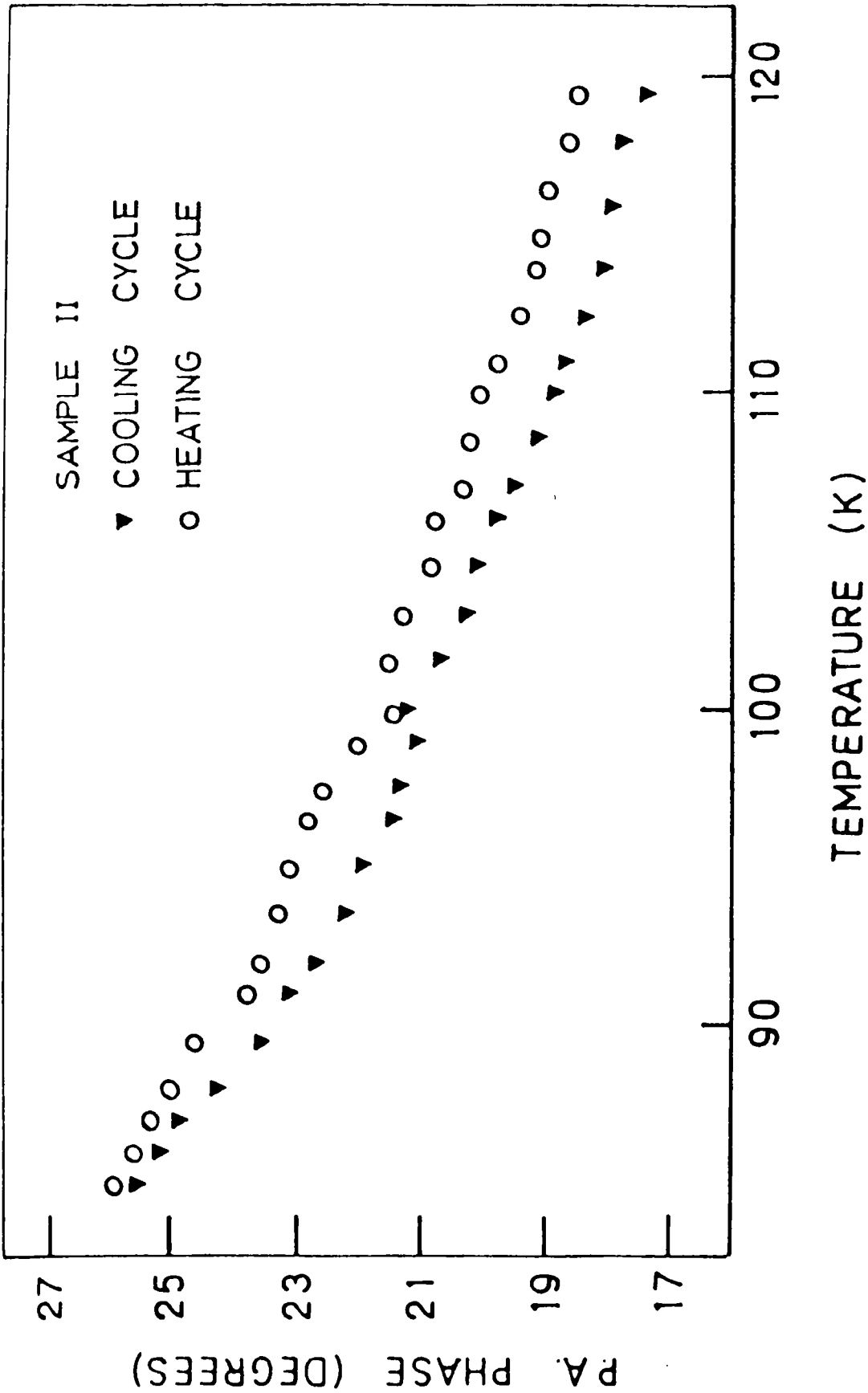


Fig.3.4: Temperature variation of the photoacoustic phase in $\text{YBa}_2\text{Cu}_3\text{O}_7$. (sample II) between 85 K and 120 K.

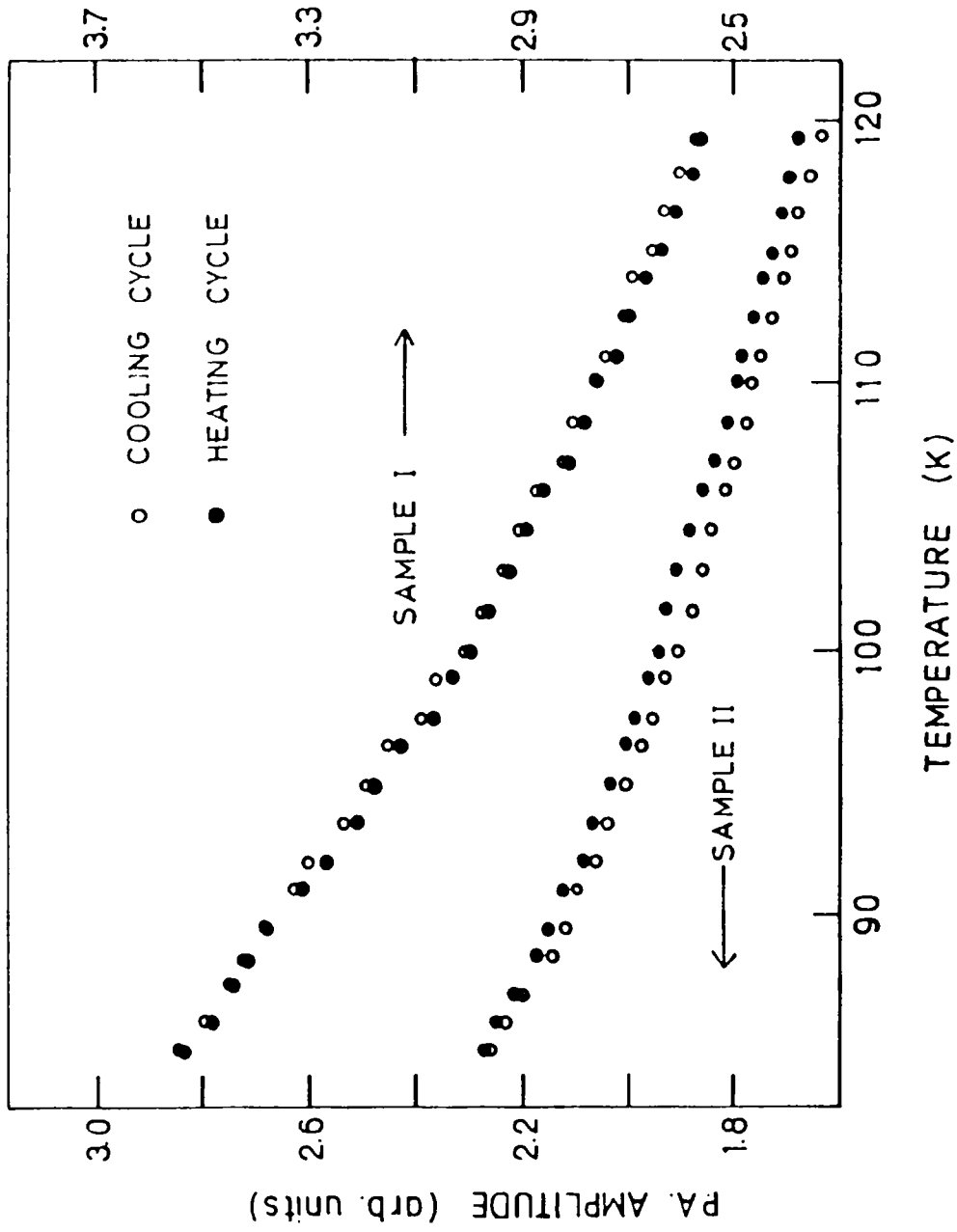


Fig.3.5: Temperature variation of the photoacoustic amplitude in $\text{YBa}_2\text{Cu}_3\text{O}_7$ (samples I and II) between 85 K and 120 K.

temperature range 80-120 K because in the higher temperature region the phase has a smooth variation which is not of much interest. The corresponding phase variation observed in sample II is shown in fig.3.4. These figures show that photoacoustic phase undergoes a clear anomalous change near T_c . A step like decrease in phase near T_c is evident in both the samples although the change is less pronounced in sample II. It may also be noticed that the minimum in phase occurs at two different temperatures during cooling and heating cycles indicating remarkable temperature hysteresis in phase variations. In fig.3.5 the temperature variation of the amplitude of the PA signal is plotted in the range 80-120 K for samples I and II. As is evident from this figure, the amplitude does not show any appreciable anomaly near the superconducting transition region. The amplitude increases as the temperature is lowered. Repeated runs lead to the same result.

Measurements have also been carried out on a non-superconducting sample of the same composition to check whether it is the superconducting transition itself that leads to the anomalous changes in phase in samples I and II. The non-superconducting sample does not show any anomaly either in phase or in amplitude anywhere in the range 80-300 K.

An interesting aspect of the above results is that only the PA phase undergoes anomalous changes near T_c without the amplitude showing any significant anomaly. According to R-G theory, for an optically opaque and thermally thick sample, in which the optical absorption length l_p is very much less than the thermal diffusion length μ , the amplitude I_{PA} of the PA signal varies as,

$$I_{PA} \propto C_p^{-\frac{1}{2}} K^{-\frac{1}{2}} \quad (3.11)$$

where C_p and K are the specific heat and thermal conductivity of the sample respectively. Reports on measurements of thermal conductivity [33-36] and specific heat [26,27] of $YBa_2Cu_3O_7$ show that the thermal conductivity increases below T_c while the specific heat decreases with temperature. This nearly opposite behaviour exhibited by K and C_p reduces their overall effect on the PA amplitude. This, however, does not fully explain the near absence of the contribution of thermal conductivity on the amplitude. One possible reason is that the assumption made earlier that the optical absorption length l_p is very much less than the thermal diffusion length μ may not strictly be valid. Optical absorption in $YBa_2Cu_3O_7$ is centered mainly in the green region of the spectrum whereas in the present measurements a substantial amount of

light falls in the other regions of the spectrum including infrared despite the IR filter. For these wavelengths the optical absorption coefficients may not be large enough to hold the above assumption true and for a sample in which $l_p > \mu$ we have,

$$I_{PA} \propto C_p^{-1} \quad (3.12)$$

Eq.(3.12) does not contain thermal conductivity. Therefore, it is reasonable to assume that the effect of thermal conductivity on the amplitude of the PA signal will be substantially reduced for value of l_p of the order of μ . The lamp-monochromator combination is found to be incapable of giving enough monochromatic light intensity to give rise to detectable PA signal in these materials. The increase in the signal amplitude as the temperature falls is due to the corresponding decrease in the specific heat of the sample. However, the small jump in specific heat as reported by other workers [26,27] is not reflected in the amplitude. One cannot expect such minute variations to be reflected in the PA amplitude which is governed by a number of other parameters as well.

The R-G theory does not account for the anomalous change observed in the photoacoustic phase during the

superconducting transition. The decrease in phase may be due to a decrease in the excited electron relaxation time when the material undergoes the transition. A faster relaxation of the optically excited levels leads to a decrease in the photoacoustic phase. This faster relaxation may be due to the creation of additional electron traps when the material changes phase. A quantitative explanation of the above observations, we believe, would evolve along with other experimental observations in the near future.

The nearly opposite behaviours of thermal conductivity and specific heat produce pronounced variations in the thermal diffusivity of $\text{YBa}_2\text{Cu}_3\text{O}_7$. Fig.3.6 shows the amplitude of the PA signal as a function of chopping frequency at various temperatures. The frequency at which the slope of the curve changes is the characteristic frequency f_c from which the thermal diffusivity α can be determined using the relation $\alpha = f_c^{-2}$. In fig.3.7 the thermal diffusivity of $\text{YBa}_2\text{Cu}_3\text{O}_7$ is plotted as a function of temperature. As is evident from the figure, there is a sharp increase in thermal diffusivity below T_c associated with the superconducting transition. Data have been recorded during cooling and heating cycles. The points follow the same curve during both the cycles.

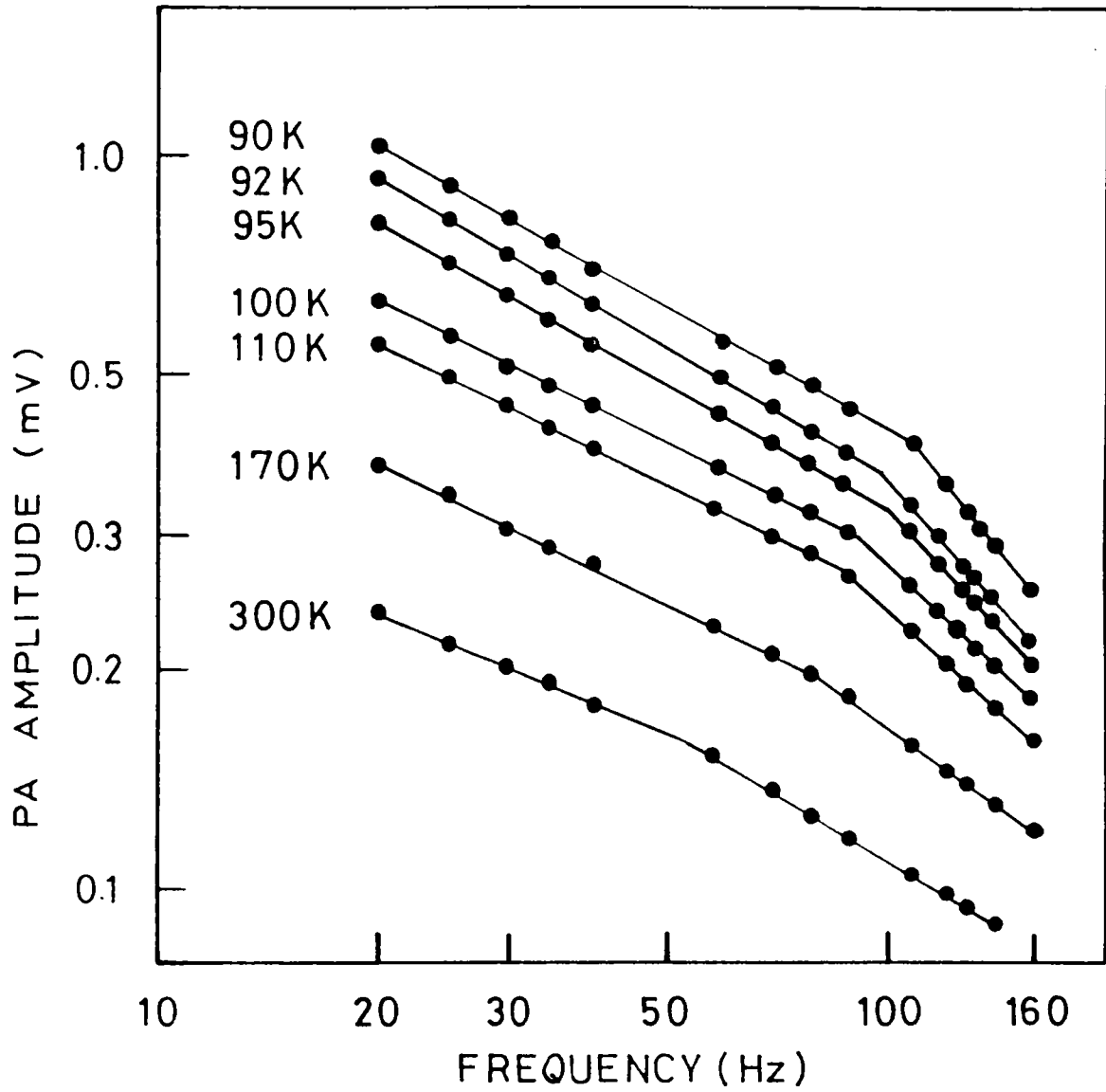


Fig.3.6: Log-log plots of variation of the PA amplitude with chopping frequency in $\text{YBa}_2\text{Cu}_3\text{O}_7$ at different temperatures.

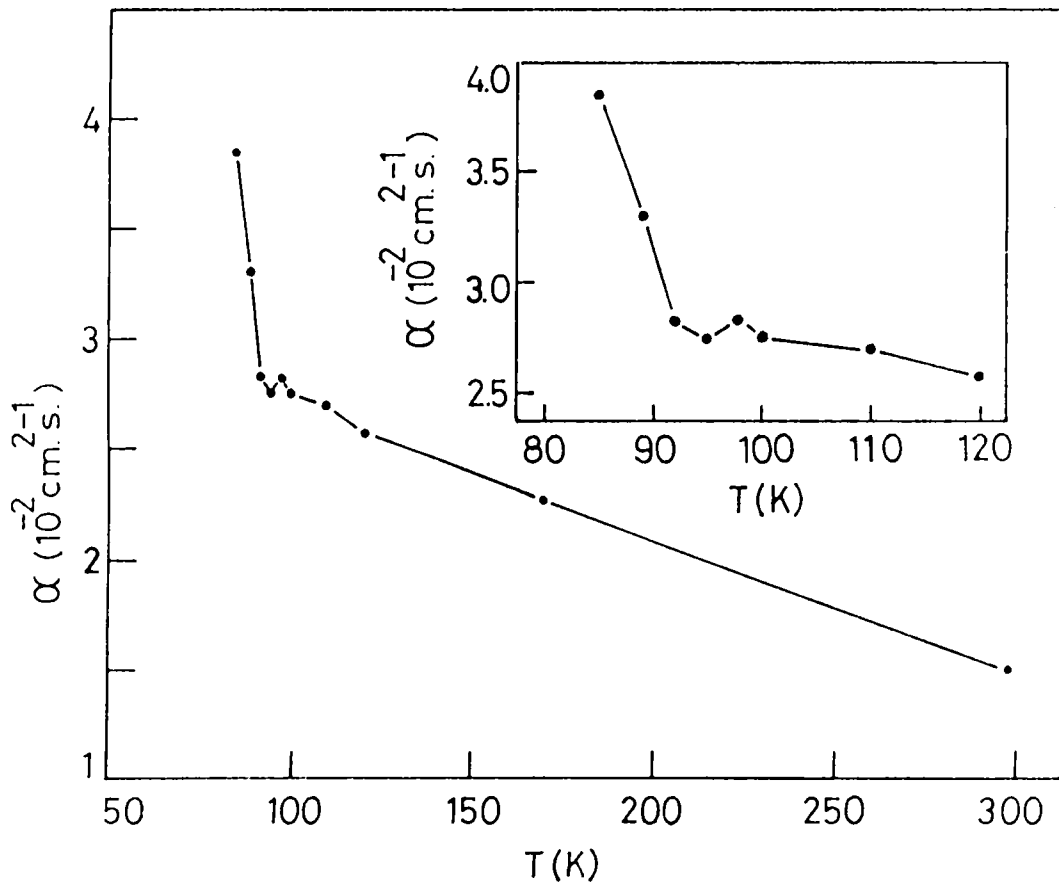


Fig.3.7: Temperature variation of the thermal diffusivity of $\text{YBa}_2\text{Cu}_3\text{O}_7$. The inset clearly shows the small anomaly in α near T_c .

When a metal becomes superconducting, electrons form Cooper pairs which cannot carry entropy and so do not contribute to thermal conductivity. Unpaired electrons in a superconductor can however transport heat but as the temperature decreases below T_c , the number of such electrons decreases exponentially. The electronic thermal conductivity of a superconductor therefore falls rapidly below T_c . On the other hand since the paired electrons no longer scatter phonons there can be an increase in phonon mean free path below T_c which increases the phononic contribution to thermal conductivity. The net temperature dependence of thermal conductivity below T_c will depend upon whether the electronic or phononic contribution dominates in the superconductor.

The thermal diffusivity α can be written as,

$$\alpha = \kappa / \rho c_p \quad (3.13)$$

where κ , ρ and c_p are the thermal conductivity, density and specific heat of the sample respectively. Substituting for κ , the phononic contribution to thermal conductivity κ_{ph} given by [44,45],

$$\kappa_{ph} = \frac{1}{3} c_p \rho \bar{v} \bar{l} \quad (3.14)$$

where \bar{v} is the average sound velocity and \bar{l} is the phonon mean free path, we get,

$$\alpha = \frac{1}{3} \bar{v} \bar{l} \quad (3.15)$$

Eq.(3.15) shows that the sudden increase in α below T_c is the result of an increase in \bar{l} which is caused by a drastic reduction in phonon carrier scattering. As the charge carriers begin to form superconducting pairs one can expect this effect. This also suggests that the major contribution to heat conduction in these materials is due to phonons.

Another feature that can be noticed in fig.3.7 is a small anomalous decrease in α and near T_c . This, we think, is a consequence of the jump in heat capacity at T_c [26,27]. In conclusion, the observed increase in thermal diffusivity below T_c is an indication of the close coupling of the charge carriers and phonon excitations in 1:2:3 superconductors.

REFERENCES

1. M.R.Beasley & T.H.Geballe, *Phys. Today* **36**, 60 (1984).
2. J.Muller, *Rep.Prog.Phys.* **43**, 663 (1980).
3. J.G.Bednorz & K.A.Muller, *Z.Phys.B* **64**, 189 (1986).
4. J.D.Jorgensen, H.B.Schuttler, D.G.Hinks, D.W.Capone II, K.Zhang, M.B.Brodskym & D.J.Scalapino, *Phys.Rev.Lett.* **58**, 1024 (1987).
5. R.J.Cava, R.B.Van Dover, B.Batlogg & E.A.Rietman, *Phys. Rev.Lett.* **58**, 408 (1987).
6. M.K.Wu, J.R.Ashburn, C.J.Torng, P.H.Hor, R.L.Meng, L.Gao, Z.J.Huang, Y.Q.Wang & C.W.Chu, *Phys.Rev.Lett.* **58**, 908 (1987).
7. D.H.Hinks, L.Doderholm, D.W.Capone II, J.D.Jorgensen, Ivan K.Schuller, C.U.Serge, K.Zhang & J.D.Grace, *Appl. Phys. Lett.* **50**, 1688 (1987).

8. P.M.Graut, R.B.Beyers, E.M.Engler, G.Lim, S.S.P.Parkin, M.L.Ramirez, V.Y.Lee, A.Nazzal, J.E.Vasquez & R.J.Savoy, Phys.Rev.B 35, 7242 (1987).
9. K.Semba, T.Tsurumi, M.Hikita, T.Iwata, J.Noda & S.Kirithara, Jpn.J.Appl.Phys. 26, L 429 (1987).
10. H.Maeda, Y.Tanaka, F.Fukutomi & T.Asano, Jpn.J.Appl.Phys. 27, L 209 (1988).
11. J.M.Tarascon, Y.LePage, P.Barboux, B.C.Bagley, L.H.Greene, W.R.Mc Kinnon, G.W.Hull, M.Giroud & D.M.Hwang, Phys.Rev.B 37, 9382 (1988).
12. Z.Z.Sheng & A.M.Herman, Nature 332, 138 (1988).
13. D.W.Murphy, S.Sunshine, R.B.van Dover, R.J.Cava, B.Batlogg, S.M.Zahurak & L.F.Shneemeyer, Phys.Rev.Lett. 58, 1888 (1987).
14. B.Batlogg, R.J.Cava, A.Jayaraman, R.B.van Dover, D.W.Murphy, L.W.Rupp, H.S.Chen, A.White, K.T.Scott, A.M.Mujsce & E.A.Rietman, Phys.Rev.Lett. 58, 2333 (1987).

15. L.C.Bourne, A.Zettl, T.W.Barbee III & M.L.Cochan, Phys. Rev.B **36**, 3990 (1987).
16. W.E.Pickett, H.Krakauer, D.A.Papaconstantopoulos & L.L.Boyer, Phys.Rev.B **35**, 7252 (1987).
17. W.Weber, Phys.Rev.Lett. **58**, 1371 (1987).
18. H.Ihara, M.Hirabayashi, N.Terada, Y.Kimura, K.Senzaki, M.Akimoto, K.Bushida, F.Kawashima & R.Uzaka, Jpn.J.Appl. Phys. **26**, L 460 (1987).
19. J.Ruvalds, Phys.Rev. B **35**, 8869 (1987).
20. C.M.Varma, R.Schmitt & E.Abrahams, Solid State Commun. **62**, 681 (1987).
21. B.K.Chakraverty, J.Phys. (Paris) **40**, L 99 (1979).
22. P.W.Anderson, Science **235**, 1196 (1987).
23. C.N.R.Rao, J.Solid State Chem. **74**, 147 (1988).
24. C.N.R.Rao (ed.), The Chemistry of Oxide Superconductors, Blackwell, Oxford (1988).

25. C.N.R.Rao (ed.) Progress in High-Temperature Superconductivity, Vol.VII, World Scientific, Singapore (1988).
26. S.E.Inderhees, M.B.Salamon, T.A.Friedmann & D.M.Ginsberg, Phys.Rev.B 36, 2401 (1987).
27. M.V.Nevitt, G.W.Crabtree & T.C.Klippert, Phys.Rev.B 36, 2398 (1987).
28. A.Junod, A.Bezinge & J.Muller, Physica C 152, 50 (1988).
29. K.Fossheim, O.M.Nes, T.Laegried, C.N.N.Darlington, D.A.O'Connor & C.E.Gough, Int.J.Med.Phys.B 2, 1171 (1988).
30. N.Okazaki, T.Hasegawa, K.Kishio, K.Kitazawa, A.Kishi, Y.Ikeda, M.Takano, K.Oda, H.Kitaguchi, J.Takada & Y.Miura, Phys.Rev.B 41, 4296 (1990).
31. A.Junod, D.Eckert, G.Triscore, V.Y.Lee & J.Muller, Physica C 159, 215 (1989).
32. C.Uher & J.L.Cohn, J.Phys.C 21, L 957 (1988).
33. C.Uher & A.B.Kaiser, Phys.Rev.B 36, 5680 (1987).

34. A.Jezowski, J.Mucha, K.Rogacki, R.Horyn, Z.Bukowski, M.Horobiowski, J.Rajalowicz, J.Stepien Damm, C.Sulkowski, E.Trojnar, A.J.Zeleski & J.Klamut, Phys.Lett.A **122**, 431 (1987).
35. D.T.Morelli, J.Heremans & D.E.Swets, Phys.Rev.B **36**, 3917 (1987).
36. J.L.Cohn, S.D.Peacor & C.Uher, Phys.Rev.B **38**, 2892 (1988).
37. M.A.Izbizky, M.Nunez Regueiro, P.Esquinazi & C.Fainstein, Phys.Rev.B **38**, 9220 (1988).
38. A.Jezowski, A.J.Zaleski, M.Ciszek, J.Mucha, J.Olejniczak, E.Trojnar & J.Klamut, Helv.Phys.Acta **61**, 438 (1988).
39. A.Jezowski, J.Mucha, A.J.Zaleski, M.Ciszek, J.Olejniczak, K.Rogacki, C.Sulkowski, M.Wolcyrz & J.Klamut, Phys.Lett. **127**, 225 (1988).
40. S.D.Peacor & C.Uher, Phys.Rev.B **39**, 11559 (1989).
41. M.F.Crommie & A.Zettl, Phys.Rev.B **41**, 10978 (1990).

42. A.Jezowski, A.J.Zaleski, H.Misiorek, E.P.Khlybov & V.V.Evdokimova, Phys.Lett. 139, 265 (1989).
43. P.Charpentier, F.Lepoutre & L.Bertrand, J.Appl.Phys. 53, 608 (1982).
44. P.G.Klemens, Solid State Physics Vol.7, F.Seitz and D.Turnbull (ed.) Academic Press, New York, (1958).
45. G.T.Meaden, K.V.Rao & K.T.Tee, Dynamical Aspects of Critical Phenomena, J.I.Budmick and M.P.Kawatra (ed.) Gordon and Breach, New York, p.349 (1972).

Chapter 4

PHOTOACOUSTIC STUDY OF THE THERMAL PROPERTIES OF THE HIGH T_c SUPERCONDUCTOR Bi-Sr-Ca-Cu-O

4.1 Introduction

The discovery of high temperature superconductivity in the two new oxide series Bi-Sr-Ca-Cu-O [1,2] and Tl-Ba-Ca-Cu-O [3] with transition temperature T_c well above 100 K has been a turning point in the search for newer high T_c oxide superconductors. The quinary nature of the Bi and Tl based oxide superconducting systems provide an array of phases with different compositions and superconducting properties. This has provided a wider variety and scope for investigating these high T_c oxides. The highest T_c obtained in Bi-Sr-Ca-Cu-O (BSCCO) system is 110 K and that in Tl-Ba-Ca-Cu-O (TBCCO) is 125 K, the highest known superconducting T_c obtained so far.

The BSCCO system has at least two important superconducting phases, one with T_c of about 80 K (the low T_c phase) [4] and the other of about 110 K (the high T_c phase) [5]. These two phases can be expressed by the general formula $\text{Bi}_2\text{Sr}_2\text{Ca}_{n-1}\text{Cu}_n\text{O}_x$ ($x = 2n + 4$) with $n = 2$ and 3. The ideal

metal atom composition for the $n = 2$ and $n = 3$ phases are 2212 and 2223, respectively. However, the Sr to Ca ratio in both the phases has some range about the ideal value and the T_c of both phases tends to decrease with increasing Ca content. The crystal structures of the two phases are similar differing only in the number (n) of $\text{CuO}_2\text{-Ca-CuO}_2$ planes inserted between double Bi-O layers and T_c is found to increase with n . Considerable efforts have been made to characterize the crystal structure and superconducting properties of BSCCO system by many previous workers [6-13].

The Bi oxide superconductors have some interesting features with regard to their practical applications. For example, a phase transition does not occur below the sintering temperature as in YBCO system, permitting better control of the material properties. The grains have a very thin planar shape with their surfaces parallel to the C-plane which will facilitate grain alignment for J_c improvement. Since cleavage of these phases occurs between the Bi-O bilayers along the C-plane, it is possible to deform the pellet samples by compaction without interrupting the high J_c current axis of the material. This suggests the possibility of the development of a preferred grain orientation with the alignment of the C-planes of each grain in the longitudinal direction of a

wire or a tape during fabrication. Most of the BSCCO films prepared by various techniques such as sputtering, evaporation and printing have a strong preferred orientation with the C-plane parallel to the substrate.

To make use of these favourable features of BSCCO, it is necessary to form the high T_c phase. However, it is very difficult, if not impossible, to prepare samples with the high T_c phase only. A tail in the resistivity transition curve usually appears due to the combined presence of the low T_c phase and the high T_c phase. The maximum volume fraction of high T_c phase obtained in a sample is about 40%. There have been several efforts to increase the volume fraction of the high T_c phase including addition of a large excess of Ca and Cu, high pressure oxygen treatment and long time sintering [14-16]. Among these efforts, partial substitution of Pb for Bi is found to be very effective in enhancing the T_c and in obtaining an increased volume fraction of the high T_c phase [17,18].

The effect of Pb doping on BSCCO superconductors have been studied by different workers before. Melting point of Pb doped material decreases as Pb concentration increases [19], and the synthesis temperature decreases as the Pb content increases [20]. Moreover, addition of Pb stabilizes

the 110 K superconducting phase and it is best when the Pb concentration is in the range 0.2 to 0.3 [19-21]. Addition of Pb beyond 0.4 leads to the formation of CaPbO_4 which may deteriorate the formation of the high T_c phase [19]. Variation of the Pb concentration however, does not influence the value of T_c significantly.

There have been a few reports of the measurement of thermal conductivity of BSCCO superconductors [22,23]. As has been pointed out in chapter 3, very useful information about the superconducting mechanism can be obtained by measuring the thermal conductivity near the transition point. Since heat is conducted by both electrons and phonons, measurement of thermal conductivity yields valuable information about the interactions between them. Thermal conductivity value increases or decreases below T_c depending upon the nature of the heat carriers and their interactions.

High temperature superconductors have electrical resistivity of the order of a milliohm-cm at room temperature which implies that the phononic contribution may be the dominant mode of heat transport. Most measurements of thermal conductivity reported so far have been on sintered polycrystalline pellets of the material. At low temperatures,

the pores present in the pellets and the grain size may impose serious limitations on the mean free path of the phonons. All the high T_c superconductors exhibit a bump like increase in thermal conductivity below T_c . This behaviour is interpreted as due to an enhancement in the phonon contribution to thermal conductivity resulting from a reduction in the electron-phonon scattering as a consequence of the formation of Cooper pairs by electrons below T_c . However, due to the very polycrystalline nature of the sample it is rather difficult to interpret the thermal conductivity variation in terms of the intrinsic electronic and phononic contributions alone. Thermal conductivity measurements made on single crystals of BSCCO [23] with varying oxygen configurations have demonstrated that near T_c the phonon-defect scattering contribution is nearly twice as large as the phonon-electron scattering contribution.

It would be very interesting and useful to study the influence of Pb doping on the thermal transport properties of BSCCO superconductor. We have measured the temperature dependence of the thermal diffusivity of four Pb doped BSCCO samples with varying Pb concentration, above and below T_c using photoacoustic technique. Details of the experiment and the results obtained are discussed below.

4.2 Sample preparation

Conventional solid-state reaction of the component oxides in stoichiometric proportions does not yield single-phase samples of Bi-based high T_c superconductors. The reason for this appears to be the relatively low melting point of Bi_2O_3 as compared to the other component oxides which leads to a loss of Bi and to intergrowth of different phases. However, through partial substitution of Pb for Bi, intergrowth of different phases can be suppressed. The volume fraction of the high T_c phase in a sample can be enhanced to $\approx 90\%$ by Pb doping.

Sintered polycrystalline samples of Pb doped BSCCO have been prepared by the well established solid state reaction method. Powder samples of Bi_2O_3 , SrCO_3 , CaCO_3 , CuO and PbO are mixed well in the required atomic proportions and calcined at 800°C for about 20 hours. The calcined material has been crushed, powdered and then made into pellets of ≈ 10 mm diameter at a pressure of about 4 metric tons. The pellets are then sintered at 820°C for nearly 100 hours. All treatments are done in air and air quenching is done after sintering.

In Pb doped samples, the Pb atoms go into Bi sites. The following four are the samples prepared for the present investigations. They have the general formula $\text{Bi}_{2.1-x}\text{Pb}_x\text{Sr}_2\text{Ca}_2\text{Cu}_3\text{O}$.

Sample I : $\text{Bi}_{1.9}\text{Pb}_{0.2}\text{Sr}_2\text{Ca}_2\text{Cu}_3\text{O}$

Sample II : $\text{Bi}_{1.8}\text{Pb}_{0.3}\text{Sr}_2\text{Ca}_2\text{Cu}_3\text{O}$

Sample III : $\text{Bi}_{1.7}\text{Pb}_{0.4}\text{Sr}_2\text{Ca}_2\text{Cu}_3\text{O}$

Sample IV : $\text{Bi}_{1.6}\text{Pb}_{0.5}\text{Sr}_2\text{Ca}_2\text{Cu}_3\text{O}$

Superconductivity property of these samples have been verified by making electrical resistivity measurements. It is found that all these samples undergo superconducting transition at ≈ 110 K.

4.3 Thermal diffusivity measurement

Thermal diffusivity measurements are carried out as described in the previous chapter. The method involves measurement of the amplitude of the PA signal as a function of the chopping frequency for a thin sample mounted on a suitable backing material. A log-log plot of the amplitude against chopping frequency shows a distinct change in slope

at the characteristic frequency f_c above which the signal is independent of the thermal properties of the backing material. Thermal diffusivity α can be obtained using the relation $\alpha = f_c l^2$, where l is the thickness of the sample.

Pellets of BSCCO samples have been thinned down to ~ 0.08 mm and mounted on a thick polished aluminium disc which acts as the backing material, using silver epoxy to ensure good thermal contact. The temperature of the sample is kept constant within $\pm 0.5^\circ\text{C}$ during the measurements.

4.4 Results and discussion

Figures 4.1 to 4.4 show log-log plots of the amplitude of the PA signal measured as a function of the chopping frequency at various temperatures for samples I to IV. The change in slope at the characteristic frequency T_c can clearly be seen in the figures. In fig.4.5(a) and (b) we have plotted the temperature variation of the thermal diffusivity of the four samples between 90 K and room temperature. Since the magnitude of α for sample IV below T_c is much lower compared to other samples, a different scale has been used for it. We have also plotted the dependence of thermal diffusivity on Pb concentration (x) at room

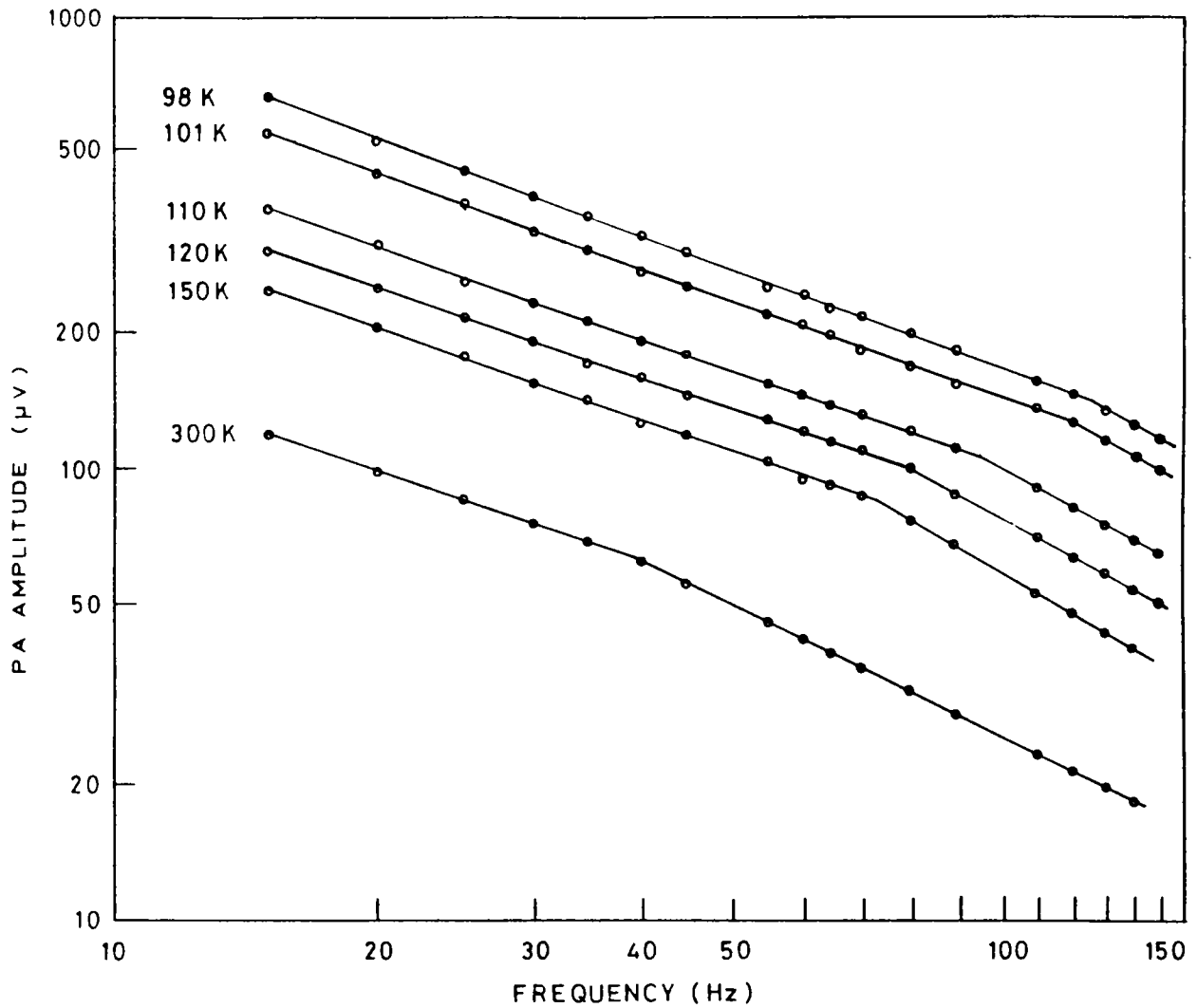


Fig.4.1: Log-log plots of variation of the PA amplitude with chopping frequency in $\text{Bi}_{1.9}\text{Pb}_{0.2}\text{Sr}_2\text{Ca}_2\text{Cu}_3\text{O}$ (sample I) at different temperatures.

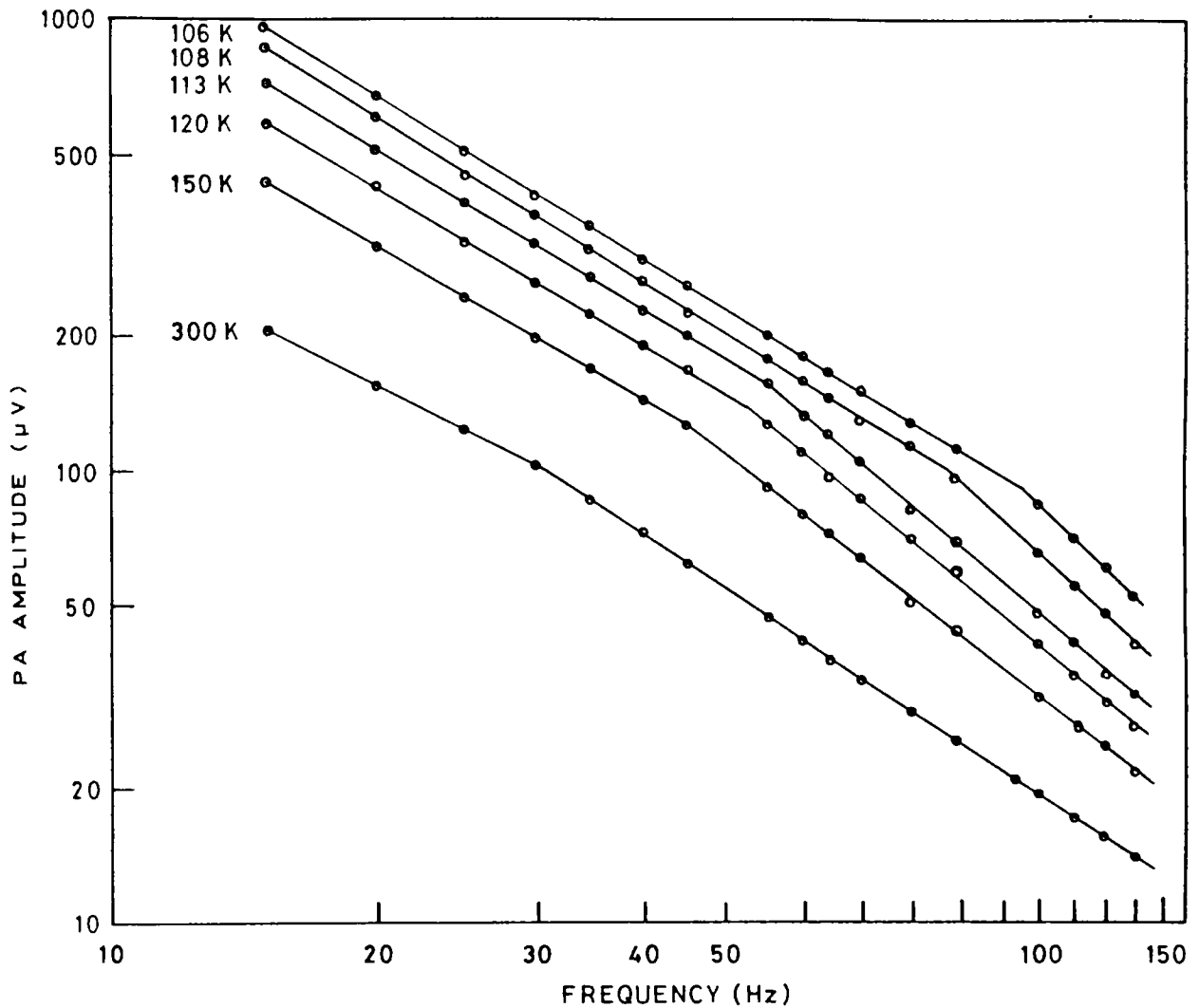


Fig.4.2: Log-log plots of variation of the PA amplitude with chopping frequency in $\text{Bi}_{1.8}\text{Pb}_{0.3}\text{Sr}_2\text{Ca}_2\text{Cu}_3\text{O}$ (sample II) at different temperatures.

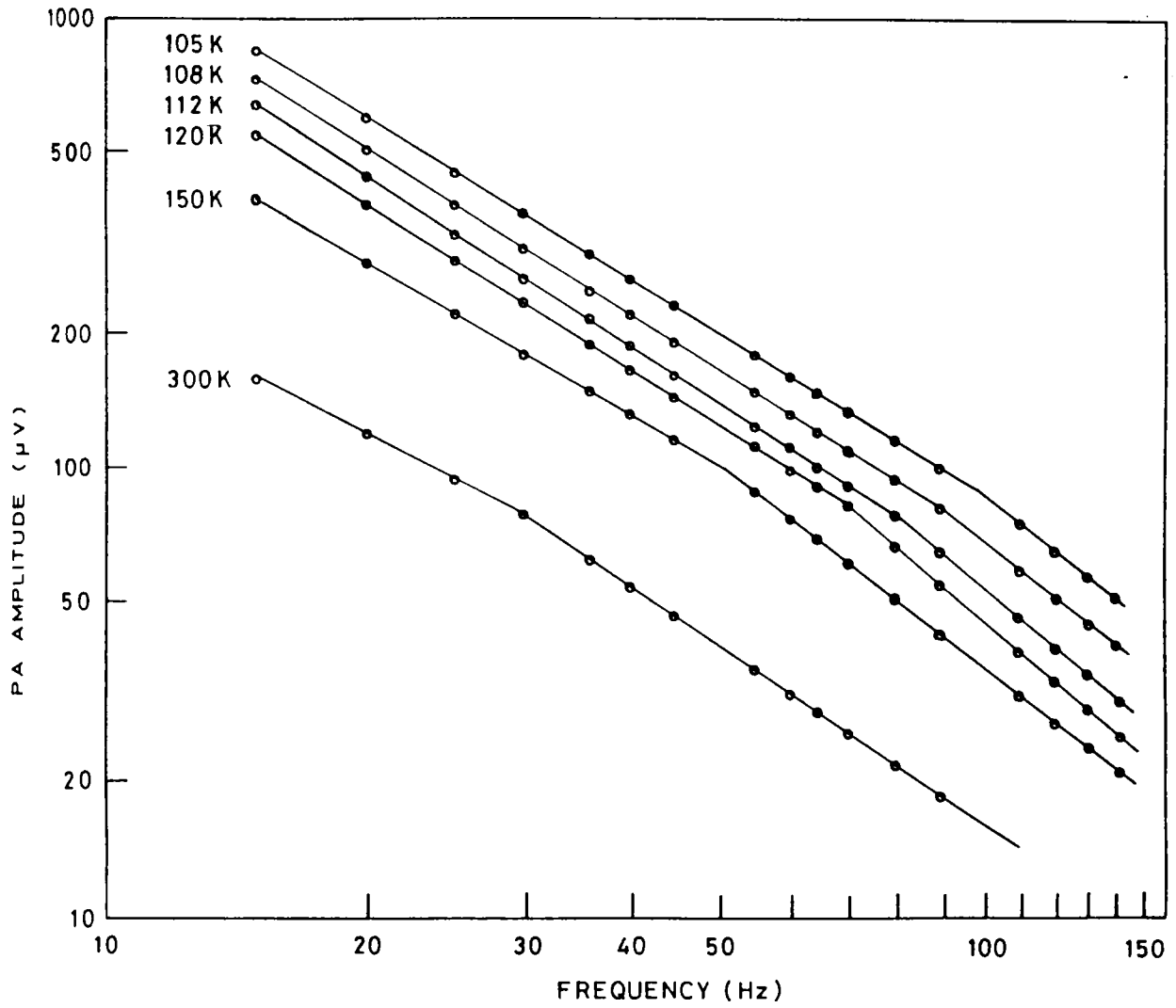


Fig.4.3: Log-log plots of variation of the PA amplitude with chopping frequency in $\text{Bi}_{1.7}\text{Pb}_{0.4}\text{Sr}_2\text{Ca}_2\text{Cu}_3\text{O}$ (sample III) at different temperatures.

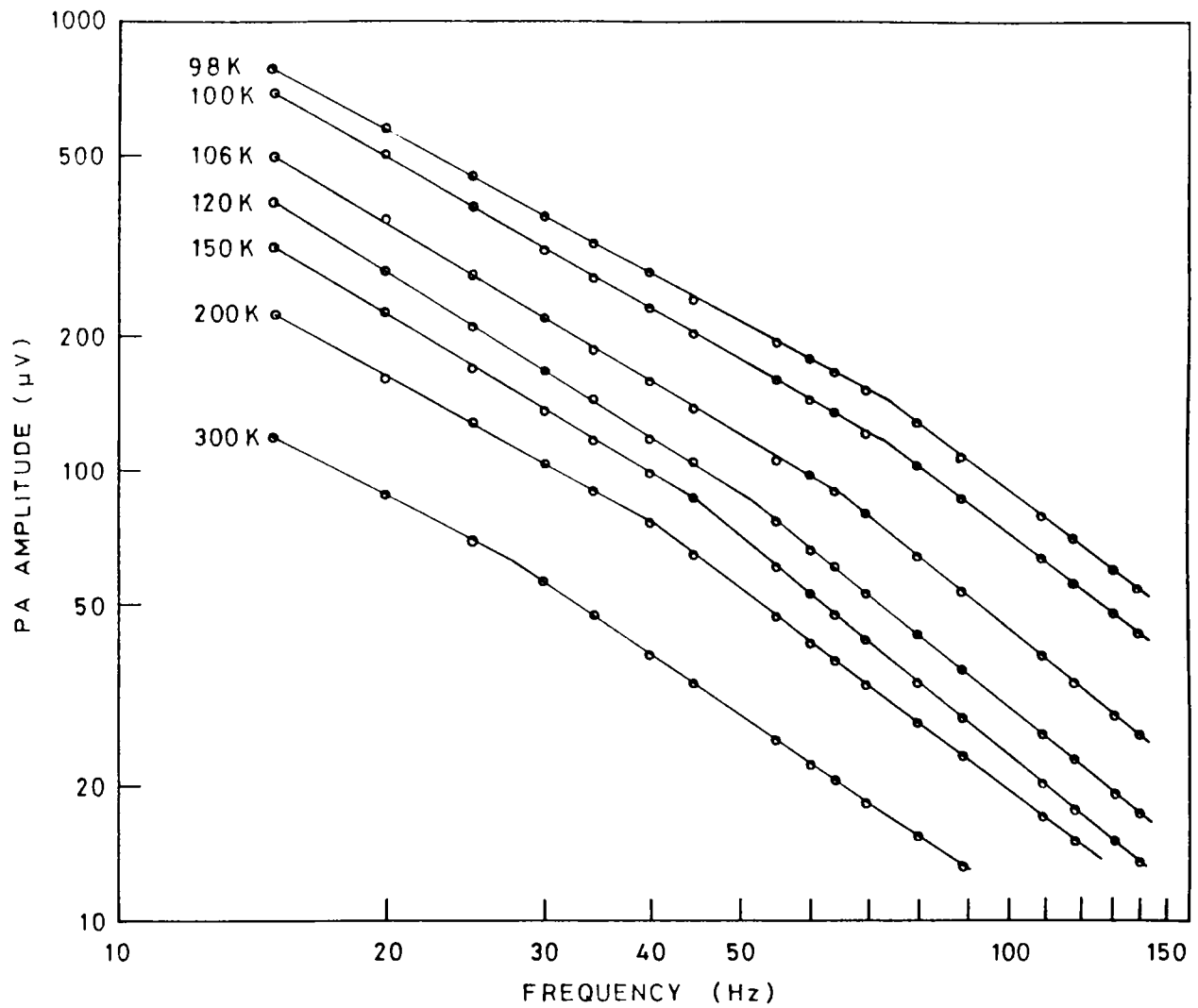


Fig.4.4: Log-log plots of variation of the PA amplitude with chopping frequency in $\text{Bi}_{1.6}\text{Pb}_{0.4}\text{Sr}_2\text{Ca}_2\text{Cu}_3\text{O}$ (sample IV) at different temperatures.

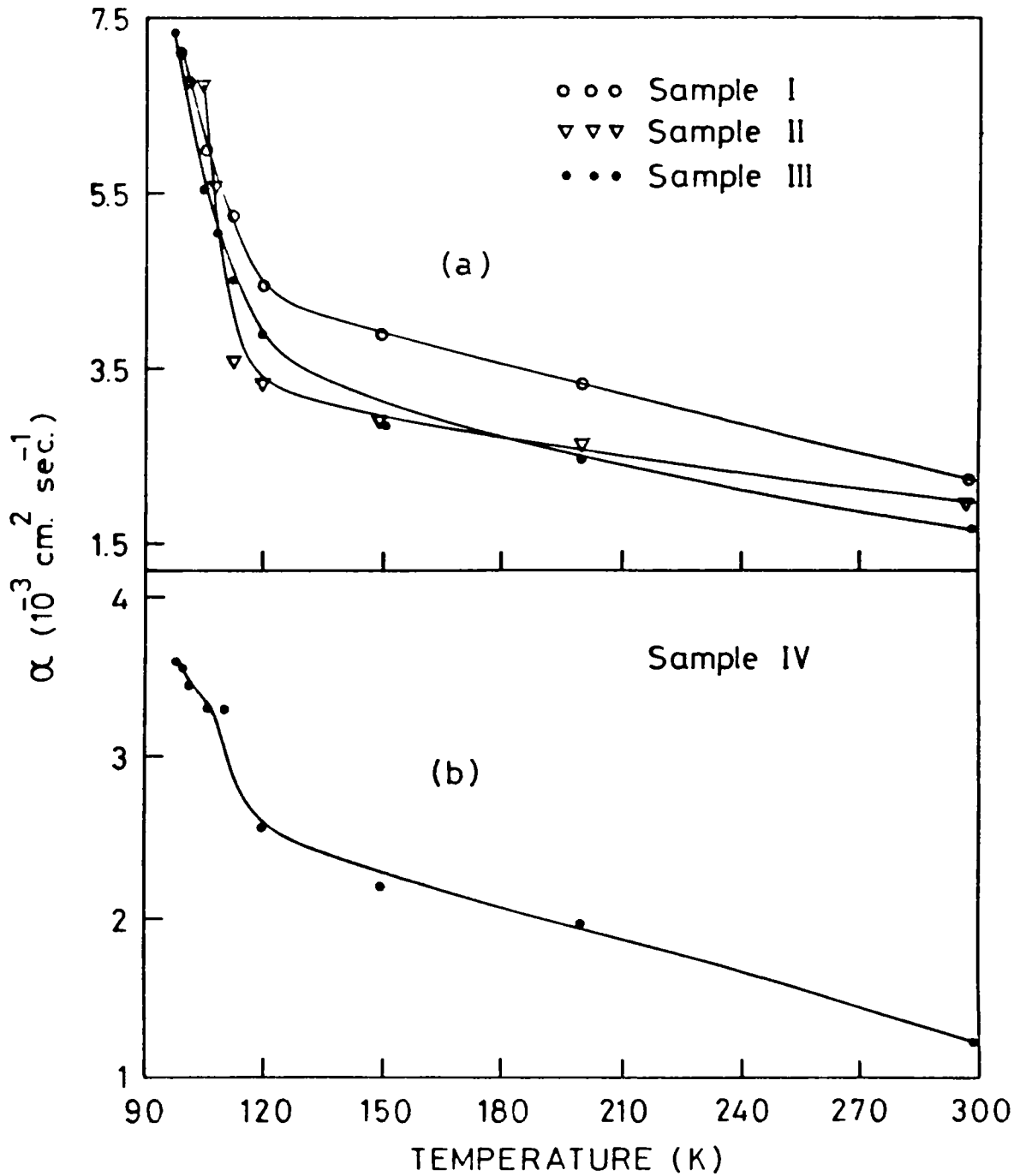


Fig.4.5(a) & (b): Temperature variation of the thermal diffusivity in samples I, II, III and IV.

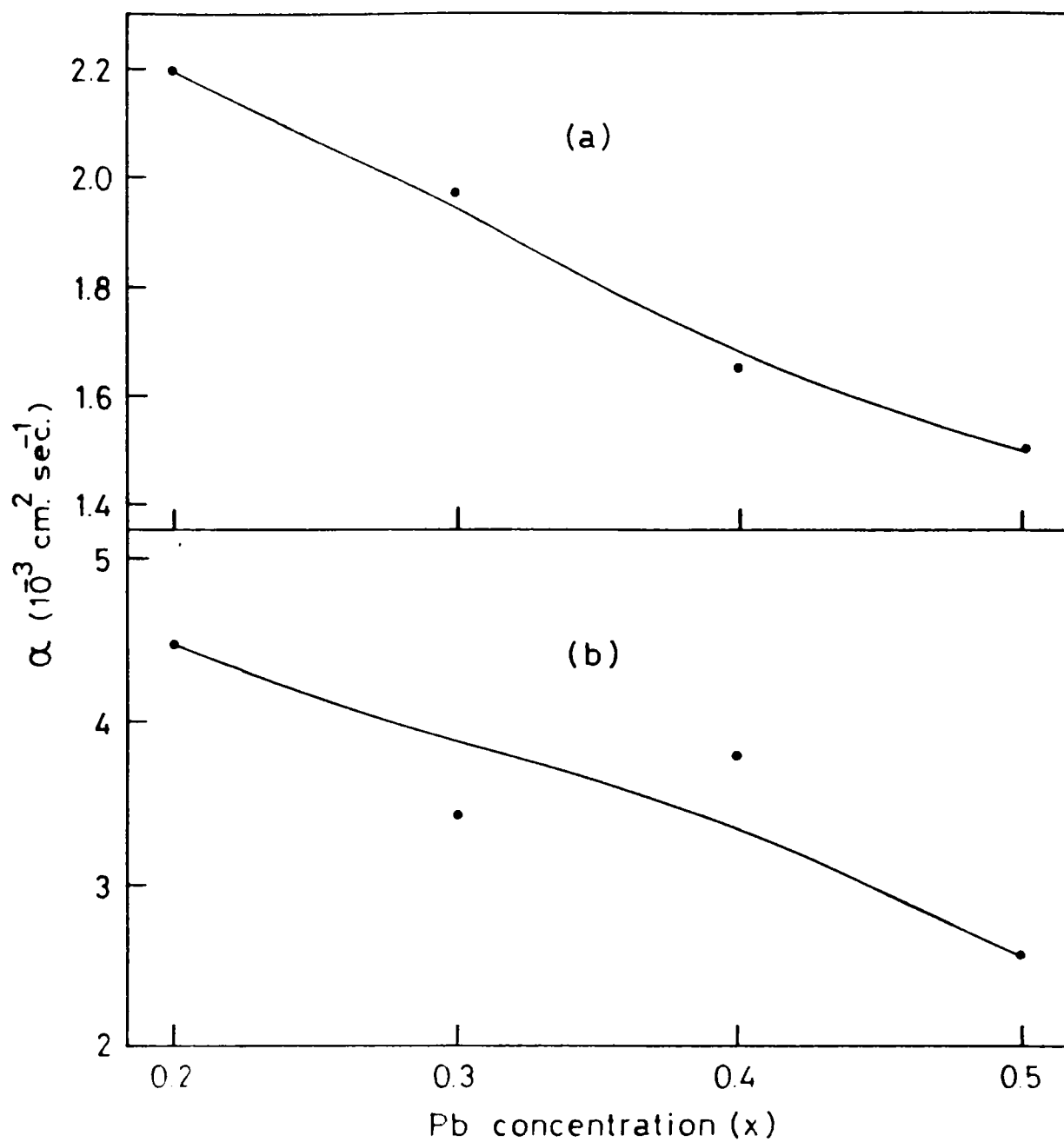


Fig.4.6(a) & (b): Variation of thermal diffusivity with Pb concentration at room temperature and 120 K.

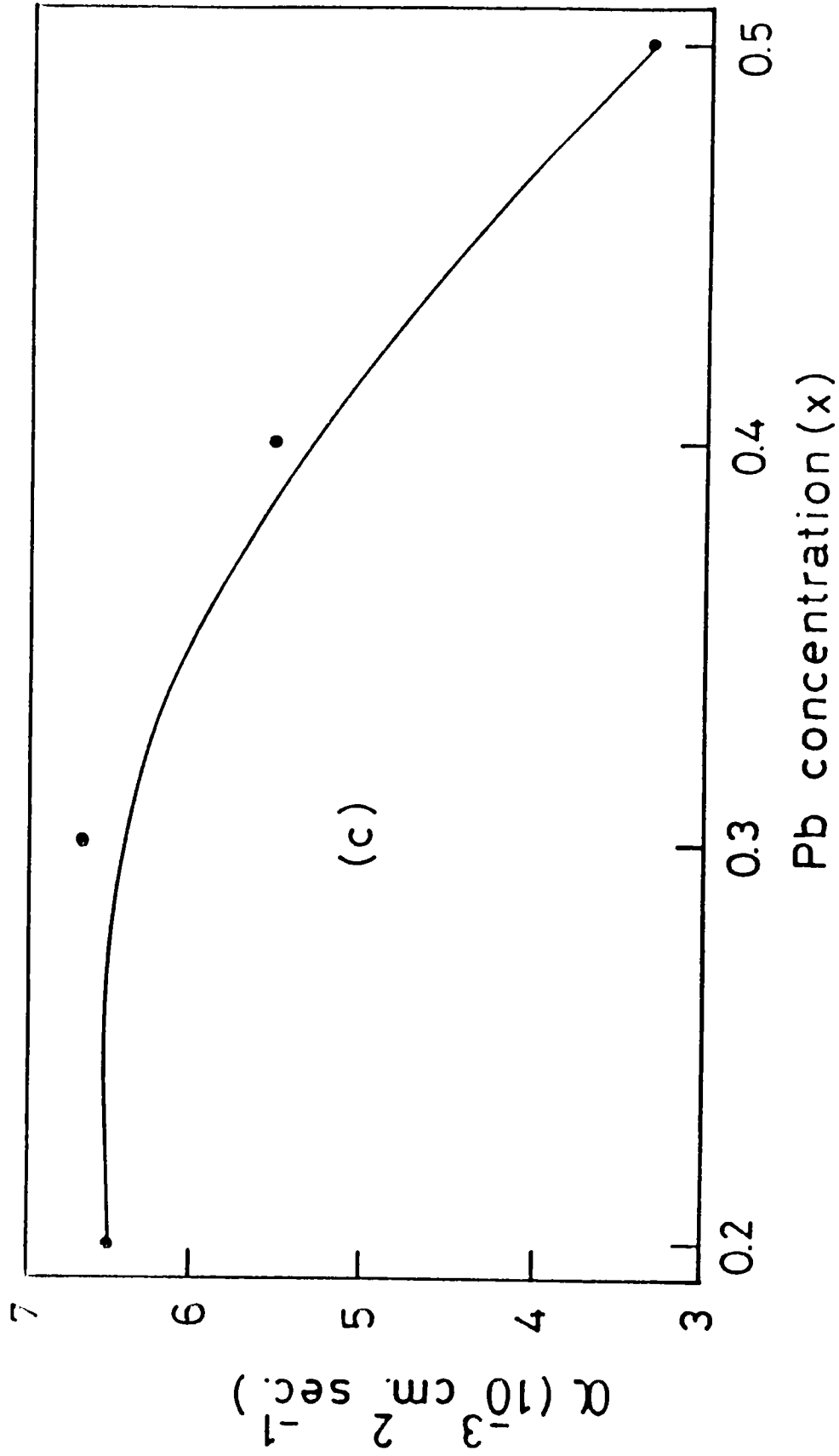


Fig.4.7: Variation of thermal diffusivity with Pb concentration at 105 K.

temperature, at 120 K (above T_c) and at 105 K (below T_c). These curves are shown in figs. 4.6(a), (b) and 4.7 respectively. It may be noted from fig. 4.7 that thermal diffusivity has a tendency to saturate below a Pb concentration of ≈ 0.3 below T_c . Such a tendency is not there for temperatures above T_c .

We have measured the density of all the samples and calculated the thermal conductivity from thermal diffusivity data taking specific heat values from literature [24]. It is found that around T_c the temperature variation of the thermal conductivity follows the corresponding thermal diffusivity curve. This is due to the fact that change in specific heat near T_c is very small and variation in thermal conductivity overshadows the corresponding specific heat variation. So an explanation for the observed thermal diffusivity variation near T_c can very well be extended to the corresponding thermal conductivity variation.

It can clearly be seen from figs. 4.5(a) and (b) that the thermal diffusivity suddenly increases just below T_c . This is similar to the behaviour shown by all high T_c superconductors, in thermal conductivity measurements. This has been attributed to the condensation of free electrons to

form Cooper pairs below T_c . The electrons which are condensed into pairs do not carry entropy and therefore cannot act as heat carriers. Moreover, the Cooper pairs so formed no longer scatter phonons so that electron-phonon scattering decreases giving rise to an increased phonon mean free path and a corresponding enhancement in the phononic part of thermal diffusivity. These observations also indicate that thermal transport in the superconducting phase is limited primarily by phonon-defect scattering. Obviously these arguments have their limitations owing to the fact that a quantitative deconvolution of thermal transport into its intrinsic electronic and phononic contributions is difficult due to the complexity of the polycrystalline system. The phonon-phonon umklapp processes can safely be ignored in our discussions as they are overshadowed by scattering from defects and electrons. Temperature dependence of the thermal conductivity measured in oxygen deficient samples of Bi-Ca-Sr-Cu-O also imply that it is determined primarily by phonon-defect scattering.

The role played by defect scattering in electrical conductivity, Hall coefficient and thermopower in Bi-Sr-Ca-Cu-O samples has been emphasized by previous workers [25,26] based on such measurements made on samples of varying oxygen

configuration. Our Pb doped polycrystalline samples in the normal state show the expected variation in thermal diffusivity at all temperatures above T_c , viz., an increase in thermal diffusivity as Pb concentration decreases. Figures 4.6(a) and (b) indicate that phonon-defect scattering plays an important role in determining thermal transport. As Pb concentration increases, the phonon mean free path decreases causing a corresponding decrease in thermal diffusivity.

Comparison of fig. 4.7 with figs. 4.6(a) and (b) makes it clear that the observed dependence of thermal diffusivity on Pb concentration is not due to change in sample density due to Pb doping. So the observed variation of thermal diffusivity is primarily due to the corresponding variation in thermal conductivity.

We consider that the most important result of this chapter is contained in fig. 4.7 where we have plotted the thermal diffusivity against Pb concentration at a temperature below T_c . We find that diffusivity tends to saturate below a Pb concentration of ≈ 0.3 . A qualitative explanation for this observation can be made in the following way.

Below T_c , the electrons in the system form Cooper pairs. When Pb atoms are added to the system to stabilize

the superconducting phase, they go into Bi sites and the free electrons contributed by Pb atoms also take part in pair formation. The Cooper pairs do not act as heat carriers and they do not contribute to thermal resistance by electron-phonon scattering. The small number of remaining normal carriers in the superconducting phase may contribute to limiting the phonon mean free path. These uncondensed carriers may participate in heat transport in the superconducting phase. But major contribution to thermal resistance is due to phonon-defect scattering below T_c . Low Pb concentration does not enhance this phonon-defect scattering considerably. But as Pb concentration increases, phonon-defect scattering begins to dominate resulting in a reduction in phonon mean free path and a corresponding decrease in thermal diffusivity. This is evident from fig. 4.7. A behaviour like this will not be seen in a corresponding electrical conductivity curve because electrical resistance is zero irrespective of the addition of Pb at this temperature.

A comparison between the curves in figs. 4.6 and 4.7 would be interesting. In fig. 4.6 the thermal transport is due to thermal energy carried by both phonons and free electrons. The phonon contribution obviously is limited by electron-phonon and phonon-defect scattering. In fig. 4.7

the free electron contribution is absent. For Pb concentrations above 0.3, one finds that this region of the curve has much higher slope in fig. 4.7 than in fig. 4.6. This difference is due to the fact that heat transport due to free electrons is considerably less in the superconducting phase.

In summary, we have undertaken photoacoustic investigation of the variation of thermal diffusivity with lead concentration in the Pb doped superconductor Bi-Sr-Ca-Cu-O above and below T_c . The results bring out the influence of phonon-defect scattering on heat transport in the superconducting phase.

REFERENCES

1. H.Maeda, Y.Tanaka, F.Fukutomi & T.Asano, *Jpn.J.Appl.Phys.* **27**, L 209 (1988).
2. J.M.Tarascon, Y.Leepage, P.Barboux, B.C.Bagley, L.H.Greene, W.R.Mc Kinnon, G.W.Hull, M.Giroud & D.M.Hwang, *Phys.Rev.B* **37**, 9382 (1988).
3. Z.Z.Sheng & A.M.Herman, *Nature* **332**, 138 (1988).
4. M.A.Subramanian, C.C.Torardi, J.C.Calabrese, J.Gopala-krishnan, K.J.Morrissey, T.R.Askew, R.B.Flippen, U.Chowdhry & A.W.Sleight, *Science* **239**, 1015 (1988).
5. H.W.Zandbergen, Y.K.Huang, M.J.V.Menken, J.N.Li, K.Kodowaki, A.A.Menovsky, G.Van Tendeloo & S.Amelincky, *Nature* **332**, 620 (1988).
6. Y.Matsui, H.Maeda, Y.Tanaka & S.Horiuchi, *Jpn.J.Appl.Phys.* **27**, L 361 (1988).
7. E.T.Muromachi, Y.Uchida, A.Ono, F.Izumi, M.Onoda, Y.Matsui, S.Takekawa & K.Kato, *Jpn.J.Appl.Phys.* **27**, L 365 (1988).

8. Y.Bando, T.Kijima, Y.Kitami, J.Tanaka, F.Izumi & M.Yokoyama, *Jpn.J.Appl.Phys.* **27**, L 358 (1988).
9. K.Hiraga, M.Hirabayashi, M.Kikuchi & Y.Shono, *Jpn.J.Appl. Phys.* **27**, L 573 (1988).
10. D.R.Veblen, P.J.Heany, R.J.Angel, L.W.Finger, R.M.Hazen, C.T.Prewitt, N.L.Ross, C.W.Chu, P.H.Hor & R.L.Menz, *Nature* **332**, 334 (1988).
11. M.Onada, A.Yamamoto, E.T.Muromachi & S.Takekawa, *Jpn.J. Appl.Phys.* **27**, L 833 (1988).
12. E.T.Muromachi, Y.Uchida, Y.Matsui, M.Onoda & K.Kato, *Jpn.J.Appl.Phys.* **27**, L 556 (1988).
13. T.M.Shaw, S.A.Shivashankar, S.J.La Placa, J.J.Cuomo, T.R.Mcguire, R.A.Roy, K.H.Keller & D.S.Yee, *Phys.Rev.B* **37**, 9856 (1988).
14. A.Sumiyama, T.Yoshitoshi, H.Endo, J.Tsuchiya, N.Kijima, M.Mizuno & Y.Oguri, *Jpn.J.Appl.Phys.* **27**, L 542 (1988).
15. N.Kijima, H.Endo, J.Tsuchiya, A.Sumiyana, M.Mizuno & Y.Oguri, *Jpn.J.Appl.Phys.* **27**, L 821 (1988).

16. H.Nobumasa, K.Shimizu, Y.Kitano & T.Kawai, Jpn.J.Appl. Phys. **27**, L 846 (1988).
17. M.Takano, J.Takada, K.Oda, H.Kitaguchi, Y.Miura, Y.Tomii & H.Mazaki, Jpn.J.Appl.Phys. **27**, L 1041 (1988).
18. M.Mizuno, H.Endo, J.Tsuchiya, N.Kijima, A.Sumiyana & Y.Oguri, Jpn.J.Appl.Phys. **27**, L 1225 (1988).
19. A.Oota, A.Kirihigashi, Y.Sasaki & K.Ohba, Jpn.J.Appl. Phys. **27**, L 2289 (1988).
20. C.K.Rhee, C.J.Kim, H.G.Lee, I.H.Kuk, J.M.Lee, I.S.Chang, C.S.Kim, P.S.Han, S.I.Pyan & D.Y.Won, Jpn.J.Appl.Phys. **28**, L 1137 (1989).
21. S.Koyama, U.Endo & T.Kawai, Jpn.J.Appl.Phys. **27**, L 1861 (1988).
22. S.D.Peacor & C.Uher, Phys.Rev.B **39**, 11559 (1989).
23. M.F.Crommie & A.Zettl, Phys.Rev.B **41**, 10978 (1990).

24. N.Okazaki, T.Hasegawa, K.Kishio, K.Kitazawa, A.Kishi, Y.Ikeda, M.Takano, K.Oda, H.Kitaguchi, J.Takada & Y.Miura, Phys.Rev.B **41**, 4296 (1990).

25. G.Briceno & A.Zettl, Phys.Rev.B **40**, 11352 (1989).

26. M.F.Crommie, A.Y.Liu, M.L.Cohn & A.Zettl, Phys.Rev.B **41**, 2526 (1990).

Chapter 5

PHOTOACOUSTIC INVESTIGATION OF THE PHASE TRANSITIONS IN KNO_3 AND TGS

5.1 Introduction

The existence of three polymorphic phases in Potassium Nitrate (KNO_3) has been well established by a variety of methods [1-6]. In the bulk form, KNO_3 has aragonite structure [7] at room temperature (Phase II) and is rhombohedral [8] above $\approx 130^\circ\text{C}$ (Phase I). On cooling, phase I does not go back directly to phase II, but changes first into an intermediate phase (Phase III) at about 120°C and then transforms to phase II at a lower temperature around 110°C . Phase III is also rhombohedral but is of lower symmetry than phase I and is ferroelectric [9]. The transition temperatures depend fairly upon the nature and history of the sample, the heating and cooling rates etc. [2,4]. Balkanski et al. [10] have reported that the intermediate phase appears only when the crystal is heated initially to about 180°C . It is known that by the application of a high pressure the phase III is realized also on heating and the temperature range corresponding to phase III on cooling is broadened [4,11].

In bulk materials, phase III is evidently metastable with respect to phase II over the short temperature range where it is observed. Depending on many factors it transforms more or less readily to phase II at lower temperatures. Contrary to this, in the thin film form of the sample, the ferroelectric phase exists over a wider range of temperatures down to $\sim 0^\circ\text{C}$ [12]. Recent reports [13] have indicated that ferroelectric KNO_3 films offer one of the most promising raw materials for fabricating non-volatile ferroelectric random access memory devices. Such films have address voltages between 2 and 6V, depending upon the thickness, and switching times as fast as 20 ns. [14]. Though these results are highly promising from the application point of view, many of the physical properties of the material are not yet well understood and many questions still remain to be answered. For example, it is not yet clear, despite several proposed models, why the temperature range over which phase III exists in the thin film sample is much wider than that in the bulk form. Equally important is the question whether the thin film ferroelectric phase is really stable or is only a metastable one. The use of the material for device applications crucially depends on the stability of the ferroelectric phase in the thin film form of the material.

For a better understanding of the nature of the different phases of KNO_3 , we have carried out investigations on the different phase transitions in the sample using photoacoustic and calorimetric techniques. We studied the behaviour of a polycrystalline powder sample which has neither the bulk form nor the thin film form. The usefulness of the relatively new PA technique for the investigation of phase transitions also become evident from the results obtained. Differential scanning calorimetric investigations have also been carried out to supplement the PA measurements. In order to re-establish the usefulness of the PA technique for the investigation of phase transitions, we have also carried out PA measurements on a Triglycine Sulphate (TGS) sample which has a well known ferroelectric phase transition at $\approx 48^\circ\text{C}$. Details of the experiments, results obtained and a discussion of the results are given below.

5.2 Experimental method

Since KNO_3 is a very weak absorber of light, it is very difficult to obtain measurable PA signals from pure samples. This difficulty is overcome by mixing the sample grains with fine particles of carbon black. In such a case the carbon particles act as the sample and KNO_3 as the backing material. At the experimental chopping frequency of

17 Hz the fine carbon particles will be thermally thin and therefore the PA signal will be governed essentially by the thermal properties of the backing material.

The experimental set up is the same as the one described in chapter 2. White light from a high power Xe lamp with the infrared portion filtered off using a water jacket is used for optical excitation of the sample. A few milligrams of the sample taken in a small aluminium pan is placed inside the PA cell, which is then sealed with a window using a silicon 'O' ring which is capable of withstanding high temperatures upto 200°C. Measurements on TGS are carried out under identical conditions. Amplitude of the PA signal is measured as a function of temperature both during heating and cooling cycles at a rate of 2°C/min. Differential scanning calorimetric data have been taken on the sample at a scanning rate of 10°C/min. during heating and cooling cycles using a Perkin-Elmer delta series differential scanning calorimeter model DSC-7.

5.3 Results and discussion

Fig.5.1 shows the amplitude of the PA signal plotted against temperature during both heating and cooling cycles for the polycrystalline KNO_3 sample. In the heating

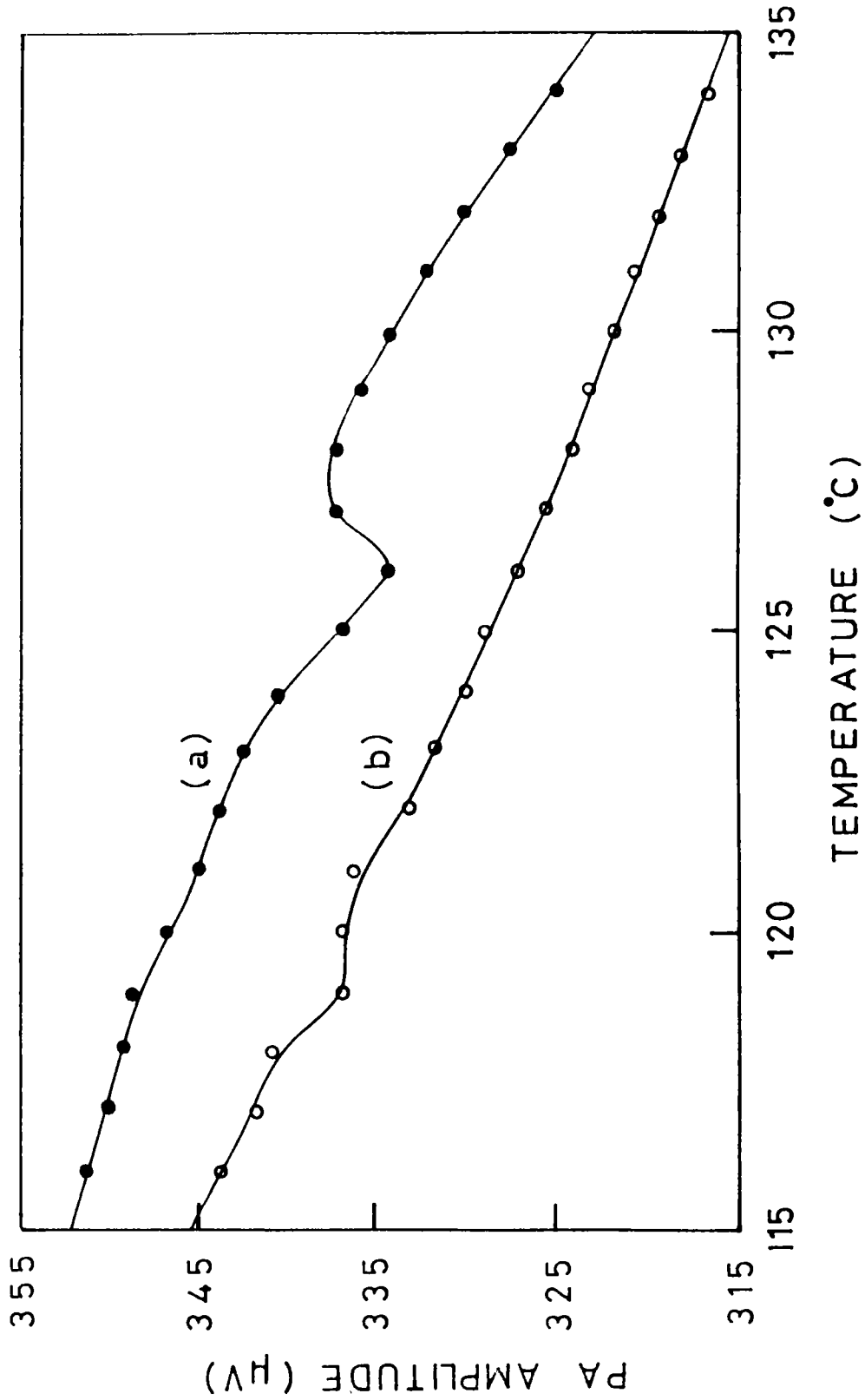


Fig.5.1: Temperature dependence of the PA signal amplitude in KNO_3 near the transition temperatures with (a) increasing temperature and (b) decreasing temperature.

curve the minimum at $\approx 126^{\circ}\text{C}$ clearly indicates the transition from phase II to I (II \rightarrow I) and in the cooling curve the minimum at $\approx 119^{\circ}\text{C}$ indicates the transition I \rightarrow III. During cooling no other anomaly has been noted down to room temperature. Data during the cooling cycle are taken with and without preheating of the sample to $\sim 190^{\circ}\text{C}$ and no difference is observed in the results between the two cases. The transition I \rightarrow III takes place in both cases which is contradictory to the behaviour in the bulk form as reported by Balkanski et al. [10].

Fig.5.2 shows the DSC curves for the above transitions. There is a good correspondence between the PA amplitude and DSC curves and none of them show any indication of the phase III \rightarrow II transition, down to room temperature. It may also be noticed that the anomaly in the PA amplitude variation in the cooling curve indicating the I \rightarrow III transition is much more diminished than the anomaly of the heating curve which indicates the II \rightarrow I transition. Correspondingly, the area under the peak of the DSC cooling curve is also much smaller than that of the heating curve. The transition temperatures obtained from the PA measurements are slightly lower than those obtained from DSC measurements. This may be due to the possible heating of the sample due to optical illumination, the temperature sensor detects the average temperature of the sample cell.

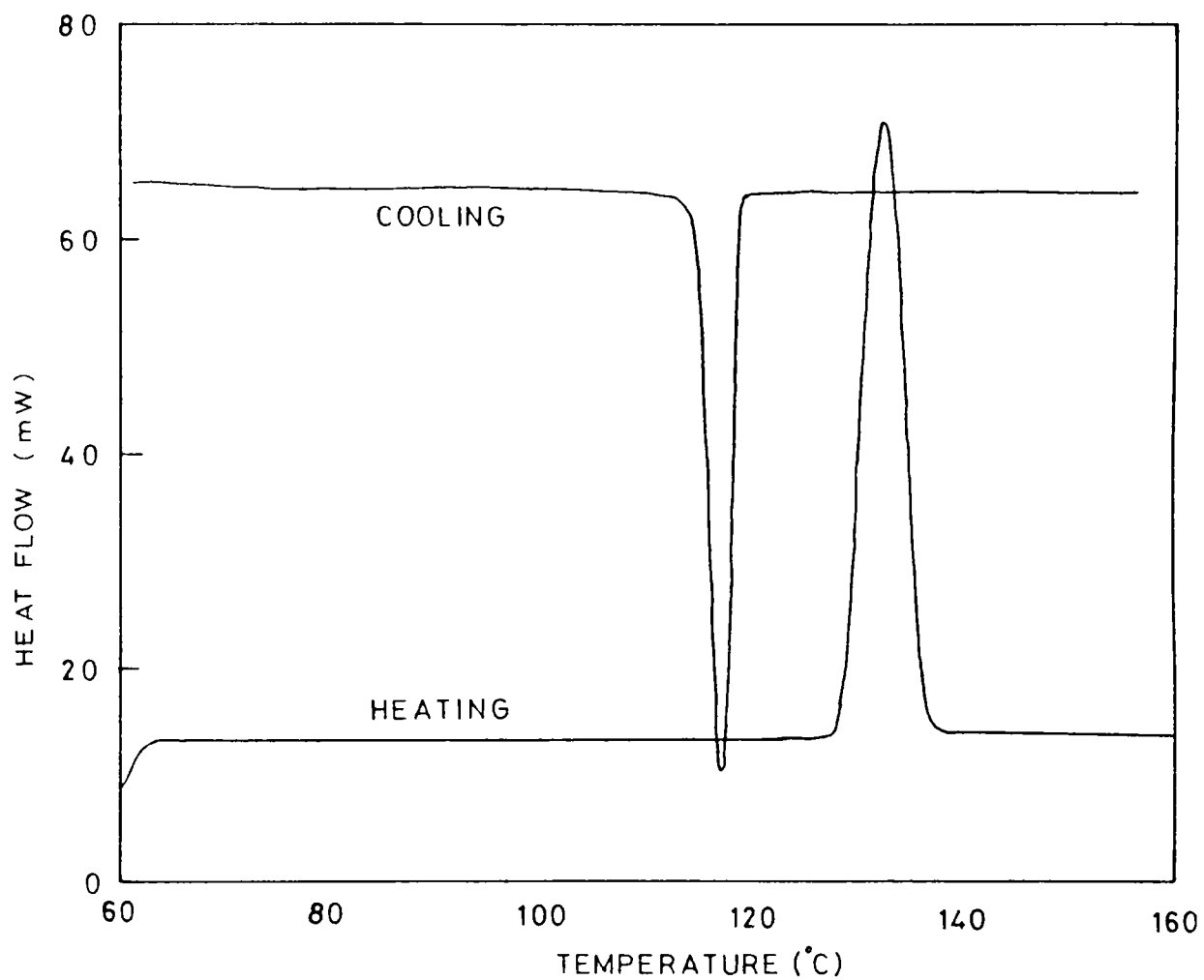


Fig.5.2: DSC curves of the phase transitions in KNO_3 obtained using Perkin-Elmer DSC-7. Scanning rate : $10^\circ\text{C}/\text{min}$.

The theory of Rosencwaig and Gersho [15] predicts the influence of the parameters which determine the thermal properties of the sample on the amplitude of the PA signal. According to the R-G theory in the case of an optically opaque and thermally thin sample, the amplitude of the PA signal is affected not by the thermal properties of the sample but by those of its backing material. In our experiments the fine particles of carbon black are thermally thin at the experimental chopping frequency of 17 Hz so that the amplitude $Q(T)$ of the PA signal at temperature T can be written as (eq.1.27)

$$Q(T) \propto g(T) \frac{\mu(T)}{K(T)} \quad (5.1)$$

where $g(T)$ stands for all the temperature dependent parameters of the PA cell and the coupling gas which affect the PA signal and $\mu(T)$ and $K(T)$ are the thermal diffusion length and thermal conductivity of the backing material (the KNO_3 sample in this case) respectively. $\mu(T)$ is defined as,

$$\mu(T) = \left(\frac{\alpha(T)}{\pi f} \right)^{\frac{1}{2}} \quad (5.2)$$

where $\alpha(T)$ is the thermal diffusivity and f is the chopping frequency. $\alpha(T)$ is given by,

$$\alpha(T) = \frac{K(T)}{\rho C(T)} \quad (5.3)$$

where ρ and $C(T)$ are the mass density and specific heat respectively. Thus eq. (5.1) can be modified as,

$$Q(T) \propto g(T) C(T)^{-\frac{1}{2}} K(T)^{-\frac{1}{2}} \quad (5.4)$$

Equation (5.4) assumes that the density of the sample does not vary with temperature in the range of the experiment. The function $g(T)$ can be obtained using a sample of known thermal properties (for example aluminium) and it is found to be inversely proportional to temperature in the range of the present experiments. Then with $g(T) \propto T^{-1}$ eq. (5.4) can be written as,

$$C(T) K(T) \propto Q^{-2}(T) T^{-2} \quad (5.5)$$

Fig.5.3 shows a plot of $Q^{-2}(T) T^{-2}$ as a function of temperature which gives relative values of $C(T) K(T)$ from eq. (5.5). The anomaly in the signal amplitude at the transition temperatures is mainly due to the corresponding specific heat variations during the transitions. Assuming that the thermal conductivity of the sample does not vary significantly over the temperature range of interest, the curves in fig.5.3

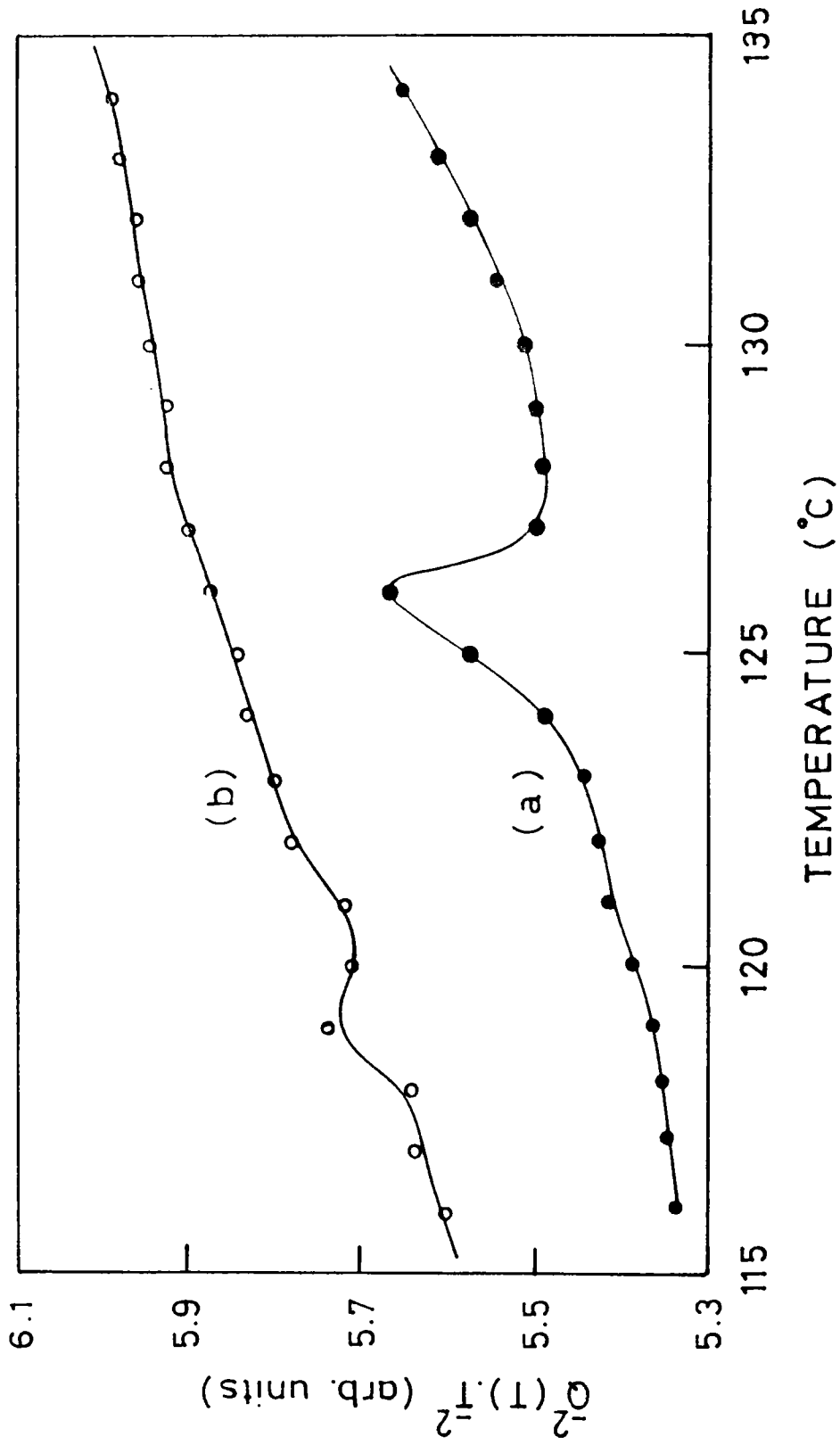


Fig. 5.3: Temperature dependence of $Q^{-2}(T) T^{-2}$ for KNO_3 sample, with (a) increasing temperature and (b) decreasing temperature.

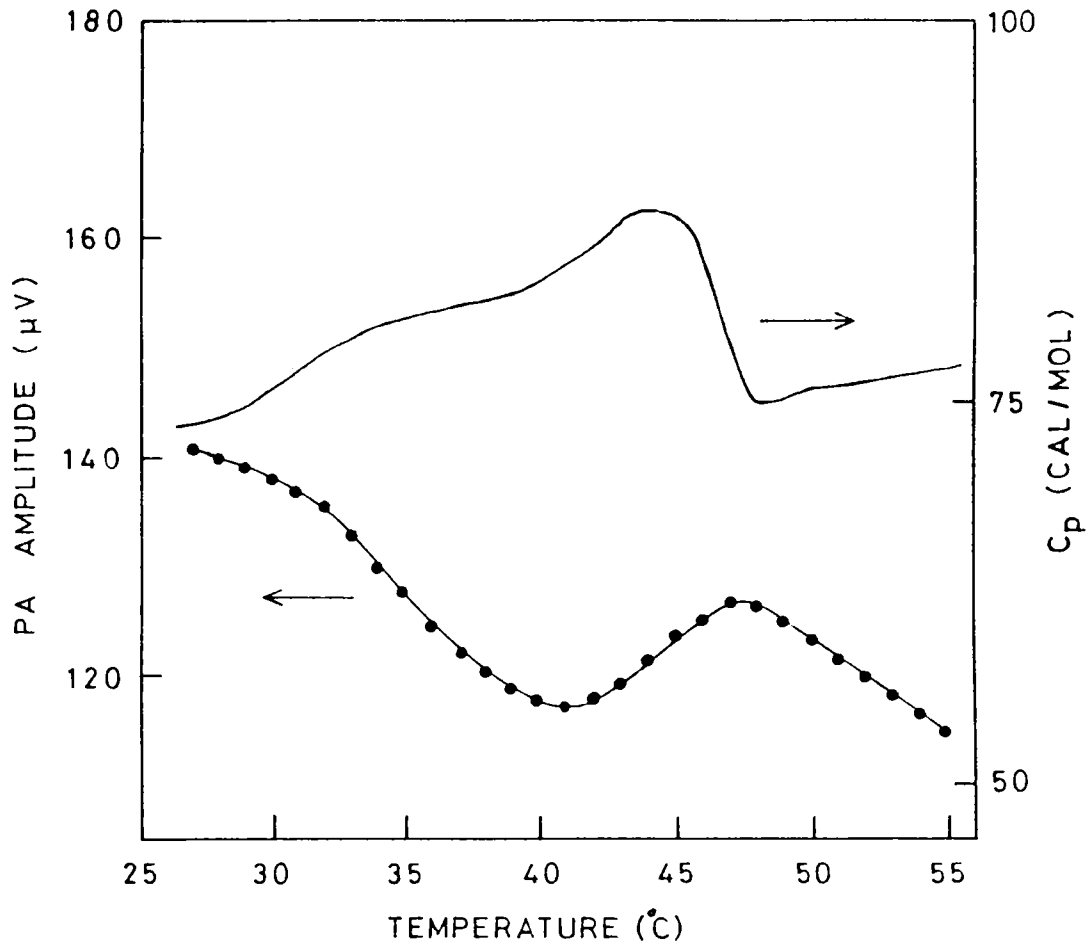


Fig.5.4: Temperature dependence of the PA signal amplitude in TGS sample around the transition temperature. Variation of the specific heat in TGS obtained from literature is also shown in the figure.

nearly follow the corresponding specific heat variation of the sample. Unfortunately no data on the temperature variation of the thermal conductivity of KNO_3 are available for a quantitative comparison.

We have carried out PA measurements on a TGS sample which has a para-ferroelectric phase transition at $\approx 48^\circ\text{C}$. The TGS sample is also powdered and mixed with carbon black to increase the signal strength. Fig.5.4 shows a plot of the PA amplitude as a function of temperature for the TGS sample. The specific heat curve obtained from literature [16] is also given in the figure for comparison. As is evident from the figure, the variation of the PA signal amplitude has a good correspondence with the specific heat variation. This also proves our assumption that the carbon black particles are thermally thin at the chopping frequency of 17 Hz is valid.

Two observations are significantly important in the results on KNO_3 presented above. First, we see that the ferroelectric phase (Phase III) exists over a wide temperature range in a polycrystalline sample contrary to the behaviour exhibited by the bulk form where it exists only over a few degrees ($\sim 120^\circ\text{C}$ to $\sim 110^\circ\text{C}$). Existence of phase III down to room temperature has been observed earlier in thin film samples as well and several mechanisms have been proposed for

the stability of phase III in thin film samples. Based on Bridgman's phase diagrams [17] which show that hydrostatic pressure considerably enhances the temperature range over which phase III exists, it has been suggested [12,18] that hydrostatic or uniaxial stress, induced by differential contraction of the film and substrate upon cooling after deposition, might be the reason for the stability of phase III. Scott et al. [19,20] on the other hand have suggested, based on Raman spectroscopic data, that the actual mechanism for the stability of phase III is the presence of large surface electric fields in the ferroelectric state. It may be noted that such models have been formulated exclusively for thin film samples and as such are not applicable to polycrystalline samples. However, the basic mechanism for the observed behaviour of phase III is expected to be the same for both the forms of the sample.

The second important observation is the difference in the heats of transition associated with the II \rightarrow I and I \rightarrow III transitions given by 63.39 J grm^{-1} and $-32.68 \text{ J grm}^{-1}$ respectively, obtained from the DSC measurements. This clearly suggests that the reentrant phase III has a larger free energy than phase II and that phase III is a metastable state with respect to phase II. The final transformation to the stable phase II may be through ageing process. One of

the reasons for the fatigue [21] observed in thin films (the decrease in apparent spontaneous polarization) after a number of polarization reversals may also be due to such a transformation. The above two observations indicate that thermodynamically phase III in KNO_3 is a metastable state.

Our experiments show that the photoacoustic technique is a powerful analytical method for the investigation of the features of phase transitions in solids. The anomalous changes in the signal amplitudes are attributed mainly to the corresponding specific heat anomalies associated with the transitions. Measurement of the PA amplitude variations during the transitions in KNO_3 enables us to draw conclusions regarding the stability of phase III. The possibility of phase III being a metastable state arises serious doubts about the possible use of KNO_3 films in ferroelectric memory devices. In conclusion, we feel from our results further work is necessary for a better understanding of the nature and stability of the ferroelectric phase in KNO_3 before considering it as a material for ferroelectric memory devices.

Our results on TGS indicate that photoacoustic technique is a useful tool to investigate features of phase

transitions in solid samples. Since extensive work has already been done on TGS using other techniques, not much emphasis has been put to analyse the results obtained from PA measurements.

REFERENCES

1. W.Borchert, Z.Krist. **95**, 28 (1936).
2. E.Cochen & H.L.Bredee, Z.Physik.Chem.A **140**, 391 (1929).
3. C.Finbak & O.Hassel, Z.Physik.Chem.B. **37**, 75 (1937).
4. F.C.Kracek, J.Phys.Chem. **34**, 225 (1930).
5. T.F.W.Barth, Z.Phys.Chem.B **34**, 448 (1939).
6. R.K.Khanna, J.Lingscheid & J.C.Decius, Spectrochimica Acta **20**, 1109 (1964).
7. D.A.Edwards, Z.Krist. **80**, 154 (1931).
8. P.E.Tahvonen, Ann.Acad-Sci.Fenn.Ser. A **1**, 44 (1947).
9. S.Sawada, S.Nomura & S.Fuji, J.Phys.Soc.Jap. **13**, 1549 (1947).
10. M.Balkanski, M.K.Teng & M.Nusimovici, Phys.Rev. **176**, 1098 (1968).
11. P.W.Bridgman, Proc.Amer.Acad. **51**, 579 (1916).

12. J.P.Nolta, N.W.Schubring & R.A.Dork, *Ferroelectricity*, E.F.Welld (ed.) Elsevier, Amsterdam 269-291 (1967).
13. R.B.Godfrey, J.F.Scott, C.A.Araujo & L.D.Mc Millán, *Ferroelectrics Letters* 5, 167 (1986).
14. C.Araujo, J.F.Scott, R.B.Godfrey & L.Mc Millan, *Appl. Phys.Lett.* 48, 1439 (1986).
15. A.Rosencwaig & A.Gersho, *J.Appl.Phys.* 47, 64 (1976).
16. S.Hoshino, T.Mitsui, F.Jona & R.Pepinsky, *Phys.Rev.* 107, 1255 (1957).
17. P.W.Bridgman, *Proc.Amer.Acad.Sci.* 51, 581 (1916); 52, 57 (1916).
18. M.H.Brooker, *Can.J.Chem.* 55, 1242 (1977).
19. J.F.Scott, Ming-Sheng Zhang, R.B.Godfrey, C.Araujo & L.Mc Millan, *Phys.Rev.B* 35, 4044 (1987).
20. J.F.Scott & B.Pouligny, *J.Appl.Phys.* 64, 1547 (1988).
21. J.F.Scott, B.Pouligny, K.Dimmler, M.Parris, D.Butler & S.Eaton, *J.Appl.Phys.* 62, 4510 (1987).

Chapter 6

PHOTOACOUSTIC INVESTIGATION OF THE PARA-FERROELECTRIC

PHASE TRANSITION IN PHOTOFERROELECTRIC SbSI

6.1 Introduction to photoferroelectric phenomena

Most of the structural phase transitions in solids, particularly ferroelectric phase transitions are associated with instability in one or more of the vibrational modes of the lattice. While the behaviour of the electronic spectrum and the electron-phonon interaction have practically been ignored until recently, a large body of experimental data has been accumulated on the effect of electrons, particularly that of nonequilibrium electrons, on ferroelectric phase transitions and the properties of the ferroelectrics well below the Curie point. Phase transitions due to such electrons are described as photostimulated in literature and the phenomena associated with the effect of nonequilibrium electrons on the ferroelectric properties, as photoferroelectric phenomena [1-4]. While photostimulated phase transitions can occur in all semiconductors that undergo phase transitions, such investigations on photoferroelectrics have the advantage that they permit photoferroelectric phenomena to be correlated with the basic

phenomenological parameters of ferroelectrics such as the Curie-Weiss constant, spontaneous polarization, heat capacity discontinuity and other independently measured parameters.

The existence of photostimulated phase transitions in solids, particularly in ferroelectrics, is of fundamental interest. When considering the mechanism of phase transitions in a crystal, the contribution that the electron subsystem makes to the total free energy of the crystal is usually neglected and thus it is assumed that the phase transition is not associated with the electron excitation in the crystal. This is because the importance of the contribution of the electrons to the free energy is determined by the ratio of the electronic heat capacity C_V^{el} to the lattice heat capacity C_V^l . Above the Debye temperature, this ratio can be written as,

$$\frac{C_V^{el}}{C_V^l} \approx \frac{kT}{E_F} \ll 1 \quad (6.1)$$

where, for a metal as well as a semiconductor, the Fermi energy E_F is of the order of several eV and $kT \approx 0.025$ eV at room temperature. Hence, for both metals and semiconductors,

the contribution of free electrons to the free energy of the crystal can be neglected above the Debye temperature and it appears that the contribution of electrons can become appreciable only near $T = 0$, where C_V^e tends to zero as T^3 .

However, the contribution of the electron subsystem to the free energy of the crystal can be substantial near the phase transition temperature, in addition to being significant at temperatures close to absolute zero. This comes about because the electrons may make an appreciable contribution, not to the heat capacity itself, but to its anomalous part which arises during the phase transition. This conclusion was first suggested by Fridkin [5] for ferroelectric phase transitions within the framework of the phenomenological theory of Landau, Ginsburg and Devonshire. Further developments in this direction have been made by Pasyukov [6,7] and the effect of electron excitation on phase transitions of a different nature has subsequently been studied.

The effect of optical illumination and the subsequent generation of nonequilibrium carriers on a ferroelectric semiconductor brings out a wide variety of phenomena. These include photo-induced shift in Curie point,

photorefraction, photodeformation effect, photodomain effect, photo-switching, anomalous photovoltaic effect etc. Photoferroelectric phenomena is hence of great importance from both scientific and technological viewpoints. One important photoferroelectric phenomena is the effect of nonequilibrium conductivity on the birefringence of ferroelectric and electro-optical crystals--the photorefractive effect [8,9]. This property has been made use of in three dimensional phase holography, where some of these materials compete with silver halides in sensitivity and resolution. Investigations on the photorefractive effect led to the discovery of a new mechanism of charge transfer in ferroelectrics, the anomalous photovoltaic effect [10,11]. A homogeneous photoferroelectric crystal might well be a possible solar energy converter.

The investigation of the intrinsic optical absorption of ferroelectrics is of significant interest. One can determine, from measurement of the intrinsic absorption edge, the anomalies in the width of the forbidden energy band at first and second order phase transitions. These anomalies are directly related to the anomalies of heat capacity and can be obtained from the thermodynamic theory of ferroelectric phase transition [12]. In the case of a ferroelectric

semiconductor, the free energy per electron-hole pair can be taken as the energy gap E_g [13], which can then be written in powers of the spontaneous polarization P as,

$$E_g = E_{g0} + \frac{1}{2} aP^2 + \frac{1}{4} bP^4 + \frac{1}{6} cP^6 + \dots \quad (6.2)$$

where E_{g0} is the energy gap in the paraelectric phase and a , b , c etc., are constants. Thus the discontinuity in a first order phase transition is approximately given by,

$$\Delta E_g \approx \frac{a}{2} P_0^2 \approx \frac{a}{4\pi} C \cdot \Delta S \quad (6.3)$$

where P_0 is the equilibrium spontaneous polarization, C is the Curie-Weiss constant and ΔS is the discontinuity in entropy. In a second order phase transition, $\Delta E_g = 0$, but there is a discontinuity in the derivatives of the energy gap $(\partial E_g / \partial T)_P$ and $(\partial E_g / \partial P)_T$. Keyes [14] developed these thermodynamic ideas and derived the general relation,

$$\left(\frac{\partial E_g}{\partial T} \right)_P \sim C_V \quad (6.4)$$

The energy gap anomaly in ferroelectric phase transition is a consequence of this. It also follows that there is such a

discontinuity in the energy gap or its derivatives in non-ferroelectric transitions. The anomaly of the energy gap is also of practical interest for identifying certain phase transitions where there is difficulty in measuring the heat of transition and heat capacity, and also in several cases where there is difficulty in measuring the dielectric anomalies because of the ambiguity of their nature.

We have carried out investigations on the temperature dependence of the optical energy gap of a representative photoferroelectric crystal antimony sulfoiodide (SbSI) using photoacoustic technique. The temperature coefficient of the energy gap $(\partial E_g / \partial T)_p$ is found to undergo a distinct change at the ferroelectric transition point. Details of the experiments, the results obtained and a discussion of the results are outlined in the following sections.

6.2 Photoacoustic determination of the temperature variation of the optical energy gap of SbSI

Antimony sulfoiodide (SbSI) and some of its isomorphous analogs belonging to the general formula $A^V B^{VI} C^{VII}$, where A is a group V atom such as Sb, Bi etc., B is a group VI atom such as S, Se etc., and C is a group VII atom such as Br, I etc., exhibit a number of interesting optical and

electronic properties and has been the subject of very extensive studies during the last few years [15]. SbSI undergoes a ferroelectric phase transition of the displacive type at $T_c \approx 20^\circ\text{C}$. Structural investigations have established that SbSI crystals are rhombic and belong to the class mmm (space group D_{2h}^{16}) above T_c and to the class mm (C_{2v}^9) below T_c [16,17]. It is a semiconducting ferroelectric with a relatively small energy gap (~ 2 eV) compared to other ferroelectrics and exhibits highly temperature dependent band gap, anomalous electro-optic and photomechanical properties in addition to being one of the strongest piezoelectric materials.

Crystalline samples of SbSI have been prepared from a melt of Sb_2S_3 and SbI_3 by the Bridgman technique. The samples obtained are in the form of thin needles oriented along the ferroelectric c-axis. The PA spectrometer already described in chapter 2 has been used for the measurements. A few milligrams of the sample is found to be enough to get measurable PA signal amplitude for the present investigations. The optical absorption spectra is obtained by measuring the amplitude of the PA signal as a function of incident wavelength for a fixed chopping frequency of 30 Hz. A high power Xe lamp in conjunction with a grating monochromator provides

the necessary monochromatic radiation as described in chapter 2. In order to avoid the effect of the spectral power density variations of the light source, the PA amplitude is normalized by dividing it by the signal from a carbon black sample at the corresponding wavelengths. The temperature of the sample is kept constant within $\pm 0.05^\circ\text{C}$ using the temperature controller described in chapter 2.

6.3 Results and discussion

Typical absorption spectra obtained from SbSI sample at various temperatures obtained from PA measurements with unpolarized incident beam is shown in figs.6.1 and 6.2. The sudden decrease in absorption beyond ~ 600 nm is due to the optical energy gap of the material lying in this range. The energy gap (E_g) values at each temperature are determined as that photon energy at which the onset of the decrease in the PA signal amplitude takes place. The values of the energy gap at various temperatures is tabulated in Table 6.1. Fig.6.3 shows the variation of the energy gap with temperature which shows a distinct change in slope at $T_c \approx 20^\circ\text{C}$. The temperature coefficient of the energy gap in the paraelectric and ferroelectric phases have been determined and are,

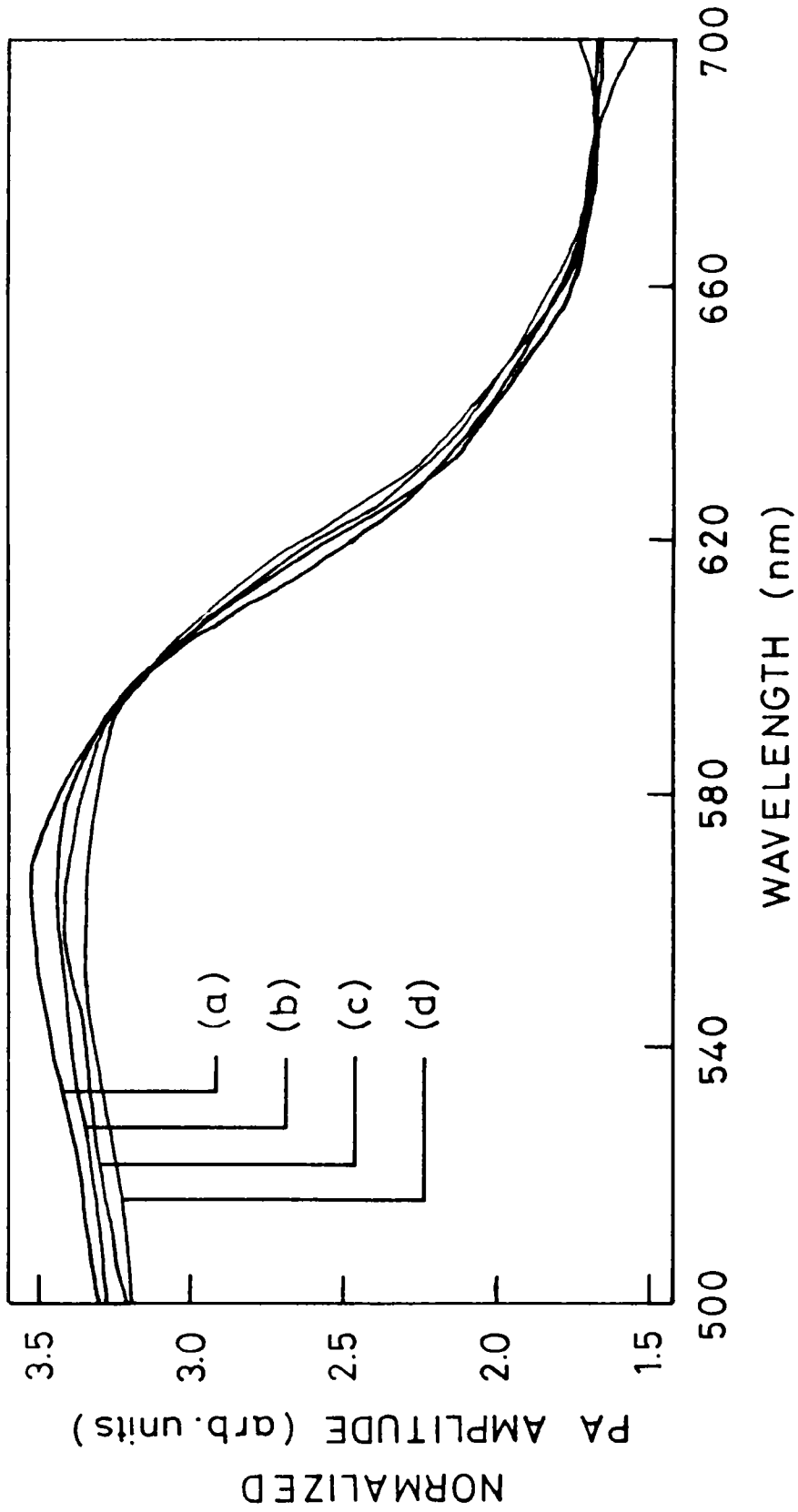


Fig.6.1: Normalized PA spectra of SbSI at different temperatures. (a) 5°C, (b) 10°C, (c) 15°C and (d) 20°C.

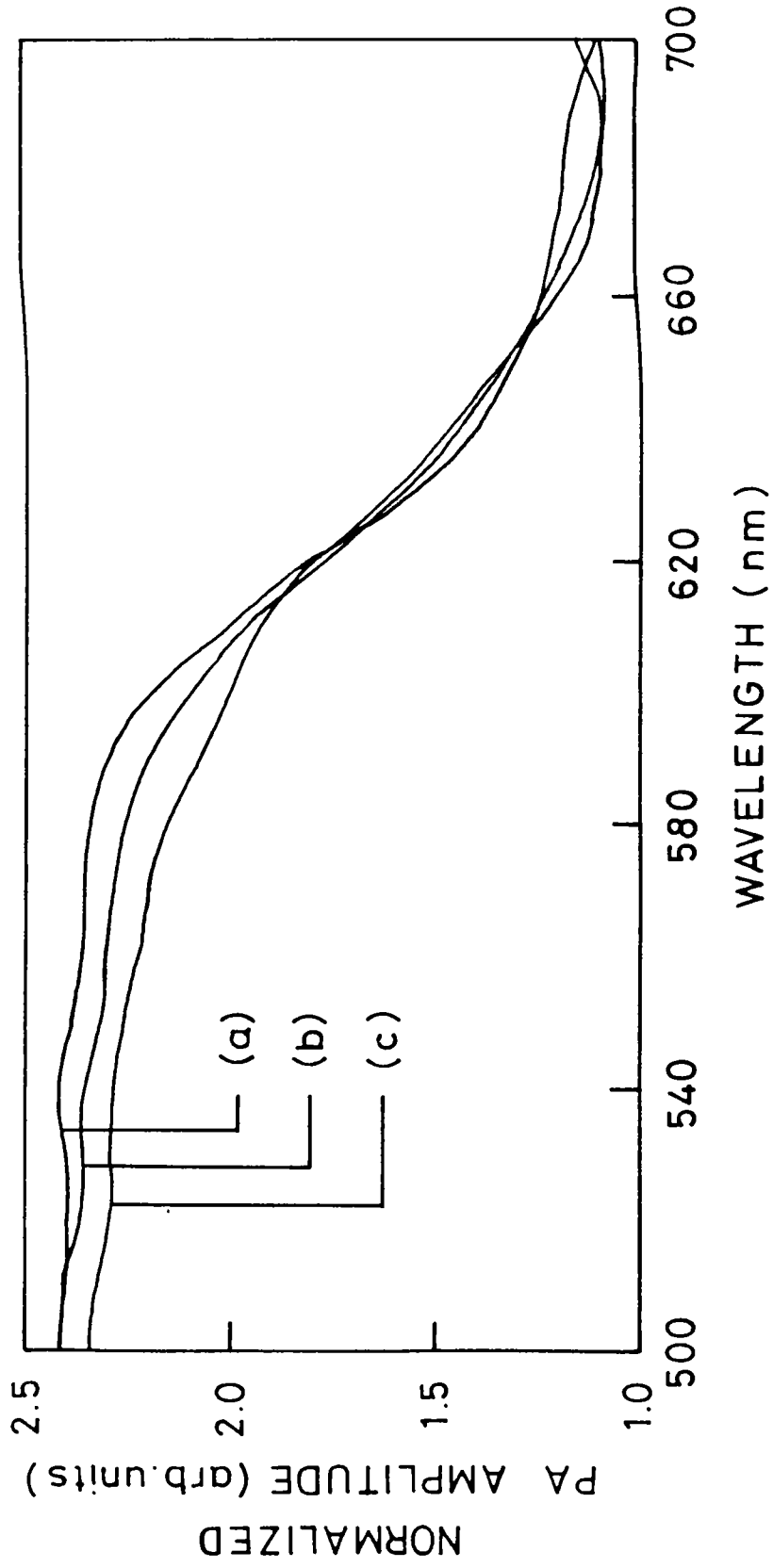


Fig.6.2: Normalized PA spectra of SbsI at different temperatures. (a) 25°C, (b) 35°C and (c) 45°C.

Temperature (°C)	Energy gap (eV)
-1	2.125
5	2.107
10	2.092
15	2.089
20	2.081
25	2.080
30	2.070
35	2.073
40	2.066
45	2.066

Table 6.1: Energy gap of SbSI at different temperatures.

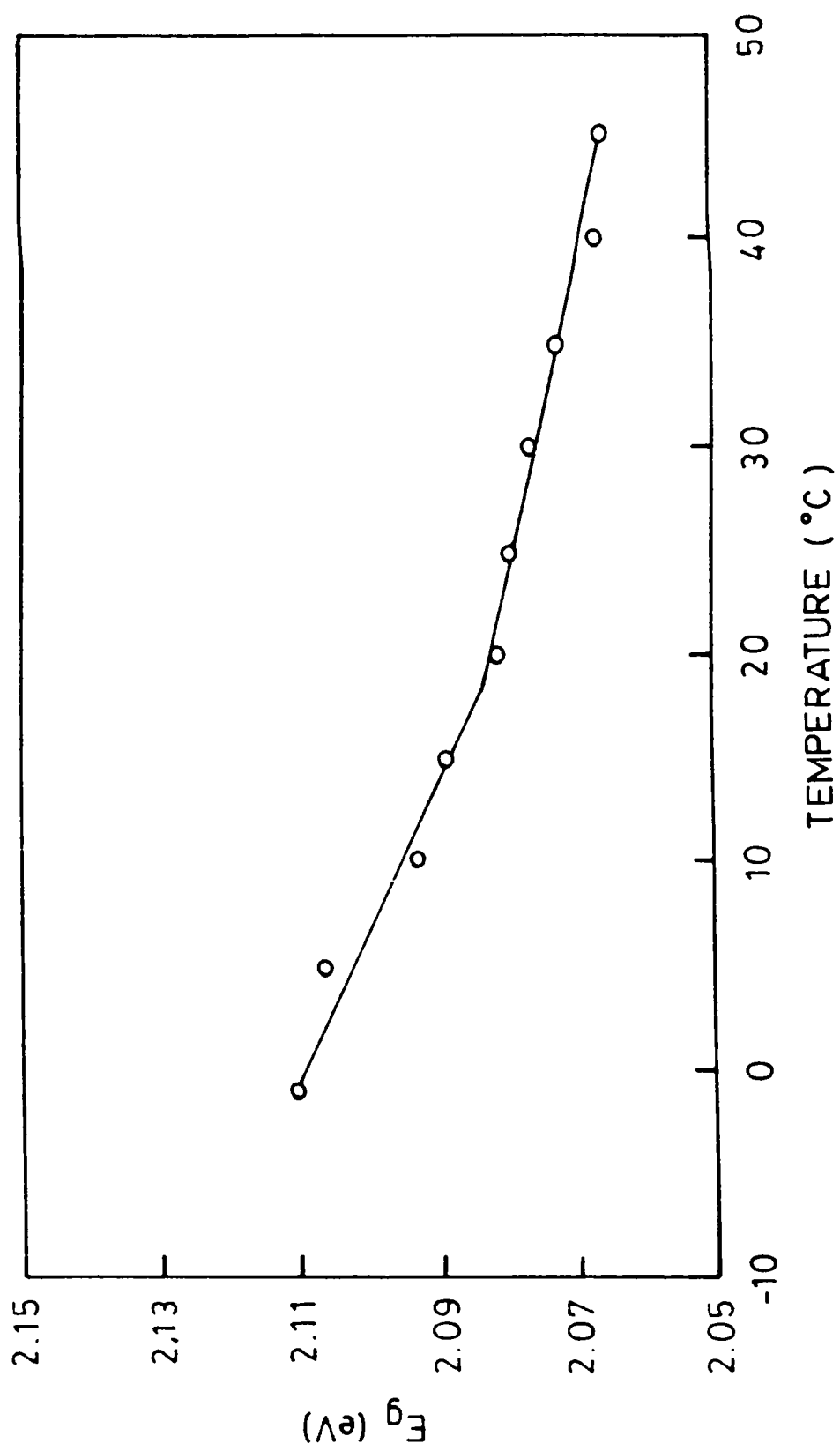


Fig.6.3: Temperature variation of the energy gap of SbSI around the transition temperature.

$$\left(\frac{\partial E_g}{\partial T}\right)_{PE} = -7 \times 10^{-4} \text{ eV K}^{-1}$$

$$\left(\frac{\partial E_g}{\partial T}\right)_{FE} = -13.8 \times 10^{-4} \text{ eV K}^{-1}$$

These values are in good agreement with the values reported earlier [18] for light polarization perpendicular to the ferroelectric c-axis. This is expected because the absorption coefficient determined for unpolarized light will be the smaller one which in this case corresponds to perpendicular polarization.

The change in the temperature shift of the energy gap at the phase transition temperature is a consequence of spontaneous polarization, while the exact mechanism may involve a number of related microscopic phenomena. Generally, the temperature shift of the energy gap is related to (i) change in the electron-phonon interaction and (ii) lattice expansion as given by,

$$\left(\frac{\partial E_g}{\partial T}\right)_P = \left(\frac{\partial E_g}{\partial T}\right)_V - \frac{\alpha}{\psi} \left(\frac{\partial E_g}{\partial P}\right)_T \quad (6.5)$$

where the first term on the right hand side of the equation stands for contribution from (i) and the second term represents contribution from (ii), α and ψ being coefficient

of volume thermal expansion and compressibility of the material respectively. Approximate calculation of the second term in eq.(6.5) for the paraelectric and ferroelectric phases gives the values 0.4×10^{-4} and -12×10^{-4} eV/K respectively [18]. It can be seen that in the paraelectric phase, the effect of the second term is negligible and the energy gap shift is predominantly due to electron-phonon interaction. However, in the ferroelectric phase the second term is significant and one should take into account the influence of the lattice expansion on the energy gap.

Thermal expansion of the lattice is caused by the anharmonicity of lattice vibrations. In the paraelectric phase, this is the dominant mechanism which determines the contribution of lattice elongation to the energy gap shift. In the ferroelectric phase the thermal expansion is greatly modified by the spontaneous polarization through its coupling to the spontaneous strain [19]. The strong piezoelectric effect observed in this material can also be regarded as a manifestation of this strain-polarization coupling. The temperature dependence of the spontaneous polarization and its coupling to the spontaneous strain are the major factors which govern the lattice elongation and the corresponding contribution to the energy gap shift in the ferroelectric phase.

In conclusion, we have successfully used the photoacoustic technique for the investigation of the absorption edge in SbSI and its temperature variation. The observations and the results obtained are in good agreement with previous reports. The increase in $(\frac{\partial E_g}{\partial T})$ in the ferroelectric phase is attributed to the lattice elongation caused by spontaneous polarization.

REFERENCES

1. V.M.Fridkin, L.M.Belyaev, A.A.Grekov & A.I.Rodin, J.Phys. Soc.Jpn. Suppl. **28**, 448 (1970).
2. F.Micheron & J.C.Trotier, Ferroelectrics **8**, 441 (1974).
3. G.A.Smolensky, V.M.Fridkin & A.A.Grekov, Ferroelectrics **6**, 1/2 (1973).
4. V.M.Fridkin, Photoferroelectrics, Springer-Verlag, Berlin, Heidelberg, (1979).
5. V.M.Fridkin, JETP Lett. **3**, 252 (1966).
6. R.E.Pasynkov, Izv.Akad.Nauk SSSR, Ser.Fiz. **34**, 2466 (1970).
7. R.E.Pasynkov, Ferroelectrics **6**, 19 (1973).
8. A.Ashkin, C.D.Boyd, T.M.Dziedzic, R.G.Smith, A.A.Ballaman, I.I.Levinstein & K.Nassau, Appl.Phys.Lett. **9**, 72 (1966).
9. A.Ashkin, B.Tell & I.M.Dziedzic, J.Quantum Electronics, **3**, 400 (1967).

10. A.M.Glass, D.von der Linde & T.J.Negran, *Appl.Phys.Lett.* **25**, 233 (1974).
11. V.M.Fridkin, B.N.Popov & K.A.Verchovskaya, *Phys.Stat.Sol.(a)* **39**, 139 (1977).
12. L.D.Landau & E.M.Lifshitz, *Statistical Physics*, Pergamon Press, Oxford (1959).
13. H.Brooks, *Adv.Electron.Electron Phys.* **7**, 117 (1955).
14. R.W.Keyes, *Solid State Physics*, (F.Seitz & D.Turnbull, Ed.), Academic Press, New York, Vol.11, (1960), p.179.
15. See, for example, a number of papers on Sulfoiodides *Proc.Int.Conf. on Ferroelectricity, in Ferroelectrics* **34/38** (1981).
16. E.Doenges, *Z.Anorg.Allg.Chem.* **263**, 112, 280 (1950).
17. R.Arndt & A.Niggli, *Naturwissenschaften* **51**, 158 (1964).
18. K.Zickus, A.Audzijonis, J.Batarunas & A.Sileika, *Phys.Stat.Sol.(b)* **125**, 645 (1984).
19. M.E.Liner & A.M.Glass, *Principles and Applications of Ferroelectrics and Related Materials*, Clarendon Press, Oxford (1977).

Chapter 7

SUMMARY AND CONCLUSION

The work presented in this thesis is centred around the relatively new photoacoustic technique and its application for the investigation of phase transitions and related phenomena in solids. The PA technique is based on the detection of an acoustic signal generated when a sample placed inside an enclosed cell containing a gas is irradiated by an intensity modulated beam of light. The PA signal detected by a sensitive microphone depends, among others, on the optical and thermal properties of the sample. Applications of PA effect cover a wide range of phenomena involving optical and thermal properties of materials.

The basic modules of the PA spectrometer which has been set up for the present investigations are a high power Xe lamp, a monochromator, an electromechanical light beam chopper, a variable temperature PA cell and a lock-in amplifier. A wide temperature range PA cell has been designed and fabricated with which measurement can be

done from 85 to 450 K. The cell incorporates a sensitive electret microphone for detecting the acoustic signal. Characterization of the cell has been done over the entire temperature range and over the frequency range of interest. An accurate temperature controller has also been designed and fabricated in order to perform the temperature dependent studies. It is a proportional, integral, derivative (PID) type controller which can be used for both measurement and control of temperature over a wide range from -200°C to $+200^{\circ}\text{C}$ with a control stability better than $\pm 0.01^{\circ}\text{C}$.

The normal to superconducting transition of the high T_c superconductor $\text{YBa}_2\text{Cu}_3\text{O}_7$ is studied using PA technique. The amplitude and phase of the PA signal is measured over a temperature range of 85-300 K, on pelletized samples prepared by solid state reaction method. The amplitude-temperature plot does not show any significant anomaly over the entire temperature range, while the phase is found to undergo a clear anomalous change in the vicinity of the superconducting transition. The amplitude behaviour manifests the absence of any large specific heat anomaly in the material during the superconducting transition. At the same time, the nearly

opposite behaviour of the specific heat and thermal conductivity below T_c cancel out each other their effect on the PA amplitude. The anomalous decrease in PA phase is considered to be due to a faster relaxation of the optically excited levels during the transition. This faster relaxation may be due to the creation of additional electron traps when the material changes phase.

The second phase of measurements on $\text{YBa}_2\text{Cu}_3\text{O}_7$ involves determination of the absolute value of the thermal diffusivity as a function of temperature using PA technique. For this, the amplitude of the PA signal is measured as a function of the chopping frequency for a sample of appropriate thickness, l , mounted on an aluminium disc. The characteristic frequency f_c above which the PA signal is independent of the thermal properties of the backing material, is determined from the amplitude-frequency plot and thermal diffusivity α is calculated using the relation $\alpha = f_c l^2$. Thermal diffusivity is determined at various temperatures above and below T_c and is found to undergo a sharp increase below T_c . The sudden increase in α below T_c is explained as due to a drastic reduction in phonon-carrier scattering as the carriers start to form superconducting pairs below T_c .

The electronic contribution to thermal conductivity decreases below T_c while that due to phonons increases. The overall increase in thermal conductivity indicates the dominance of the phonon contribution in this material in the normal state. The relatively large value of the normal state electrical resistivity also supports this view. The abrupt increase in thermal diffusion below T_c is also an indication of the close coupling of phonons and charge carriers in these systems. Thermal diffusivity of superconducting Bi-(Pb)-Sr-Ca-Cu-O has also been measured as a function of temperature which shows similar behaviour as described above. Measurements have been carried out on samples with varying Pb doping concentration in order to study the effect of Pb doping on thermal diffusivity. It is found that above T_c the thermal diffusivity increases as the Pb concentration decreases, while below T_c it tends to saturate below a particular Pb concentration. This behaviour suggests that the phonon-defect scattering plays a dominant role in the thermal transport processes of the material.

The successive phase transitions in potassium nitrate (KNO_3) have been investigated using PA technique.

Measurements have been carried out on polycrystalline powdered samples mixed with fine particles of carbon black to enhance the optical absorption. During heating, the amplitude of the PA signal measured as a function of temperature clearly shows an anomaly at $\approx 126^\circ\text{C}$ indicating the transition from phase II to phase I. Upon cooling phase I transforms to phase III, which is ferroelectric, showing another anomaly at $\approx 120^\circ\text{C}$. In the bulk form of the sample the ferroelectric phase (phase III) exists only over a small temperature range and transforms to phase II at around 110°C . In the polycrystalline sample, the PA measurements do not show any indication of a III \rightarrow II transition down to room temperature. Calorimetric measurements performed with a differential scanning calorimeter (DSC) support the PA observations. The behaviour exhibited by the polycrystalline sample is similar to that of thin film samples. However, existing models for the stability of the phase III in KNO_3 are exclusively for thin film samples and are as such not applicable to a polycrystalline powder sample. It is also found from PA and DSC measurements that the heat of transition associated with the I \rightarrow III transition is much less than that of the II \rightarrow I transition indicating an excess of

free energy for phase III than phase II. This suggests the possibility of phase III being only a metastable state with respect to phase II arising serious doubts about the application of KNO_3 films as the raw material for non-volatile random access memory devices.

The variation of the optical energy gap with temperature around the para-ferroelectric transition in the photoferroelectric material antimony sulfoiodide (SbSI) has been investigated using PA technique. Optical absorption spectra of SbSI at various temperatures have been obtained by plotting the normalized amplitude of the PA signal as a function of the incident wavelength. The temperature coefficient of the energy gap is found to undergo a distinct change at T_c . This change at T_c is regarded as a consequence of the spontaneous polarization which appears below T_c . The microscopic mechanism for this observation seems to be the elongation of the lattice caused by the spontaneous polarization through its coupling to the spontaneous strain.

In summary, we have carried out the investigation of various phenomena associated with phase transitions

in different solid materials, using photoacoustic technique. The results obtained are important not only in understanding the physics of the respective systems in a better way, but also in establishing the potentiality of the photoacoustic technique to study properties of solids. As is evident from the present work, the most striking characteristic of the PA technique is the diversity of phenomena that can be studied and the variety of ways in which the method can be applied. Incorporating both calorimetric and spectroscopic aspects of the photoacoustic effect, the photoacoustic technique offers a unique and powerful method for the investigation of various phenomena associated with phase transitions observed in a wide range of materials.